THE REPUBLIC OF TURKEY
BAHÇEŞEHİR UNIVERSITY

SIMULATION BASED PERFORMANCE ANALYSIS OF LTE SYSTEMS

Master's Thesis

ÖMER TURA

İSTANBUL, 2012

THE REPUBLIC OF TURKEY
BAHÇEŞEHİR UNIVERSITY

THE GRADUATE SCHOOL OF NATURAL AND APPLIED SCIENCE

ELECTRICAL AND ELECTRONICS ENGINEERING

SIMULATION BASED PERFORMANCE ANALYSIS OF LTE SYSTEMS

Master's Thesis

ÖMER TURA

Supervisor: Asst. Prof. ALKAN SOYSAL

İSTANBUL, 2012

THE REPUBLIC OF TURKEY
BAHÇEŞEHİR ÜNİVERSİTESİ

THE GRADUATE SCHOOL OF NATURAL AND APPLIED SCIENCES
ELECTRICAL AND ELECTRONICS ENGINEERING

Title of Thesis: Simulation Based Performance Analysis of LTE Systems
Name of the Student: Ömer Tura
Date of Thesis Defense:

The thesis has been approved by the Graduate School of Natural and Applied Science.

Assoc. Prof. Tunç BOZBURA
Director

This is to certify that we have read this thesis and that we find it fully adequate in scope quality and content, as a thesis for the degree of Master of Science.

Assoc. Prof. Ufuk TÜRELİ
Program Coordinator

Examining Committee Members: Signature

Asst. Prof. ALKAN SOYSAL ----------

Assoc. Prof. Ufuk TÜRELİ ----------

Asst. Prof. Çağrı GÜNGÖR ----------

ACKNOWLEDGEMENTS

I am thankful to my advisor Asst. Prof. Alkan Soysal for all of his support, insight, and invaluable help for this thesis as well as for making it possible for me to my master's work at Bahçesehir University.

I would also like to thank to my thesis committee members for their time. Especially, thanks to my friends and colleagues for being sources of inspiration to me. Mustafa Alnaqeeb, Mehmet Bay, Mustafa Kılıç, Erinç Topdemir and everyone else I have not mentioned, I say big thanks.

Finally, special thanks go to my parents for their love, support, and encouragement.

Before I conclude this text, I would also like to note that I also appreciate Prof. Dr. Tuncay Ertaş who taught and endeared me communication during my undergraduate education. Also I am thankful for his letter of recommendation that helped me to be accepted for master's education.

Ömer TURA

İstanbul, September 2012

ABSTRACT

SIMULATION BASED PERFORMANCE ANALYSIS OF LTE SYSTEMS

Ömer Tura

Electrical Electronics Engineering

Thesis Supervisor: Asst. Prof. ALKAN SOYSAL

August 2012, 91 pages

In this Master's thesis, a performance analysis of 3GPP Long Term Evolution (LTE) Release 8 is provided. LTE is the evolution of the Universal Mobile Telecommunications System (UMTS). It allows mobile users to reach high data rates and access Internet through their devices (mobile telephones, laptop, tablet PC, etc.). LTE intends to deliver rich multimedia services (Full HD video stream, video call...) to next generation users. LTE mobile broadband technology has been used in more than 30 countries and by 70 operators and in the coming years it will be widely used in many countries with more than 100 LTE user devices such as notebooks, tablet PCs, smartphones, hotspots, gaming devices and video cameras.

The Long Term Evolution provides high data rates and can operate using different bandwidths ranging from 1.4MHz up to 20MHz. Furthermore LTE supports Multiple Input Multiple Output (MIMO) systems up to four antennas and can reach higher peak data rates than Single Input Single Output (SISO) systems (326 Mb/s in the DL and 150 Mb/s in the UL with 4 antennas). LTE supports transmit diversity and spatial multiplexing with multi antenna technology to have more reliable communication and to increase the data rate respectively. LTE also improves system capacity and coverage by using more bandwidth and different frequency bands and also it reduces operating costs with IP based infrastructure. The two main frequency bands that will be used in LTE are 2600 MHz and 800 MHz bands. The 2600 MHz band is a choice for more capacity since it provides 190 MHz bandwidth and the 800 MHz band is more ideal for coverage since its wavelength is higher than the other.

In LTE, resource allocation is another important technique to reach that much high rates. The resources (time and frequency) can be scheduled to users fairly or just the user with the best channel condition can be scheduled. In this study, the Round Robin, the Proportional Fair and the Best CQI scheduling algorithms have been considered.

In this Master's thesis, we compared 800 MHz and 2600 MHz frequency bands in terms of coverage and examined the impact of the scheduling algorithms and the MIMO modes on the average cell and cell edge throughputs for the different environments.

Keywords: LTE, MIMO, Scheduling, Spatial Multiplexing, Transmirt Diversity, Capacity, Coverage

ÖZET

LTE SİSTEMLERİNİN BENZETİM TABANLI PERFORMANS ANALİZİ

Ömer Tura

Elektrik Elektronik Mühendisliği

Tez Danışmanı: Yrd. Doç. Dr. ALKAN SOYSAL

Ağustos 2012, 91 sayfa

Bu yüksek lisans tezinde, The 3rd Generation Partnership Project (3GPP) Long Term Evolution (LTE – Uzun Vadeli Evrim) 8. Versiyonunun performans analizi sunulmuştur. LTE Evrensel Mobil Telekomünikasyon Sisteminin (UMTS) gelişimidir. LTE, mobil kullanıcılarının yüksek veri hızlarına çıkmalarına ve cihazlar (cep telefonu, laptop, tablet PC) üzerinden internete erişimine olanak sağlamaktadır. LTE gelecek nesil kullanıcılara zengin çoklu ortam servisleri (Full HD video yayını, görüntülü konuşma) ulaştırmayı hedeflemektedir. LTE mobil geniş bant teknolojisi 30'dan fazla ülkede ve 70'den fazla operatör tarafından kullanılmaktadır ve gelecek yıllarda bir çok ülkede ve notebook, tablet PC, akıllı telefon, modem, oyun cihazları ve video kamera gibi 100'den fazla LTE destekli kullanıcı cihazları ile yaygın olarak kullanılacaktır.

LTE yüksek veri hızları sağlayabilmekte ve 1.4MHz ile 20MHz arasında farklı bant genişliklerinde çalışabilmektedir. Bunun yanında, LTE dört antene kadar Çoklu Giriş Çoklu Çıkış (MIMO) Sistemlerini desteklemekte ve Tek Giriş Tek Çıkış (SISO) Sistemlerine göre daha yüksek tepe hızlarına (4 anten ile aşağı yolda 326 Mb/s ve yukarı yolda 150 Mb/s) ulaşabilmektedir. LTE çoklu anten teknolojisi ile daha güvenli iletişime sahip olmak ve veri hızını artırmak için sırasıyla iletim çeşitlemesi ve uzamsal çoklamayı desteklemektedir. LTE ayrıca, daha fazla bant genişliği ve farklı frekans bantları kullanarak sistem kapasite ve kapsamasını artırabilmektedir ve ekipmanlarında IP tabanlı altyapı kullanarak operasyon giderlerini azaltmaktadır. LTE'de kullanılacak iki temel frekans bantları 2600 MHz ve 800 MHz bantlarıdır. 2600 MHz bandı, 190 MHZ bant genişliği sağladığından kapasite için tercih edilmekte ve 800 MHz bandı ise dalga boyu daha büyük olduğu için kapsama için daha idealdir.

LTE'de böyle yüksek tepe hızlarına ulaşmak için kaynak ataması önemli tekniklerden biridir. Kaynaklar (zaman ve frekans) tüm kullanıcılara adil olarak atanabilir ya da sadece kanal durumu en iyi olan kullanıcıya atanır. Bu çalışmada Round Robin, Proportional Fair ve Best CQI çizelgeleme algoritmaları kullanılmıştır.

Bu yüksek lisans tezinde, 800 MHz ve 2600 MHz frekans bantlarının kapsamalarını karşılaştırdım ve çizelgeleme algoritmaları ve MIMO yöntemlerinin farklı ortamlar için ortalama hücre ve hücre sınırı hızları üzerine etkisini inceledim.

Anahtar Kelimeler: LTE, MIMO, Çizelgeleme, Uzamsal Çoklama, İletim Çeşitlemesi, Kapasite, Kapsama

CONTENTS

TABLES

FIGURES

ABBREVIATIONS

3GPP	:	Third Generation Partnership Project
ADSL	:	Asymmetric Digital Subscriber Line
AMC	:	Adaptive Modulation and Coding
AWGN	:	Additive White Gaussian Noise
BER	:	Bit Error Rate
BLER	:	Block Error Rate
BP	:	Belief Propagation
BPSK	:	Binary Phase Key Shifting
CB	:	Circular Buffer
CFR	:	Channel Frequency Response
CP	:	Cyclic Prefix
CQI	:	Channel Quality Indication
CRC	:	Cyclic Redundancy Check
DAB	:	Digital Audio Broadcast
DFT	:	Discrete Fourier transform
DL	:	Downlink
DVB	:	Digital Video Broadcast
FDD	:	Frequency Division Duplex
FEC	:	Forward Error Correction
FFT	:	Fast Fourier Transform
FIR	:	Finite-Length Impulse Response
GSM	:	Global System for Mobile Communications
HARQ	:	Hybrid Automatic Repeat Request
ICI	:	Inter-carrier interference
IMT	:	International Mobile Telecommunications
ISI	:	Inter-symbol interference
ITU	:	International Telecommunicatiıon Union
LDPC	:	Low Parity Check Code

LS	:	Least Square
LTE	:	Long Term Evolution
MAC	:	Medium Access Control
MCS	:	Modulation and Coding Scheme
MIMO	:	Multi-Input Multi-Output
ML	:	Maximum Likelihood
MMSE	:	Minimum Mean Square Error
OFDM	:	Orthogonal Frequency Division Multiplexing
OFDMA	:	Orthogonal Frequency Division Multiple Access
PAPR	:	Peak To Average Power Ratio
PDCCH	:	Physical Downlink Control Channel
PDSCH	:	Physical Downlink Shared Channel
PMI	:	Precoding Matrix Indicator
PSS	:	Primary Synchronization Signal
PUCCH	:	Physical Uplink Control Channel
PUSCH	:	Physical Uplink Shared Channel
QAM	:	Quadrature Amplitude Modulation
QoS	:	Quality of Service
QPP	:	Quadratic Polynomial Permutation
QPSK	:	Quadrature Phase Shift Keying
RB	:	Resource Block
RE	:	Resource Element
RF	:	Radio Frequency
RI	:	Rank Indicator
RM	:	Rate Matching
RRC	:	Radio Resource Control
RS	:	Reference Signals
SC-FDMA	:	Single Carrier-Frequency Division Multiple Access
SINR	:	Signal to Interference and Noise Ratio
SISO	:	Single Input Single Output
SPA	:	Sum Product Algorithm

SSS	:	Secondary Synchronization Signal
SVD	:	Singular Value Decomposition
TDD	:	Time Division Duplex
TDMA	:	Time Division Multiple Access
TTI	:	Transmission Time Interval
UE	:	User Equipment
UL	:	Uplink
UMTS	:	Universal Mobile Telecommunications System
VA	:	Viterbi Algorithm
WLAN	:	Wireless Local Area network
WSSUS	:	Wide-Sense Stationary Uncorrelated Scattering
ZC	:	Zadoff-Chu

SYMBOLS

Autocovariance Matrix of H : $\underline{R}_{HH}$

Autocovariance Matrix of Y : $\underline{R}_{YY}$

Autocovariance Matrix of h : $\underline{R}_{hh}$

Noise Variance : σ^2

Estimated Symbol Vector : $\hat{S}$

Kronecker product : $\otimes$

Maximum Excess Delay : τ_{max}

LS Estimate of H : $\hat{H}^{LS}$

MMSE Estimate of H : $\hat{H}_{MMSE}$

1. INTRODUCTION

In the last decade, the number of mobile subscribers exceeded one billion and this number is growing exponentially as illustrated in Figure 1.1. In the second generation mobile network (Global System for Mobile Communication - GSM), voice traffic was dominant and technologies like GPRS (General packet radio service) and EDGE (Enhanced Data rates for GSM Evolution) allowed mobile subscribers to access data from their mobile phones (Holma – Toskala 2009).

Figure 1.1: Growth of mobile subscribers

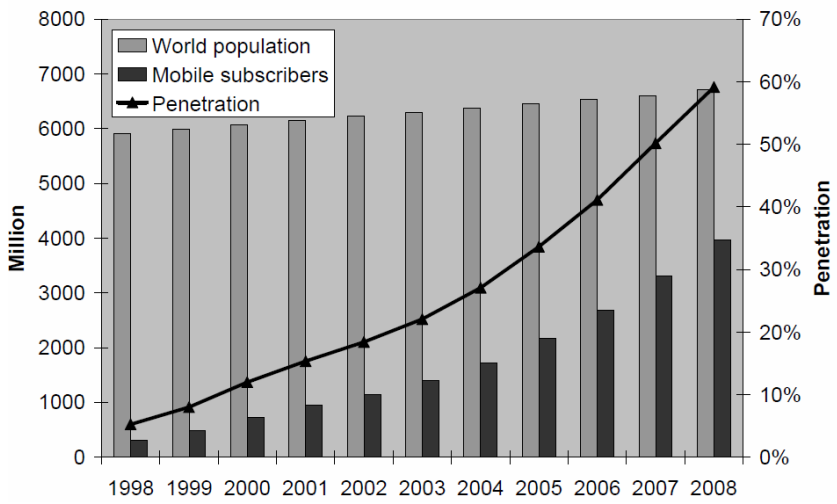

Source: Holma and Toskala, (2009)

Nevertheless, voice traffic was dominant although the data traffic has increased. Then, the third generation network was introduced with HSDPA (High Speed Downlink Packet Access) and standardized by 3GPP (Third Geneartion Partnership Project) Release 5 which is a collaboration between groups of telecommunications associations, known as the Organizational Partners. The initial scope of 3GPP was to make a globally applicable third-generation (3G) mobile phone system specification based on evolved Global System for Mobile Communications (GSM) specifications within the scope of the International Mobile Telecommunications-2000 project of the International Telecommunication Union (ITU). HSDPA allowed mobile subscribers to have data rates over 1 Mbit/s and data traffic volume exceeded voice traffic volume in many cases as shown in Figure 1.2 (Holma – Toskala 2009).

Figure 1.2: HSDPA data volume exceeds voice volume

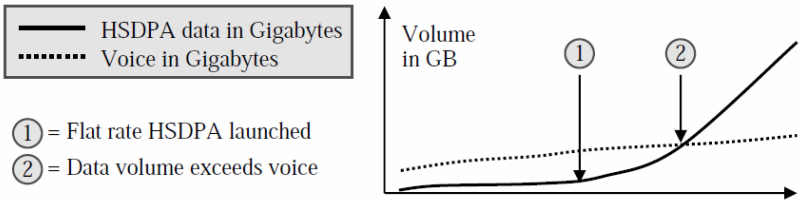

Source: Holma and Toskala, (2009)

In subsequent years, data usage became possible with various devices like laptops and smart phones. These devices are used for many purposes including internet access, video on demand, voice over IP, blogging, interactive gaming which are bandwidth hungry applications and takes 10 to 100 times more capacity compared to voice traffic. In the future, it is expected that broadband internet connection will be available almost anywhere in the world. So, there will be a need for more capacity with extensive use of wireless access to offer true broadband connectivity to the mobile subscribers.

3GPP started to work on LTE (Long Term Evolution) in 2004 which was standardized as 3GPP Release 8. The new mobile network technology is called 3.9G. Although marketed as 4G LTE, it does not meet the all requirments of 4G introduced by ITU-R (ITU - Radiocommunication Sector). 3GPP LTE Release 8 standard was finalized in December 2008 (3GPP 2012). The schedule of 3GPP standards and their commercial deployment is shown in Figure 1.3.

Figure 1.3: Schedule of 3GPP standard and their commercial deployments

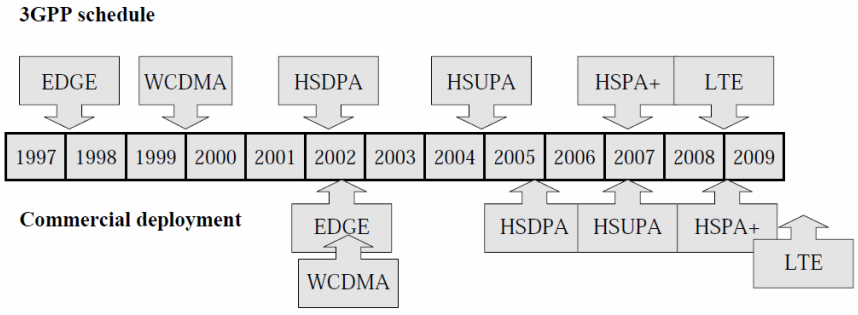

Source: Holma and Toskala, (2009)

LTE uses different multiple access schemes from the previous third generation technologies, which are, Orthogonal Frequency Division Multiple Access (OFDMA) in downlink and Single Carrier Frequency Division Multiple Access (SC-FDMA) in

uplink. Both in uplink and downlink, resource allocation takes place in the frequency domain with a resolution of 180 kHz. Also, the frequency domain packet scheduling is one of the reasons for high LTE capacity. LTE supports scalable carrier bandwidths, from 1.4 MHz to 20 MHz and supports both frequency division duplexing (FDD) and time-division duplexing (TDD).

The LTE specification with 20 MHz bandwith utilization provides downlink peak rates of 150 Mbit/s with 2x2 MIMO configuration, downlink peak rates of 300 Mbit/s with 4x4 MIMO and uplink peak rates of 75 Mbit/s. The evolution of peak data rates from second generation standards to LTE is illustrated in Figure 1.4. QoS provisions permitting a transfer latency of less than 5 ms in the radio access network. LTE has the ability to manage fast-moving mobiles and supports multi-cast and broadcast streams.

Figure 1.4: Peak data rate evolution of 3GPP technologies

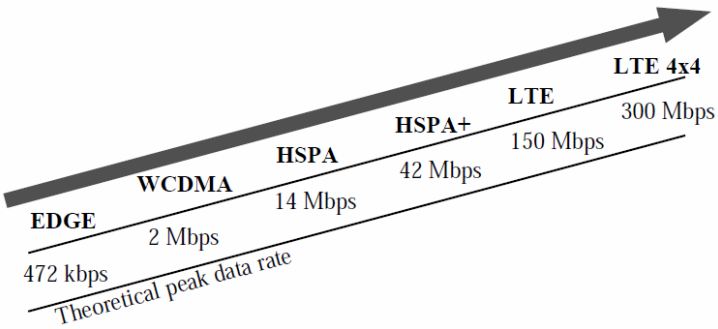

Source: Holma and Toskala, (2009)

LTE will use new frequency bands in addition to refarming coexisting frequency bands. The main frequency band to be used is 2600 MHz. Also refarming 900 MHz and 1800 MHz bands are discussed. There are 17 paired and 8 unpaired bands defined currently in 3GPP specifications that are shown in Figure 1.5 and Figure 1.6 respectively. In the USA, LTE was deployed using 700 MHz bands and also 1700/2100 Mhz bands are planned to be deployed. In Japan, LTE was deployed in the 2100 band and this band will be followed later by 800, 1500 and 1700 MHz bands (3GPP TR 36.942 2009).

In 2007, ITU-R World Radiocommunicaiton Conference (WRC-07) worked to idfentify the new spectrum also including LTE as illustrated in Figure 1.7. The goal of identifying new bands is to increase coverage with low frequency bands and capacity with high frequency bands. The main coverage band was identified between 790-862

MHz sub-band in Europe and Asia-Pacific which is currently used for terrestrial TV broadcasting (Tura and et al 2011). When analog to digital switchover is completed, this sub-band will be available for LTE. In the USA, the sub-band 698-806 MHz was identified and already auctioned for the operators. On the other hand, the capacity bands will be in 3.4-4.2 GHz for IMT in Europe and Asia-Pacific as well as 2.3-2.4 GHz band for IMT-2000 in China (Holma – Toskala 2009)..

Figure 1.5: Frequency bands for paired bands in 3GPP specifications

Operating band	3GPP name	Total spectrum	Uplink [MHz]	Downlink [MHz]
Band 1	2100	2x60 MHz	1920-1980	2110-2170
Band 2	1900	2x60 MHz	1850-1910	1930-1990
Band 3	1800	2x75 MHz	1710-1785	1805-1880
Band 4	1700/2100	2x45 MHz	1710-1755	2110-2155
Band 5	850	2x25 MHz	824-849	869-894
Band 6	800	2x10 MHz	830-840	875-885
Band 7	2600	2x70 MHz	2500-2570	2620-2690
Band 8	900	2x35 MHz	880-915	925-960
Band 9	1700	2x35 MHz	1750-1785	1845-1880
Band 10	1700/2100	2x60 MHz	1710-1770	2110-2170
Band 11	1500	2x25 MHz	1427.9-1452.9	1475.9-1500.9
Band 12	US700	2x18 MHz	698-716	728-746
Band 13	US700	2x10 MHz	777-787	746-756
Band 14	US700	2x10 MHz	788-798	758-768
Band 17	US700	2x10 MHz	704-716	734-746
Band 18	Japan800	2x30 MHz	815-830	860-875
Band 19	Japan800	2x30 MHz	830-845	875-890

Source: Holma and Toskala, (2009)

Figure 1.6: Frequency bands for unpaired bands in 3GPP specifications

Operating band	3GPP name	Total spectrum	Uplink and downlink [MHz]
Band 33	UMTS TDD1	1x20 MHz	1900-1920
Band 34	UMTS TDD2	1x15 MHz	2010-2025
Band 35	US1900 UL	1x60 MHz	1850-1910
Band 36	US1900 DL	1x60 MHz	1930-1990
Band 37	US1900	1x20 MHz	1910-1930
Band 38	2600	1x50 MHz	2570-2620
Band 39	UMTS TDD	1x40 MHz	1880-1920
Band 40	2300	1x50 MHz	2300-2400

Source: Holma and Toskala, (2009)

Figure 1.7: Main new frequencies identified for IMT in WRC-07

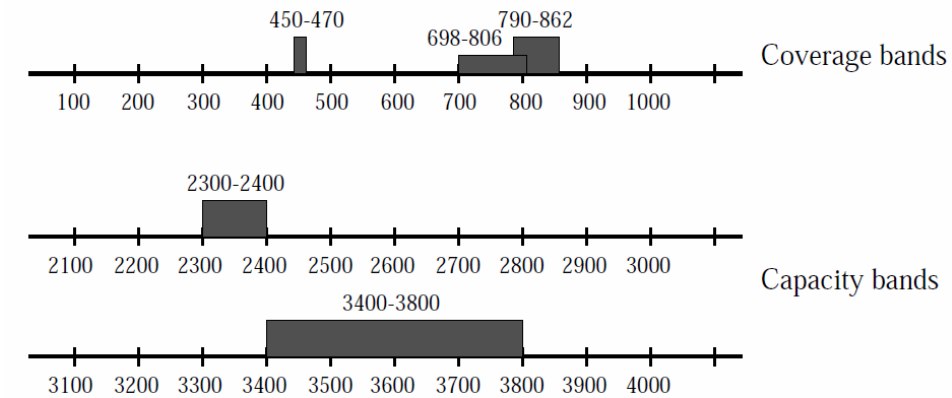

Source: Holma and Toskala, (2009)

1.1 THESIS GOAL

In this study, the performance analysis of LTE systems in terms of coverage and capacity are investigated. The system level simulator is used to create different environments (urban, rural), path loss models (e.g. COST 231 Hata model, COST 231 Walfish- Ikegami model), single and multiple antenna configurations, frequency bands, scheduling algorithms so as to simulate with very similar to real scenarios. The results are investigated in four different environments which are urban-micro, urban-macro, suburban-macro and rural-macro environments. Each environment has different characretistics such as in urban-micro environment users are pedestrian with 3 km/h speed while in rural-macro environment users are in high speed vehicles with 120 km/h. Also inter site distance, path loss models, transmitter antenna heights, powers and gains are different for each environment.

The coverage analysis is made in two main frequency bands to be used in LTE which are 800 Mhz and 2600 MHz. The results are compared according to Signal to Interference and Noise Ratio (SINR) values for different distances form the base station and the furthest distance that can be served (cell-edge).

The capacity analysis is based on average cell and cell-edge throughputs. These values are compared with utilizing various techniques such as single or multiple antenna selection, different multiple antenna modes (e.g. diverstiy, spatial multiplexing), scheduling algorithms, channel models, user speeds and frequency bands. Main idea of

capacity analyse is to show the effects of the single antenna, diversity and spatial multiplexing techniques and different scheduling algorithms on average cell throughput and cell-edge throughput in 800 MHz and 2600 MHz bands and in four different environments. In single antenna technique, there is only one data stream transmitted while in diversity and spatial multiplexing there are two data streams transmitted simultaneously. But in diversity technique both of the streams carry the same data. However, spatial multiplexing allows to transmit two distinct data streams from each antenna. Nevertheless, it does not mean that it is always possible to have higher data rates. Spatial multiplexing technique is more vulnerable to channel variations according to diversity technique and in bad channel conditions (e.g. cell-edge) diversity technique is more accurate and can give higher throughputs. But almost in all cases, spatial multiplexing performs better than single antenna technique. Also, scheduling algorithms effect the throughput since the resource allocation is based on the chosen scheduling algorithm. These algorithms are Round Robin, Proportional Fair and Best CQI. Scheduling algorithms are compared with a fairness index which indicates fairness between the users also dealing with the cell throughput. Scheduling algorithms performance changes depending on average cell throughput or cell-edge throughput is simulated. While evaluating the average cell throughput, the scheduler can perform the best, but for the cell-edge case, the results can be opposite, i.e. Best CQI scheduler allocates resource to user who has the best channel condition but in cell-edge it is almost imposible use this scheduler since the channel condition is very bad in all area. So it is very critical to choose the appropriate scheduler depending on the channel condition of the user.

2. PHYSICAL LAYER FOR LTE DOWNLINK

2.1 ORTHOGONAL FREQUENCY DIVISION MULTIPLE ACCESS (OFDMA)

2.1.1 Orthogonal Frequency Division Multiplexing (OFDM)

Orthogonal Frequency Division Multiplexing (OFDM) is a special case of frequency-division multiplexing and a digital multi-carrier modulation method which benefits from efficient use of bandwidth with orthogonality principle (Sesia and et al 2009). OFDM has been used successfully in wireline applications such as Digital Audio Broadcast (DAB), Digital Video Broadcast (DVB) and Asymmetric Digital Subscriber Line (ADSL). Also, it has been widely used in some wireless systems such as 802.11 family, WiMAX, UMB and LTE (Sesia and et al 2009). Since OFDM system is well suited for use in multipath environments, in mobile case it is possible to reach high data rates which is important in multimedia applications and video conference.

The main idea in OFDM is orthogonality of the subcarriers. OFDM has an advantage over single carrier modulation systems by subdividing the available bandwidth into many narrower frequency bands which delivers better bandwidth efficiency to transmit the information in parallel streams. OFDM signals are closely placed continuous waves in frequency domain which are represented by sinc functions shown in Figure 2.1. The trick that makes OFDM efficient is the subcarrier spacing such that the peak of a subcarrier, line up with the nulls of the adjacent subcarriers. The subcarrier spacing in OFDM is 15 kHz and the symbol time is 66.7 μs which is reciprocal of the subcarrier spacing (Sesia and et al 2009). Each subcarrier can be modulated using different levels of modulation, e.g. QPSK, QAM depending on signal quality.

OFDM is based on digital technology and it uses Discrete Fourier transform (DFT) and Inverse Discrete Fourier transform (IDFT) to transform between frequency and time domain signals. In practical implementations FFT (Fast Fourier Transform) and IFFT is used.

Figure 2.1: OFDM signal generation and the orthogonality principle

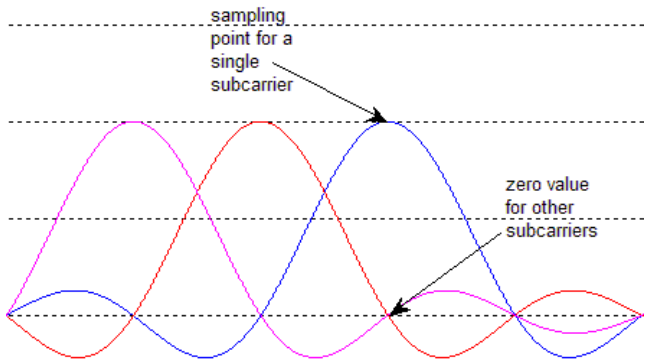

In OFDM, information carrying high rate data symbols firstly converted serial-to-parallel for modulation onto N parallel subcarriers, each of which are 15 kHz. Therefore, symbol duration T_s increases on the order of N which is significantly longer than the delay spread T_d. So, the channel impulse response remains constant during the transmission of each modulated symbol. Also this procedure has another advantage that less complex equalization procedure is required in the receiver. A Serial to Parallel (S/P) converter allocates serial data symbols to subcarriers. As additional information, it is possible to use different level modulation schemes (e.g. QPSK or 64QAM) on each subcarrier since the channel is frequency selective and the channel gain may be different between subcarriers. Thus, this results variable data rates for different subcarriers. After S/P, IFFT block converts frequency domain signal to time domain signal. In the next step, cyclic extension is added. Cyclic extension is a guard period between symbols to eliminate the Inter-symbol interference (ISI) which is caused by multipath propagation in the channel. The guard period used in OFDM is called cyclic prefix. Cyclic prefix is created by copying a part of the symbol at the end and adding it to the beginning as shown in Figure 2.2. The length of cyclic prefix is chosen such that the longest channel impulse response must be shorter than the cyclic prefix length. The cyclic prefix also ensures circular convolution which is compatible with DFT. In the last step, Parallel-to-Serial (P/S) conversion is performed to the output of the IFFT for transmission through the channel (Sesia and et al 2009).

Figure 2.2: LTE OFDM symbol and cyclic prefix lengths.

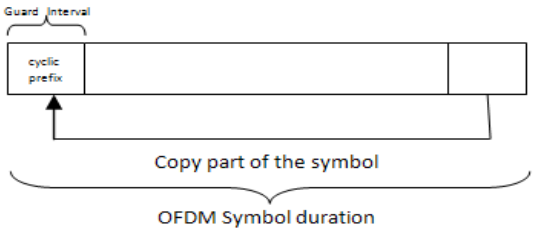

The reverse operations are implemented at the receiver for the OFDM signal demodulation. Cyclic prefix is removed in order to process with DFT only the samples which are ISI-free. After DFT process, equalization is performed. Finally, the output of the equalization is demodulated to receive the information carrying bits. A general the transmitter and the receiver of an OFDM system is shown in Figure 2.3.

Figure 2.3: OFDM transmitter and receiver

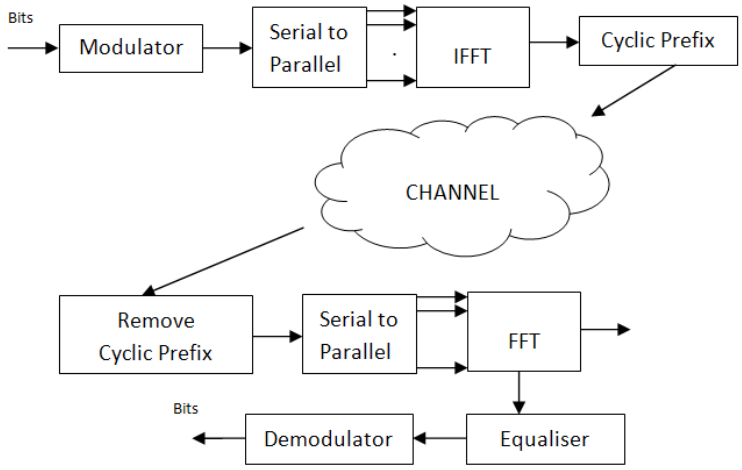

In addition to the advantages of OFDM that have been mentioned so far, there are also some disadvantages of OFDM. One of them is the high Peak-to-Average Power Ratio (PAPR) (Rumney 2008). In frequency domain, the OFDM transmission is formed of parallel subcarriers. In time domain it corresponds to multiple sinusoidal waves with very high amplitude variations. Thus, OFDM symbols in time domain leads to the Gaussian distribution. In cellular systems, power consumption is a critical issue. Power amplifiers operate linearly in a very limited range. Since OFDM signals have large envelope variation, power amplifiers need large back-off in order to stay in the linear region. But this leads to inefficient amplifier power or expensive RF transmitters. This has effect to uplink coverage range. If the output power is high, coverage range will

increase so as the battery consumption. Otherwise, it will result in shorter coverage range. This trade-off may not be important for downlink transmission since the base station (eNodeB) does not have a power consumption problem but for the user equipments (UE) it is a big challenge since they have limited battery. Because of this reason 3GPP decided to use SC-FDMA in the uplink direction which is mentioned in the next section.

Another disadvantage of the OFDM system is the sensitivity to frequency errors. The transmitter and the receiver should operate in the same frequency. If it is not maintained then the orthogonality between the subcarriers is lost and Inter-carrier interference (ICI) occurs. One of the main reasons that cause frequency error is the local oscillator reference frequencies mismatch between the transmitter and the receiver. Also, Doppler Effect which is related to relative speed between transmitter and receiver causes frequency errors (Sesia and et al 2009).

2.1.2 Orthogonal Frequency Division Multiple Access (OFDMA)

Orthogonal Frequency Division Multiple Access (OFDMA) is the multiplexing scheme for the 3GPP LTE downlink. OFDMA is an implementation of a multiuser communication which allocates subcarriers to different users to enable multiple users to be scheduled to receive data. Generally, a group of continuous subcarriers are allocated so that the overhead for indicating which user has been allocated to related subcarrier can be reduced.

OFDMA is based on multicarrier FDMA in which a set of randomly selected subcarriers assigned to each user. OFDMA also gets benefit from multiuser diversity by enabling OFDM. So, adaptive user to subcarrier assignment based on feedback information about the channel can be performed to enhance total system spectral efficiency. Resources can be partitioned in the time-frequency plane with a group of subcarriers for a specific time block which is a combination of OFDMA used with Time Division Multiple Access (TDMA). Such blocks called Resource Blocks (RB) in LTE. A Resource Block consists of 12 subcarriers. A minimum bandwidth allocation for a user is an RB. In time domain, respective allocation is 1ms. So, the resource allocation

for a user for the downlink transmission fills the 180 kHz blocks with the 1 ms resolution, as shown in Figure 2.4.

Figure 2.4: OFDMA resource allocation in LTE

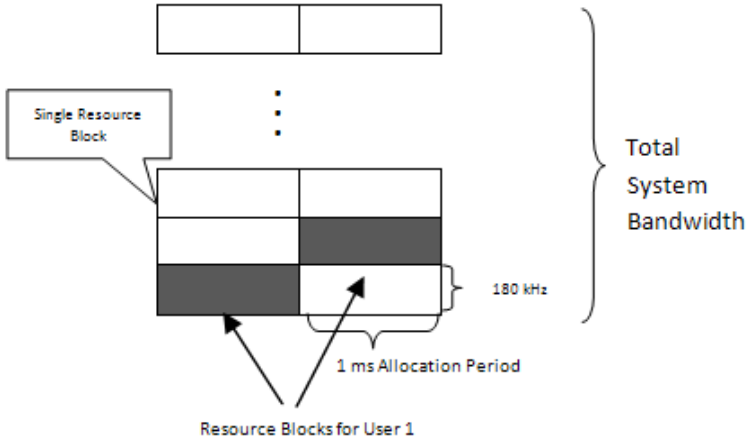

2.1.3 Single Carrier Frequency Division Multiple Access (SC-FDMA)

3GPP decided to use Single Carrier Frequency Divison Multiple Access (SC-FDMA) for LTE uplink direction (Zyren 2011). One of the main reasons of using SC-FDMA for uplink transmission is power consumption of the user equipment (UE). As mentioned previously, high PAPR results in shorter battery life for the UE. SC-FDMA and OFDMA have many common functional blocks, thus in principle, LTE downlink design is very similar to uplink design except for low PAPR. SC-FDMA signal is a representation of the single carrier by the discrete subcarriers unlike OFDM. Since the SC-FDMA subcarriers are modulated independently, it results in a lower PAPR than for OFDM. So, SC-FDMA is a combination of multipath resistance and flexible subcarrier frequency allocation characteristic of the OFDM transmission scheme with the low PAPR of a single carrier transmission scheme.

In SC-FDMA, the allocated bandwidth is divided into parallel subcarriers. Orthogonality between subcarriers is guaranteed by the use of a Cyclic Prefix (CP) as in OFDM so that Inter-Symbol Interference (ISI) can be prevented between SC-FDMA blocks. In addition to recovery of ISI, linear convolution is transformed into a circular convolution, thus performing the equalization in the receiver is just scaling each subcarrier by the channel gain.

Since only a single modulation symbol is transmitted at a time, all the transmitted subcarriers carry a component of each modulated symbol of an SC-FDMA signal in each symbol period, the modulation method dominates the waveform characteristics and the good envelope properties of the system are preserved. However, in OFDM, each subcarrier is modulated by data symbols independently. The single carrier character of SC-FDMA results in a very low PAPR than OFDM multicarrier scheme. Thus, this allows efficient use of the power amplifier and lowers the user equipment power consumption.

SC-FDMA has two types of signal generation techniques which are in the time-domain or the frequency-domain. Both techniques have equivalent functionalities but the time-domain technique is less efficient due to filtering and ramp-up and ramp-down times interrelated to filtering. In frequency-domain, signal generation can be done both in localized and distributed manners as shown in Figure 2.5. In localized transmission, a group of adjacent subcarriers are allocated to a user. In distributed transmission, equally spaced subcarriers are allocated to a user.

Figure 2.5: Localized and distributed subcarrier mapping in SC-FDMA

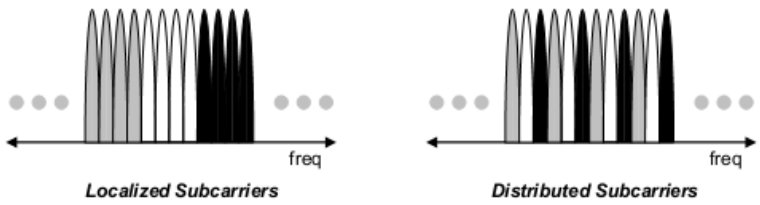

Source: Zyren, (2007)

2.1.4 LTE Downlink Physical Resource Structure

The Long Term Evolution (LTE) downlink physical layer which is elaborated in (3GPP 2012, 3GPP TS 36.211 2009, 3GPP TS 36.212 2009) aims to improve capability of radio interface between the base station and user equipment. The LTE downlink transmission resources consist of frequency, time and space dimensions. The space dimension exploits multiple spatial layers which are achieved by multiple antenna transmission and reception schemes (Section 3).

LTE supports both paired spectrum for Frequency Division Duplex, FDD and unpaired spectrum for Time Division Duplex, TDD operation for transmission. Radio frames forms the radio interface of physical resources. There are two types of radio frame structures supported: frame type 1, is applicable for FDD in paired spectrum, and frame type 2, is applicable for TDD in unpaired spectrum (Sesia and et al 2009). In this study, only frame type 1 is shown. The generic frame structure can be applied to both the downlink and uplink for FDD operation.

The following structure is used for the time-frequency resource subdivision in frame type 1: in time domain, largest unit is the radio frame which is 10 ms length. Radio frame consists of ten sub frames each has 1 ms length. The smallest unit is the slot which splits sub frame into two consecutive parts each of 0.5 ms duration. One slot is composed of a group of OFDM subcarriers along with a number of OFDM symbols. In the frequency domain, 12 OFDM subcarriers forming a group (thus occupying a 180 kHz bandwidth) in one slot time is called a Resource Block (RB). Also, each slot contains seven or six OFDM symbols depending on the cyclic prefix length (normal or extended). One subcarrier for duration of one OFDM symbol in a slot is named the Resource Element (RE) which is the smallest unit of resource. A resource block thus contains 84 resource elements when normal cyclic prefix preferred and 72 resource elements for the extended cyclic prefix. In Figure 2.6, the detailed resource structure with the assumption of a radio frame type 1 with normal cyclic prefix (i.e., seven OFDM symbols per slot) is shown.

In resource structure, some resource elements have specific tasks and they are utilized to meet the required objective. These specific purposes are: reference signals, synchronization signals, control signaling and critical broadcast system information. The remaining resource elements are utilized for data transmission.

Figure 2.6: Frame structure in LTE

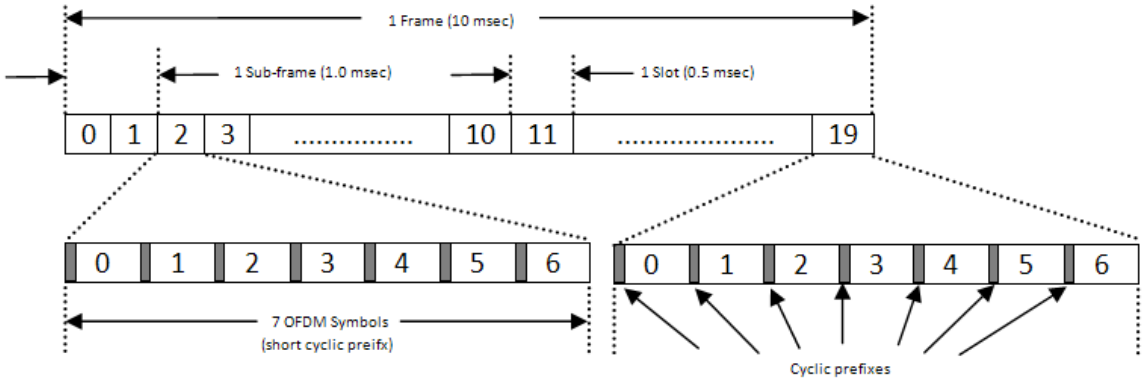

2.1.4.1 Reference signals

In LTE, downlink channel estimation is facilitated by using the special reference signals (Coleri and et al 2002). Reference signals are located in predetermined resource elements in time-frequency grid. Reference signals are transmitted in the first and third last OFDM symbols of each slot in the time domain. In the frequency domain, reference signals are located over every six subcarriers. Thus, two dimensional time-frequency interpolation may be implemented for channel estimation to obtain precise estimation of the channel frequency response within the slot time interval.

In a multi-input multi-output (MIMO) antenna scheme, user equipment should be able to estimate the channel response of each path. This can be achieved by transmitting reference signals of each antenna on different subcarriers to avoid interference with each other (Simko 2009). Also, if a resource element in one antenna is used for transmitting reference signal. Then in other antennas, that resource element is not used for data transmission. In Figure 2.7, reference signal allocation example for two antenna transmission is illustrated.

Figure 2.7: Reference signal distribution for 1 antenna and 2 antennas cases

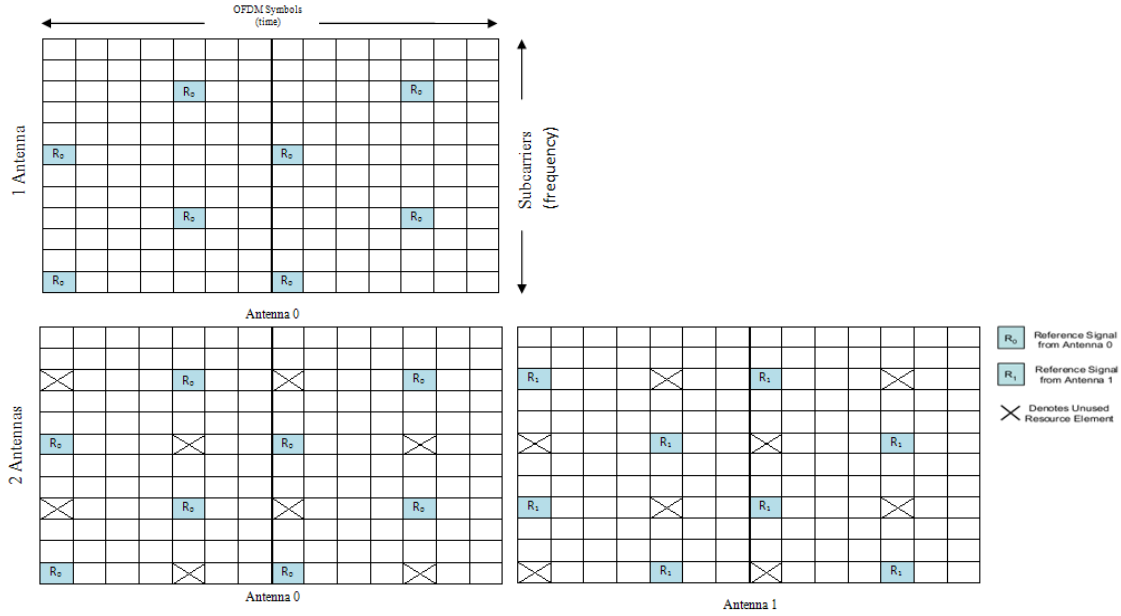

2.2 CHANNEL ESTIMATION AND REFERENCE SIGNALS FOR LTE

2.2.1 Reference Signal Design

In wireless communication systems, perfect knowledge of the channel is assumed for simplicity of calculations. But in real life, the channel is not perfect and should be estimated for equalization. Since the channel modifies the transmitted signal, the receiver should accurately estimate the channel to recover the transmitted information.

In wireless systems, channel estimation is a challenging problem. The radio channel is highly random and its characteristic of statistic changes depending on the environment (Tse - Viswanath 2004). While the transmitted signal travels to the receiver, many disruptive effects corrupts the signal and it results in degradation on the system performance. Transmitted signals arrive at receivers along multiple paths due to reflections and scattering, and this causes Inter-symbol Interference (ISI). Another disruptive effect occurs because of moving receivers, transmitters or scattering objects. This results rapidly changing channel response over time. Multipath propagation, mobility, and local scattering cause the signal to be spread in frequency, time, and angle. Selectivity of the channel is related to these spreads which have remarkable

impacts on the received signal. These statistics have direct effect on channel estimation performance (Madhow 2008).

When the channel knowledge is exploited, the detection method is said to be coherent, otherwise it is called non-coherent. Coherent detection can use the transmitted signal amplitude and phase information, but non-coherent detection can use only amplitude information. Therefore, coherent detection requires precise estimation of the channel which is valid for both downlink and uplink and also for Time Division Duplex (TDD) and Frequency Division Duplex (FDD). Coherent detection is simpler to implement in terms of algorithms compared to non-coherent detection for equivalent detection. But in coherent detection, to be able to estimate the channel requires an overhead. This overhead consists of known signals both to transmitter and receiver. These known signals do not carry data, so they cause spectral inefficiency.

In OFDM based systems there are two main categories of channel estimation: blind estimation and non-blind estimation (Ozdemir - Arslan 2007). The blind channel estimation uses received signal statistics and require a large amount of data. In fast fading channels, performance reduces heavily. However, in the non-blind channel estimation, the receiver exploits previous channel estimation information or a part of the transmitted signal for the channel estimation.

Generally, known signals in other words reference signals (or pilot signals) can be embedded into the transmitted signal in different ways. One of the ways is multiplexing the reference signals with the data symbols in either the frequency, time or code domain. In time domain, multiplexing is performed as preamble-based training in which the reference signals (RS) are transmitted at the beginning of each data. Also, reference symbols can be sent on top of unknown data without necessarily perpendicular to each other.

The OFDM transmission in LTE downlink can be described by a two-dimensional lattice in time and frequency as described in previous sections. The multiplexing of the reference signals is made possible with this structure. The reference signals are mapped

to prearranged Resource Elements (REs) of the two-dimensional lattice as shown in Figure 2.8.

In OFDM based systems, reference symbols are arranged such that they are equidistant to each other in time-frequency lattice to achieve the minimum mean squared error estimation. Also, a 'diamond shape' is optimal if a uniform reference symbol grid is used in time-frequency plane. These principles are used to arrange the symbols which take the place for the cell specific reference symbols in time-frequency plane. The reference symbol arrangement is shown in Figure 2.8.

Figure 2.8: Reference symbol arrangement in time-frequency plane

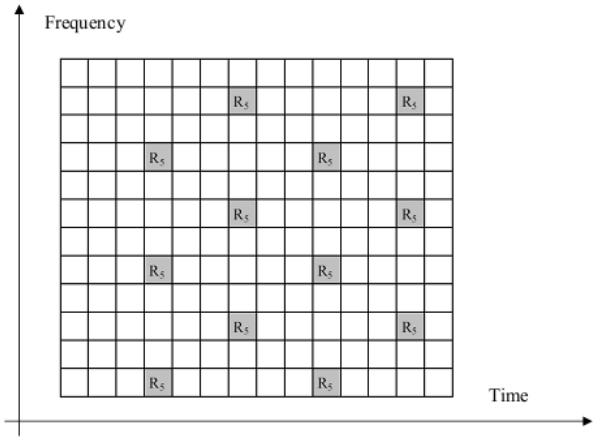

Source: Sesia, Toufik, Baker, (2009)

Since the channel estimation is performed in specified time-frequency which contains reference symbols, all correlations between channel coefficients in time and frequency should be considered to estimate the channel accurately. The channel estimation for the resource elements which do not contain reference signals are computed with the help of interpolation (Akram 2007). Two-dimensional Wiener filter interpolation is the optimal choice for channel estimation in terms of mean squared error, but since it's a complex filter, using one-dimensional filter is another choice to achieve a trade-off between accuracy and complexity.

In basic OFDM system reference symbol allocation in time-frequency plane has different options (Akram 2007). There are three such options as illustrated in Figure 2.9. In the first case, a whole OFDM symbol may be allocated as a reference symbol as

shown in Figure 2.9a. That kind of allocation is called block-type pilot subcarrier arrangement which is the most suitable for channel estimation when the channel is highly frequency-dispersive and has a low Doppler spread although it decreases data rate. In the second case, specific subcarriers might be allocated reference symbols during the whole transmission period as shown in Figure 2.9b. This choice is called comb-type pilot subcarrier arrangement which is beneficial in rather frequency selective and high Doppler channels. Furthermore, reference symbols can be allocated in distributed way in time and frequency as illustrated in Figure 2.9c. Both high frequency-selective and high Doppler channels will be worked well via this kind of allocation strategy, depends on channel properties and the time-frequency pilot spacing.

Figure 2.9: Different possibilities for pilot allocation

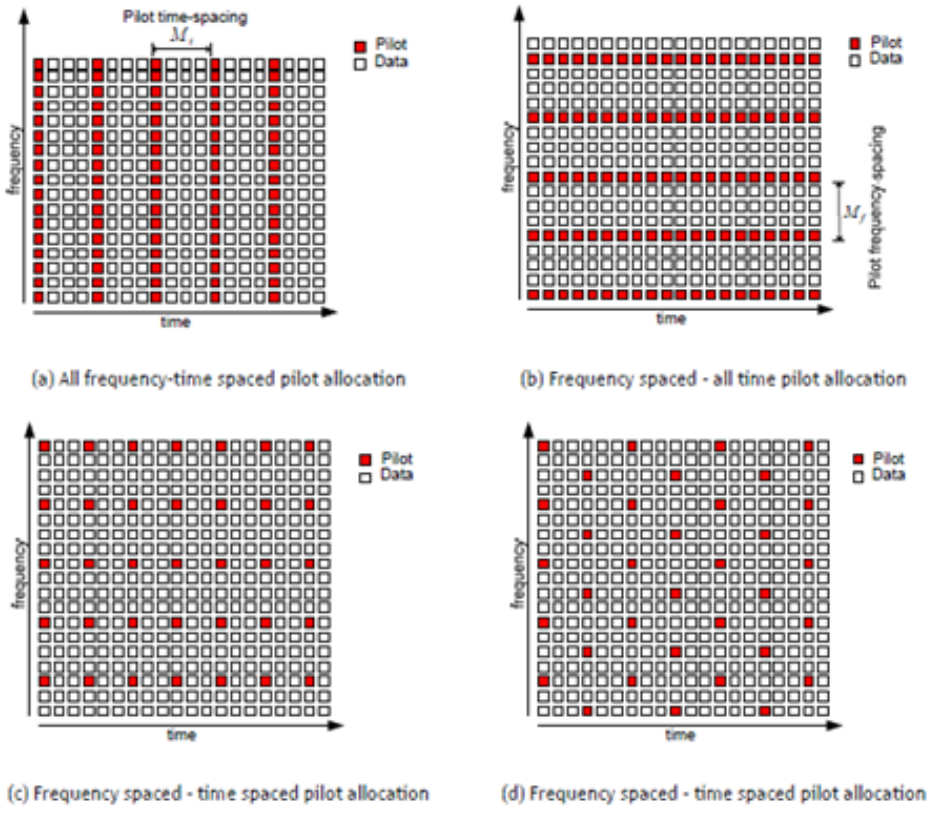

Source: Akram, (2007)

One of the advantages of LTE with respect to other mobile network technology (e.g. UMTS, GSM) is the ability to work under high-mobility (3GPP 2012). Unlike LTE, WLAN systems support pedestrian-level mobility and a preamble-based training sequence is used for channel estimation.

For the channel estimation with reference symbol, the reference symbol spacing should be decided meticulously. In frequency domain, reference symbols spacing depends on the coherence bandwidth of the channel which is related to the channel delay spread. There is one reference symbol every six subcarriers on each OFDM symbols, but these are gradually arranged within each Resource Block (RB) so that there is one reference symbol every 3 subcarriers in frequency domain. The number of subcarrier spacing between the reference symbols in frequency domain depends on the Nyquist sampling theorem that provides a prescription for the nominal sampling interval required to avoid aliasing, such that the channel variations in frequency can be all taken, which is

$$D_p \leq \frac{1}{\tau_{\max} \Delta df} \qquad \textbf{(2.1)}$$

where τ max is the maximum excess delay of channel. Reference symbol spacing in frequency should be sufficient, so as to satisfy the above to estimate the channel completely (Sakram 2009).

In time domain, spacing between the reference symbols is decided by the maximum Doppler spread to be supported. In LTE, it corresponds 500 km/h (3GPP 2012). The Doppler spread varies the channel across OFDM symbols, so the reference symbols should be inserted at some ratio to be able to track the variation of channel in time domain. This ratio is a function of coherence time and the maximum reference symbol spacing is given by,

$$D_t \leq \frac{1}{2 fd_{\max} Tf} \qquad \textbf{(2.2)}$$

where f_d max is the maximum Doppler spread and T_f is the OFDM symbol duration. For comb-type pilot arrangements, the reference symbols are inserted for every OFDM symbol and spacing between them should satisfy the Nyquist criteria (Sakram 2009).

LTE supports to work with multiple transmit antennas in downlink direction and this is detailed in Chapter 3. Reference symbol allocation for multiple antenna ports is characterized at the eNodeB. Implementation of an antenna port may be either single transmit antenna or combination of multiple antenna elements. Each antenna port is defined by the transmitted reference symbols from the point of view of the UE so that the channel estimation for the related antenna can be derived by the UE which might be a single radio channel from one physical antenna or a combined channel from a combination of multiple antenna elements those forming the antenna port.

LTE eNodeB supports up to four antennas which mean a UE should estimate up to four distinct channels (3GPP 2012). Reference symbol pattern for each antenna port must be designed carefully in order to minimize the intra-cell interference between the multiple antenna ports.

Figure 2.10: Reference symbol allocation for four antenna ports

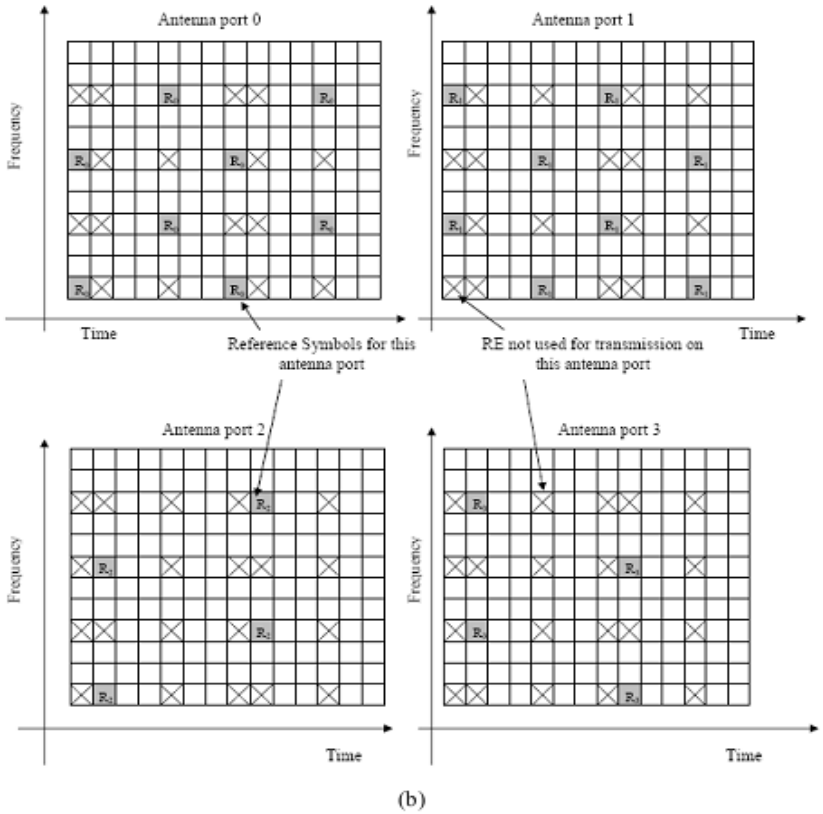

Source: Sesia, Toufik, Baker, (2009)

Reference symbol allocation for four antenna ports is illustrated in Figure 2.10 where R_p is the reference symbol on antenna port p. When a reference symbol is transmitted on one antenna port, on the other antennas, the corresponding resource element is not used to limit the interference. Furthermore, on the third and fourth antenna ports, reference symbol density is half of the first to minimize the spectral inefficiency. Also, Peak-to-Average Power Ratio is considered so that only QPSK modulation is used for all the reference symbols (Sesia and et al 2009).

2.2.2 Channel Models

Physical propagation characteristics determine the channel model which directly affects the channel estimation. These characteristics are carrier frequency, relative speed between the transmitter and the receiver (Doppler speed), transmission bandwidth, number of transmit and receive antennas and cell configuration (Yang 2010). While scattering nature of the channel is related to the carrier frequency and system bandwidth; delay spread, multipath and spatial correlation is governed by the cell deployment; and the time-varying properties of the channel is set by the relative speed between eNodeB and UE receivers (Sesia and et al 2009).

The channel correlation function which is in a three dimensional space including time, frequency and spatial domains, is featured by the propagation conditions. Generally, spatial scattering conditions depending on each MIMO (Multiple-Input Multiple Output) multipath channel component can be different but related which leads to a full three-dimensional correlation function between the domains. But it is assumed that each spatial channel experience the same scattering conditions for simplicity. So, it is possible to apart spatial correlation from the frequency and time domain correlations. A channel model and its corresponding correlation properties are derived which are then used for channel estimation techniques (Sakram 2009).

In mobile communication, a commonly used channel model for the multipath channel is the Wide-Sense Stationary Uncorrelated Scattering (WSSUS) channel. A more general exposition of WSSUS models is given in (Proakis 2001). Beside the channel delays and Doppler spread which produce time and frequency correlation, the spatial scattering induces spatial correlation. In LTE, Kronecker model is used as a spatial correlation

model to evaluate the performance (Sesia and et al 2009). Kronecker model is commonly used for the theoretical analysis of MIMO systems but to obtain verifiable results it is limited up to two or three antennas at both eNodeB and UE.

In a narrowband MIMO channel system with N_{TX} transmitting antennas and N_{RX} receiving antennas, the narrowband N_{RX} x N_{TX} channel matrix is

$$\mathrm{H} = \begin{pmatrix} h_{0,0} & \cdots & h_{0,N_{TX}-1} \\ \vdots & \ddots & \vdots \\ h_{N_{RX}-1,N_{TX}-1} & \cdots & h_{N_{RX}-1,N_{TX}-1} \end{pmatrix} \quad \textbf{(2.3)}$$

where each component $h_{n,m}$ suits the narrowband OFDM systems as they can be seen as the complex channel coefficient of each spatial link at a given subcarrier index. The correlation matrix can be identified by taking expectation of the H matrix with its transpose as

$$C_S = E[\mathrm{vec}(H)\ \mathrm{vec}(H)^H] \quad \textbf{(2.4)}$$

where $\{.\}^H$ is the Hermitian operation. The result of (2.4) is the full correlation matrix of the MIMO channel.

In the Kronecker model, separate spatial correlations at the transmitter and receiver give the full correlation. So it is possible to write the full correlation matrix in terms of the transmitter and receiver correlation matrices with the Kronecker product ($\otimes$). For instance, for the case of a 2 x 2 MIMO channel, the MIMO correlation matrix is expressed as (Pagès 2009)

$$C_S = C_{TX} \otimes C_{RX} = \begin{bmatrix} 1 & \beta & \alpha & \alpha\beta \\ \beta^* & 1 & \alpha\beta^* & \alpha \\ \alpha^* & \alpha^*\beta & 1 & \beta \\ \alpha\beta & \alpha^* & \beta^* & 1 \end{bmatrix} \quad \textbf{(2.5)}$$

where $C_{TX} = \begin{bmatrix} 1 & \alpha \\ \alpha^* & 1 \end{bmatrix}$ and $C_{RX} = \begin{bmatrix} 1 & \beta \\ \beta^* & 1 \end{bmatrix}$.

2.2.3 Channel Estimation Methods

In OFDM systems, channel estimation should be applied in time-frequency domain. Therefore, it is possible to perform two dimensional methods to estimate the channel from resource elements containing reference symbols (pilot tones). However, two dimensional estimators have high computational complexity, so only in time or frequency domain estimation can be applied to reduce the complexity. One dimensional estimation has two steps. Firstly, the channel estimation is applied in time (or frequency) domain then the channel estimation is applied in frequency (or time) domain.

Channel estimation for OFDM systems can be classified into two types (Coleri and et al 2002):

i. Block Type Channel Estimation
ii. Comb-Type Channel Estimation

Let $\bar{X}=[X_0 X_1 \ldots X_{N_c-1}]^T$ and $\bar{Y}=[Y_{0,i} Y_{1,i} \ldots Y_{N_c-1}]^T$ indicate the input data of IDFT block at the transmitter and the output data of DFT block at the receiver, respectively.
Let $\bar{h}=[h_0 h_1 \ldots h_{N_c-1}]^T$ and $\bar{n}=[n_0 n_1 \ldots n_{N_c-1}]^T$ indicate the sampled channel impulse response and AWGN, respectively. Define the input matrix $\underline{X}$ = diag ($\bar{X}$) and the DFT-matrix,

$$\underline{F} = \begin{pmatrix} W_N^{00} & \cdots & W_N^{0(N-1)} \\ \vdots & \ddots & \vdots \\ W_N^{(N-1)0} & \cdots & W_N^{(N-1)(N-1)} \end{pmatrix} \quad \textbf{(2.6)}$$

where $W_N^{i,k} = \left(1/\sqrt{N}\right)^{-j2\pi(ik/N)}$. Also after DFT operation $\bar{\mathrm{H}} = \mathrm{DFT_N}(\bar{h}) = \underline{F}\ \bar{h}$ and $\bar{\mathrm{N}} = \underline{F}\ \bar{\mathrm{n}}$. Thus in an OFDM system, a transmission of data over a set of parallel channels can be explained as,

$$\bar{\mathrm{Y}} = DFT_N(IDFT_N(\bar{X}) \otimes \bar{h} + \bar{\mathrm{n}}) = \underline{X}\underline{F}\bar{h} + \bar{N} = \underline{X}\bar{H} + \bar{N} \quad \textbf{(2.7)}$$

The OFDM system with fading channel can be considered as a two-dimensional lattice in time and frequency as described in previous sections. It is sampled at reference symbol containing resource elements and interpolation is applied to find the channel response between two reference symbols positions. The main criterion in channel estimation design is to find optimal solution with a trade-off between complexity and performance.

In Figure 2.11, two types of channel estimation are shown. The first channel estimation method is the block-type which is on the left figure. This type of channel estimator is useful in slow fading channel and all sub-carriers of OFDM symbols are inserted with reference symbols within a particular period. The other one is the comb-type channel estimation which is designed to perform when the channel changes so fast even between adjacent OFDM blocks. In this case, specific sub-carriers are reserved for reference symbol insertion and the spacing between two subsequent sub-carriers is decided by the coherence time of the channel (Shen – Martinez 2006).

Figure 2.11: Block-type and comb-type channel estimation

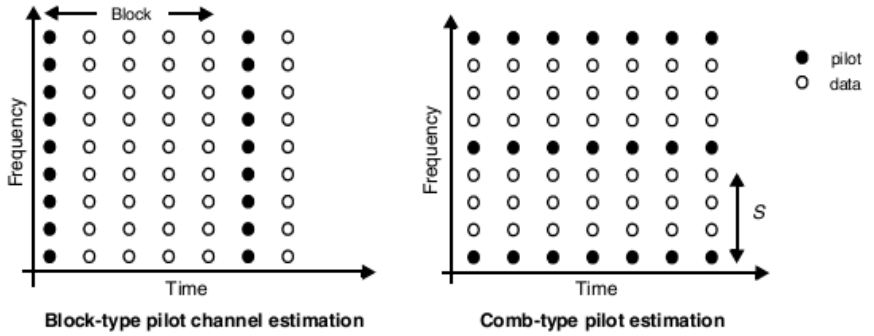

Source: Coleri, Ergen, Puri, Bahai, (2002)

2.2.3.1 Block-type channel estimation

In block-type pilot based channel estimation, all subcarriers are allocated with reference symbols and these symbols are transmitted periodically as shown in Figure 2.11. The task is to determine the channel statistics from the known transmitted reference symbol and received signals.

The estimated channel is used by the receiver to decode the data block. The estimated channel is valid until the next channel estimation. The estimation of the channel statistics can be based on least square (LS), minimum mean-square error (MMSE) or modified MMSE (Sesia and et al 2009).

2.2.3.1.1 Least square estimator

The least square (LS) channel estimator for subcarriers on reference symbols can be found by minimizing the parameter $(\bar{Y} - \underline{\underline{X}}\bar{H})^{H}(\bar{Y} - \underline{\underline{X}}\bar{H})$, where $(.)^{H}$ is the conjugate transpose operation (Sakram 2007). The LS estimator of $\bar{H}$ is given by

$$\hat{H}^{LS} = \underline{\underline{X}}_{p}^{-1}\bar{Y}_{p} = \left[Y_{p} / X_{p} \right] \qquad \textbf{(2.8)}$$

where p denotes the reference symbol positions. LS estimator is a low complexity channel estimator. However, it does not exploit the statistics of the channel, so it suffers from a high mean-square error.

2.2.3.1.2 Minimum mean-square error (MMSE) estimator

The Minimum mean-square error (MMSE) requires the second order statistics of the channel and the noise. It performs better than the LS estimator in terms of mean square error but it requires higher computational complexity (Sakram 2007).

The MMSE channel estimate can be obtained by filtering the LS estimate. The auto covariance matrices of $\bar{h}$, $\bar{H}$ and $\bar{Y}$ are denoted by $\underline{R}_{hh}$, $\underline{R}_{HH}$, $\underline{R}_{YY}$, respectively. Also, $\underline{R}_{hY}$ is the cross covariance matrix between $\bar{h}$ and $\bar{Y}$. The variance of the noise is denoted by σ_N^2. Assuming the time domain channel vector $\bar{\mathrm{h}}$ is Gaussian and uncorrelated with the noise $\bar{N}$, then $\underline{R}_{HH}$, $\underline{R}_{hY}$ and $\underline{R}_{YY}$ are derived as

$$\underline{R}_{HH} = E\left\{\bar{H}\bar{H}^H\right\} = E\left\{\left(\underline{F}\bar{h}\right)\left(\underline{F}\bar{h}\right)^H\right\} = \underline{F}\underline{R}_{hh}\underline{F}^H \qquad \textbf{(2.9)}$$

$$\underline{R}_{hY} = E\left\{\bar{h}\bar{Y}^H\right\} = E\left\{\bar{h}\left(\underline{X}\underline{F}\bar{h} + \bar{N}\right)^H\right\} = \underline{R}_{hh}\underline{F}^H\underline{X}^H \qquad \textbf{(2.10)}$$

$$\underline{R}_{YY} = E\left\{\bar{Y}\bar{Y}^H\right\} = \underline{X}\underline{F}\underline{R}_{hh}\underline{F}^H\underline{X}^H + \sigma_N^2\underline{I}_N \qquad \textbf{(2.11)}$$

The time domain MMSE estimate of $\bar{h}$, assuming $\underline{R}_{HH}$ and σ_N^2 are known at the receiver is given by $\hat{h}_{MMSE} = \underline{R}_{hY}\underline{R}_{YY}^{-1}\bar{Y}$. Thus, the frequency domain MMSE estimate can be written as

$$\hat{H}_{MMSE} = \underline{F}\hat{h}_{MMSE} = \underline{F}\left[\left(\underline{F}^{H}\underline{X}^{H}\right)^{-1}\underline{R}_{hh}{}^{-1}\sigma_N^2 + \underline{X}\underline{F}\right]^{-1}\bar{Y} \quad \textbf{(2.12)}$$

$$= \underline{R}_{HH}\left[\underline{R}_{HH} + \sigma_N^2\left(\underline{X}\underline{X}^{H}\right)^{-1}\right]^{-1}\hat{H}^{LS} \quad \textbf{(2.13)}$$

The MMSE estimate is therefore obtained by filtering the LS channel estimate with the matrix $\underline{R}_{HH}\left[\underline{R}_{HH} + \sigma_N^2\left(\underline{X}\underline{X}^{H}\right)^{-1}\right]^{-1}$. The MMSE estimator is better than LS estimator in terms of performance especially under the low SNR conditions; however the implementation of the MMSE estimator requires the inversion of a large matrix, so it has a high computational complexity (Simko 2009).

2.2.3.1.3 Modified MMSE estimator

The Minimum mean-square error (MMSE) estimate performs better than the LS estimate for channel estimation. But, the major drawback of the MMSE estimate is its high computational complexity, depending on the observation samples. Modified MMSE estimators are studied widely which have low rank approximation and use the frequency correlation of the channel. The main idea to reduce the complexity for the MMSE estimator is using the singular-value decomposition (SVD). There are some other simplification techniques which are used to derive modified MMSE estimator. The first simplification is averaging over the transmitted data in equation (2.13), i.e. replacing the term $\left(\underline{X}\underline{X}^{H}\right)^{-1}$ with its expectation $E\left\{\left(\underline{X}\underline{X}^{H}\right)^{-1}\right\}$ (Sakram 2007). Also, assuming the same signal constellation on all symbols and equal probability on all constellation points, it is derived that

$$E\left\{\left(\underline{X}\underline{X}^{H}\right)^{-1}\right\} = E\left\{\left|1/X_k\right|^2\right\}\underline{I} \quad \textbf{(2.14)}$$

where $\underline{I}$ is the identity matrix. Defining the average signal-to-noise ratio (SNR) as $\overline{\text{SNR}} = E\left\{|X_k|^2\right\}/\sigma_N^2$ and the term $\beta = E\left\{|X_k|^2\right\} / E\left\{|1/X_k|^2\right\}$ which is a constant depending on the signal constellation, then the simplified estimator can be obtained as

$$\hat{H}_{M-MMSE} = \underline{R}_{HH}\left[\underline{R}_{HH} + \frac{\beta}{SNR} I\right]^{-1} \hat{H}^{LS} \qquad \textbf{(2.15)}$$

The second simplification is considering the channel taps in terms of energy they contain. Thus, the channel taps with significant energy is used which is the upper left corner of the auto covariance matrix $\underline{R}_{hh}$ (Simko 2009).

The third simplification uses the singular-value decomposition (SVD) which is obtained by exclusion of base vectors corresponding to the smallest values (Goldsmith 2005). The SVD of the channel correlation matrix is denoted as

$$\underline{R}_{HH} = \underline{U}\,\underline{\Lambda}\,\underline{U}^H \qquad \textbf{(2.16)}$$

Where $\underline{U}$ is a unitary matrix containing the singular vectors and $\underline{\Lambda}$ is a diagonal matrix containing the singular values on its diagonal (Goldsmith 2005). Thus, the estimator can be written

$$\hat{H}_{M-MMSE} = \underline{U}\,\underline{\Delta}\,\underline{U}^H \hat{H}^{LS} \qquad \textbf{(2.17)}$$

where $\underline{\Delta}$ is a diagonal matrix containing the values

$$f_k = \frac{\lambda_k}{\lambda_k + \dfrac{\beta}{SNR}}, \quad \text{k=0,1,……,p-1} \qquad \textbf{(2.18)}$$

on its diagonal. The best rank-p approximation of the estimator becomes

$$\hat{H}_{M-MMSE} = \underline{U}\begin{pmatrix} \underline{\Delta}_p & 0 \\ 0 & 0 \end{pmatrix}\underline{U}^H \hat{H}^{LS} \quad \textbf{(2.19)}$$

where $\underline{\Delta}_p$ is the upper left *p*x*p* corner of $\underline{\Delta}$.

The computational complexity decreases with smaller *p*. However, the approximation error increases simultaneously. Also it is expected *p* to be in the cyclic prefix samples range.

2.2.3.2 Comb-type channel estimation

In the fast fading channels, block type channel estimation is not suitable since the estimated channel parameters are completely lost even after one symbol duration (Simko 2009). Comb-type pilot based channel estimation is used for the fast fading channels where reference symbols K_p are uniformly inserted into $\underline{X}$ (Coleri and et al 2001). That is, the total N subcarriers are divided into K_p groups, each apart from each other as N/K_p.

Reference symbol locations $\overline{P}$, input values $\overline{X}_p$ and the received signals $\overline{Y}_p$ are known by the receiver. Thus, the estimation of reference symbols based on LS estimation at pilot subcarriers are given by

$$\hat{H}_k^{LS} = \left[\, \underline{X}_k^{-1}\overline{Y}_k \,\right]^T, \quad (k=0,\ldots\ldots,Kp\text{-}1) \quad \textbf{(2.20)}$$

Once the LS estimate at pilot subcarriers obtained, then the channel conditions at the data subcarriers can be estimated by interpolation (Sakram 2007).

There are different types of one dimensional interpolation schemes such as; linear interpolation, low-pass interpolation, spline-cubic interpolation, second-order interpolation and time domain interpolation (Simko 2009).

Interpolation in the frequency domain for comb-type pilot structure is mandatory to obtain the channel frequency response (CFR) at data subcarriers. Piecewise-linear and piecewise-constant interpolation are together the simplest methods. Higher-order interpolation such as piecewise second-order, low-pass and spline-cubic methods yield better channel interpolation (Sakram 2007).

2.2.3.2.1 Linear interpolation

The linear interpolation performs better than the piecewise-constant interpolation. The channel estimation at the data subcarrier between two pilots $\hat{H}_{LS}^{k}(k)$ and $\hat{H}_{LS}^{k}(k+1)$, by using linear interpolation channel estimate of data subcarriers are given by

$$\hat{H}_{LS}^{k} = \left[Y_k / X_k \right]^T, \quad (\text{k}=0,\ldots\ldots,Kp\text{-}1) \qquad \textbf{(2.21)}$$

2.2.3.2.2 Low-pass interpolation

In the low-pass interpolation method, firstly, zeros are inserted into the original $\hat{H}_{LS}^{k}$ sequence and a low pass finite-length impulse response (FIR) filter is applied so that the original data passes from the filter without any changing. This method also interpolates between the interpolated points and their ideal values such that the mean-square error is minimized.

2.2.3.2.3 Spline-cubic interpolation

The spline-cubic interpolation is based on producing a smooth and continuous polynomial fitted to given data.

2.2.3.2.4 Time domain interpolation

The time interpolation is a high-resolution interpolation which is based on zero-padding and DFT-IDFT. When the channel estimation $\hat{H}_{LS}^{k}$ is obtained, then it is transformed to time domain by IDFT. The time domain estimated sequence is interpolated to *N* points with piecewise-constant method. Finally, the interpolated time domain estimated sequence is converted to the frequency domain via DFT.

2.2.3.3 Channel estimators for MIMO-OFDM systems

Multiple transmit and receive antennas in OFDM systems increase the capacity and improve the quality of the communication. In the OFDM systems with multiple transmit antennas (N_t) and receive antennas (M_r), the LS channel estimation for MIMO-OFDM system between n^{th} transmitter and m^{th} receiver antenna is (Bagadi – Das 2010)

$$\hat{H}_{LS}^{(n,m)} = \bar{Y}^{(m)} / \underline{X}^{(n)} \tag{2.22}$$

And similarly MMSE channel estimation for MIMO-OFDM system between n^{th} transmitter and m^{th} receiver antenna is (Bagadi – Das 2010)

$$\hat{H}_{MMSE}^{(n,m)} = \underline{\underline{F}}\underline{\underline{R}}_{hY}\underline{R}_{YY}^{-1}\bar{Y}^{(m)} \tag{2.23}$$

where

$$\underline{R}_{hY} = \underline{R}_{hh}^{(m,n)}\underline{F}^{H}(\underline{X}^{(n)})^{H} \tag{2.24}$$

$$\underline{R}_{YY} = \underline{X}^{(n)}\underline{\underline{F}}\underline{\underline{R}}_{hh}^{(n,m)}\underline{F}^{H}(\underline{X}^{(n)})^{H} + \sigma_N^2\underline{I}_N \tag{2.25}$$

$X^{(n)}$ is an *NxN* diagonal matrix whose diagonal elements are the reference symbols of each n^{th} transmitter antenna and $Y^{(m)}$ is *N* length received vector at receiver antenna m.

2.3 LINK ADAPTATION AND CHANNEL CODING IN LTE

In LTE, the UE can be configured to measure and report the instantaneous channel quality from the downlink received signal, typically by measuring the downlink reference signals. The measurement of the channel quality is then fed back to the eNodeB by means of channel quality indicators (CQIs), thus, the eNodeB selects the appropriate modulation and coding scheme (MCS) for the downlink transmission. The UE does not report exact SINR, but the reported CQI consists the highest order MCS such that the UE can decode the received signal with a block error rate probability less than or equal to 10% (Furht - Ahson 2009). Therefore, the received channel quality as well as the characteristics of the UE receiver is also considered by the eNodeB. Hence, a UE with advanced signal processing capability can feedback better channel quality information, so the eNodeB selects higher MCS. Thus, in the downlink direction, the UE can receive data with a higher rate.

2.3.1 Adaptive Modulation and Coding

In LTE, different order quadrature amplitude modulations (QAM), ranging from binary phase key shifting (BPSK) to 64 QAM can be used (3GPP TS 36.211 2009). When the channel conditions are good, higher data rates can be achieved with the possibility of using higher order modulations, but this decreases robustness. The aim of adaptive modulation is to keep the bit error rate (BER) small while improving data throughput without exceeding a predetermined level. The instantaneous channel quality, i.e. the CQI value is used for the transmitted signal to achieve the target BER. The term ‘Adaptive Modulation and Coding (AMC)’ refers to the fact that the coding scheme may be modified according to the instantaneous channel conditions for each user (3GPP TS 36.211 2009). It is possible to change both modulation and coding scheme in both time and frequency domains, thus the transmitter can adapt the signal to the varying channel conditions. The transmission reliability can be increased using redundancy which is determined by the coding scheme and added to the transmitted data. The

effective coding rate R depends on the length of the redundancy between the original data and the coded data length. There is a trade-off between the link quality and the amount of redundancy. If the link quality condition is good, then a high-order modulation scheme can be preferred (more bits per symbol) as well as a low coding rate (less redundancy). However, under poor link conditions, a lower order modulation schemes must be used together with higher coding rates in order to maintain the requested QoS (Quality of Service) level. A predefined set of modulation and coding schemes (MCSs) are defined in LTE specifications corresponding to each CQI level (3GPP 36.213).

2.3.2 CQI Reporting in LTE

The CQI signaling brings an overhead in the uplink. So an efficient CQI design has a trade-off between the link adaptation performance and uplink signaling overhead. An appropriate choice for CQI value can be decided by Block Error Rate (BLER) threshold, as shown in Figure 2.12 by an example.

The MCS selection for a UE is based on the CQI value that ensures BLER$\leq 10^{-1}$ which is decided by the measured signal quality in the receiver. In Table 2.1, the list of all modulation schemes and code rates for different CQI indexes are shown which are defined according to 3GPP technical specifications (3GPP 36.213).

The eNodeB makes use of the fed back CQI values indicating the downlink channel quality by the UE for the selection of modulation and coding scheme, the time and frequency selective scheduling, interference management and the transmission power control for physical channels.

The CQI value fed back for each UE can be used by allocating the time and frequency resources which is under the control of the eNodeB.

Figure 2.12: Reference BLER and throughput curves for the 15 MCSs

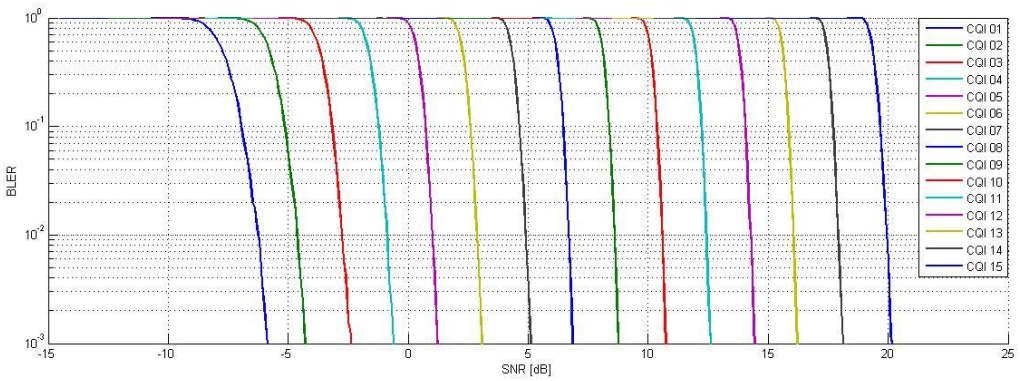

Table 2.1: Modulation and coding schemes for each CQI value

CQI index	Modulation	Approximate code rate	Efficiency (information bits per symbol)
0	No transmission	—	—
1	QPSK	0.076	0.1523
2	QPSK	0.12	0.2344
3	QPSK	0.19	0.3770
4	QPSK	0.3	0.6016
5	QPSK	0.44	0.8770
6	QPSK	0.59	1.1758
7	16QAM	0.37	1.4766
8	16QAM	0.48	1.9141
9	16QAM	0.6	2.4063
10	64QAM	0.45	2.7305
11	64QAM	0.55	3.3223
12	64QAM	0.65	3.9023
13	64QAM	0.75	4.5234
14	64QAM	0.85	5.1152
15	64QAM	0.93	5.5547

Source: Sesia, Toufik, Baker, (2009)

In time domain, the more CQI reporting density, the more accurate matching to channel and interference variations. Also in the frequency domain, the resolution of the CQI reports is utilized by means of frequency domain scheduling. However, the amount of CQI information in both domains leads to feedback overhead in the uplink.

2.3.3 Channel Coding in LTE

In digital communication, channel coding has been widely used to improve performance and reliability in the transmission. In a wireless channel, redundant information needs to be added to information bits to detect and correct some of the errors due to the effects of channel impairments, such as multipath fading, selective frequency fading and multiple access interference. The purpose of channel coding is that, reducing energy per bit over

noise for a given probability of error or vice versa. Convolutional coding and Viterbi decoding are suitable when the signal is corrupted by Additive White Gaussian Noise (AWGN). In wireless communication, convolutional coding is not the best technique. There are more advanced and appropriate channel coding technologies which are turbo coding and Low Parity Check (LDPC) codes (Sesia and et al 2009).

2.3.4 Interleaver

The interleaver is used to rearrange its own input bits or symbols such that consecutive bits or symbols are spaced far apart at its own output. The interleaver is widely used in communication after error correct coding and signal mapping to overcome correlated channel noise such as fading or burst error. The de-interleaver arranges the bits or symbol back into the original sequence at the receiver end as shown in Figure 2.13 (Goldsmith 2005).

Therefore, the interleaver process makes the correlated noise introduced in the channel statistically independent in order to enable the decoder to estimate the received bits or symbols effectively as shown in Figure 2.14.

There are two types of interleavers; block type and random type (Goldsmith 2005). In the block type interleaver, the data bits or symbols are written as one row and read out one column at a time. The inverse of this process is performed by the de-interleaver. In the random type interleaver, the input bits or symbols are mapped to the output positions randomly according to the permutation order with using a fixed random permutation. The random interleaver is simple to implement and has improved BER performance than the block interleaver.

Figure 2.13: The Interleaving and the de-interleaving process

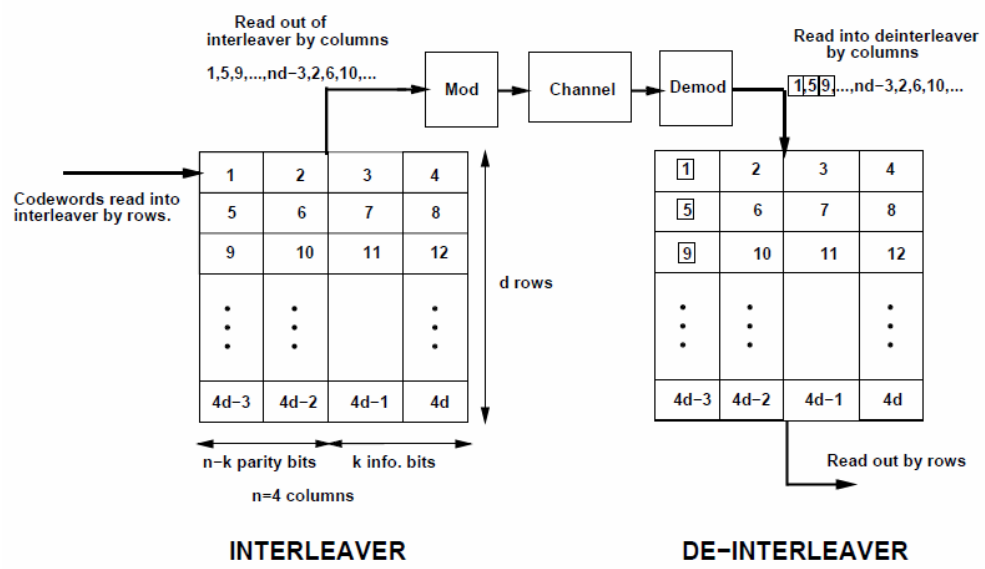

Source: Goldsmith, 2005

Figure 2.14: Schematic representation of coding and interleaving the information

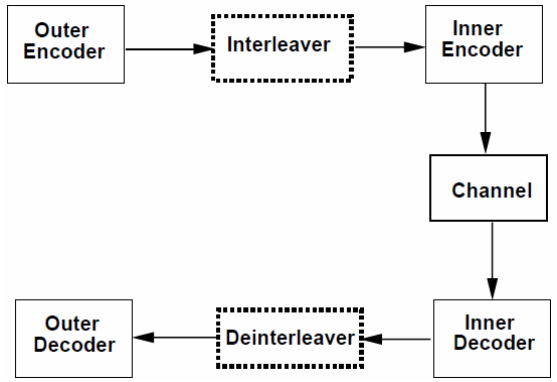

Source: Goldsmith, 2005

In LTE, a quadratic polynomial permutation (QPP) interleaver is used to reduce the complexity in turbo coder (3GPP TS 36.212 2009). A QPP interleaver for an information block size K can be defined by the following polynomial.

$$\Pi(\mathrm{i})=(f_1 i+f_2 i^2)\bmod K \qquad \textbf{(2.26)}$$

where $\Pi(\mathrm{i})$ is the bit index before interleaving, i is the output index, and f_1 and f_2 are the permutation coefficients. These coefficients are related to the factorization of K where f_1 is relative prime to block size K and all prime factors of K also factor f_2. The QPP

interleaver holds the maximum contention-free property which is a great advantage from a hardware implementation perspective and provides maximum flexibility in supported parallelism i.e. any *M* that factors *K* is a supported parallelism. For example, for a QPP interleaver with *K*=2048, any supported parallelism factor $M=2^x$, $0<x\leq11$, is a valid choice for *M*. In practice very large values for *M* is impractical.

2.3.5 HARQ

The physical layer in LTE supports Hybrid Automatic repeat Request (HARQ) which is a combination of ARQ and error correcting codes (Furht - Ahson 2009). HARQ is performed by both the MAC layer and the physical layer while ARQ is performed only by the MAC layer.

In ARQ, if an error is detected in a packet, the incorrect packet is canceled then a retransmission is requested (Goldsmith 2005). But the previous error detected packet is thrown away when the retransmission is preformed. So the useful information is also thrown away with that packet. However in HARQ, if an error is detected in a packet by the MAC layer (i.e., Cyclic Redundancy Check (CRC) fails), a NAK is sent to request retransmission and the newly retransmitted packet is combined with the original packet in the physical layer to enhance the accuracy of Forward error correction (FEC) decoding. If the combined packet passes CRC, an ACK is sent to the transmitter and the HARQ process ends. If the combined packet still contains error, then a NAK is sent to the transmitter to request another retransmission of the packet for HARQ usage.

HARQ requires higher computational complexity in its implementation then a traditional ARQ, but it gives a better performance than ARQ techniques.

Typically, there are two types of HARQ retransmission strategies; chase combining and incremental redundancy (Holma – Toskala 2009). In chase combining or type I HARQ, each retransmission is identical to the original transmission. In other words, the retransmitted packets have the same FEC decoding scheme as in the original packet. For instance, if the original packet bits are coded using a rate ¾ convolutional code, then any retransmission of the same packet should also use the same rate, i.e., ¾ convolutional code. In chase combining, once the original transport block is received,

CRC (Goldsmith 2005) is performed to check if there is an error in the packet with comparing it with the original CRC sequence. After CRC comparison, if an error or errors are detected in the packet, then a retransmission is requested by the receiver which is answered by the transmitter by sending the same transport block. Meanwhile, the original erroneous transport block is kept at the receiver so that it can be combined with the retransmitted transport block to yield more successful decoding probability. An example process for the chase combining is depicted in Figure 2.15.

Figure 2.15: Chase combining technique

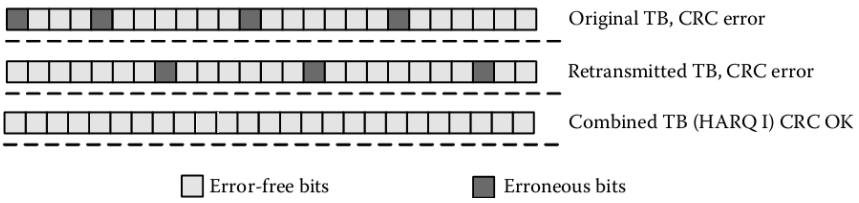

Source: Furht, Ahson, (2009)

In incremental redundancy or type II HARQ, a transport block with FEC coded is sent to the receiver (Holma – Toskala 2009). This transport block contains the systematic bits and a few parity bits to correct errors. A retransmission request is sent to the transmitter upon an error occurred in the decoding process. The retransmitted transport blocks use different FEC-coding scheme and additional parity bits are transmitted incrementally in each retransmitted packet. The retransmitted transport blocks are combined jointly with the original packet to check the error with CRC calculation. Until a successful decoding is performed or the retransmission limit is reached (i.e., unsuccessful decoding), the process is repeated which is illustrated in Figure 2.16.

In LTE, HARQ retransmission strategy is only supported on the physical downlink and uplink shared channels (PDSCH and PUSCH). HARQ process is based on stop-and-wait ARQ (Goldsmith 2005).

Since the process of decoding the original transport block plus the retransmitted packet should be finished and then an ACK or NAK command should be sent for the transmitter to send a new packet or retransmit the previous packet. In LTE FDD operation, both uplink and downlink is limited with eight stop-and-wait (SAW) HARQ processes with a typical Round-Trip Time (RTT) of 8ms (Holma – Toskala 2009).

Figure 2.16: Incremental redundancy HARQ at code word level

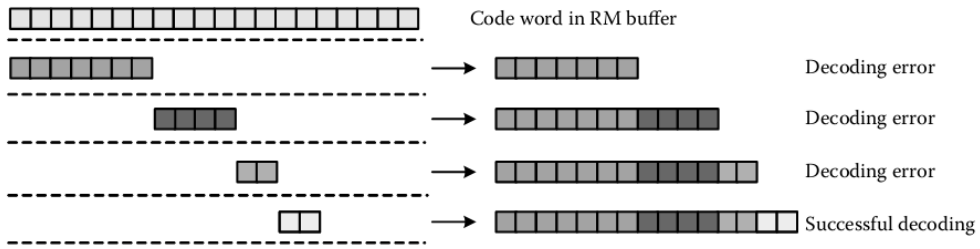

Source: Furht, Ahson, (2009)

In the downlink, HARQ process for LTE is asynchronous and adaptive which means, retransmissions may occur at any time and each process is identified with an explicit HARQ process number. On the other hand, uplink HARQ process is synchronous, and either non-adaptive or adaptive, in which the initial transmission time determines the retransmission instant. Therefore, it is possible to obtain process number indirectly.

3. MULTIPLE ANTENNA TECHNIQUE IN LTE

Multiple input multiple output (MIMO) techniques support multiple antennas at the transmitter and at the receiver. The aim of MIMO is to achieve different kinds of gains, namely: spatial diversity and spatial multiplexing (Lee and et al 2009).

Spatial multiplexing increases the capacity by transmitting different streams of data simultaneously in parallel from different antennas. Spatial diversity can be used to increase the robustness of communication in fading channels by transmitting multiple replicas of the transmitted signal from different antennas. Thus MIMO can be used to improve the cell capacity (Ball and et al 2009).

One of the main advantages of LTE is different MIMO modes support. LTE Release 8 supports up to two antennas in UE and up to four antennas in eNodeB (Lee and et al 2009). It is possible to reach up to 300 Mbps with four antennas in the downlink and 75 Mbps in the uplink. In LTE, MIMO technologies have been widely used to improve downlink peak rate, cell coverage, as well as average cell throughput. To achieve this diverse set of objectives, LTE adopted various MIMO technologies including transmit diversity and single user MIMO (SU-MIMO) (Sesia and et al 2009). SU-MIMO scheme is specified for the configuration with two or four transmit antennas in the downlink, which supports transmission of multiple spatial layers with up to four layers to a given UE. There are two operation modes in SU-MIMO spatial multiplexing: the closed-loop spatial multiplexing mode and the open-loop spatial multiplexing mode (Ball and et al 2009).

In the closed-loop spatial multiplexing mode, the base station (also known as eNodeB) applies the spatial domain precoding on the transmitted signal taking into account the precoding matrix indicator (PMI) reported by the UE so that the transmitted signal matches with the spatial channel experienced by the UE. The closed-loop spatial multiplexing with M layers and N transmit antennas ($N \geq M$) is illustrated in Figure 3.1. To support the closed-loop spatial multiplexing in the downlink, the UE needs to feedback the rank indicator (RI), the PMI, and the channel quality indicator (CQI) in the

uplink. The RI indicates the number of spatial layers that can be supported by the current channel experienced at the UE. The eNodeB may decide the transmission rank, M, taking into account the RI reported by the UE as well as other factors such as traffic pattern, available transmission power, etc. The CQI feedback indicates a combination of modulation scheme and channel coding rate that the eNodeB should use to ensure that the block error probability experienced at the UE will not exceed 10% (Lee and et al 2009).

The open-loop spatial multiplexing may be operated when reliable PMI feedback is not available at the eNodeB, for example, when the UE speed is not slow enough or when the feedback overhead on uplink is too high. The open-loop spatial multiplexing with M layers and N transmit antennas (N ≥ M) is illustrated in Figure 3.2. The feedback consists of the RI and the CQI in open-loop spatial multiplexing (Lee and et al 2009).

Figure 3.1: Closed-loop spatial multiplexing with N antennas and M layers.

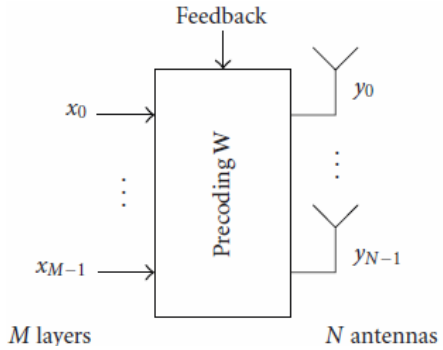

Source: Lee, Han, Zhang, (2009)

In contrast to the closed-loop spatial multiplexing, the eNodeB only determines the transmission rank and a fixed set of precoding matrices are applied cyclically across all the scheduled subcarriers in the frequency domain.

It is noted that in order to cope with the situation that the spatial multiplexing is not possible due to channel variation, the eNodeB can instantaneously schedule downlink transmission using the transmit diversity even though the UE has been configured to be in the spatial multiplexing mode.

Figure 3.2: Open-loop spatial multiplexing with *N* antennas and *M* layers.

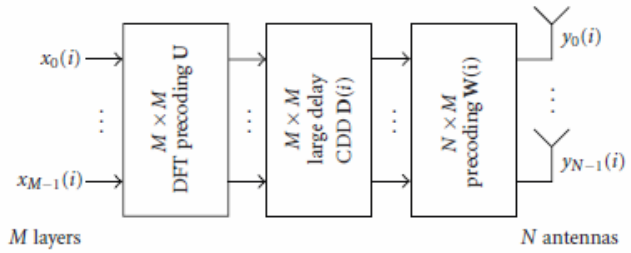

Source: Lee, Han, Zhang, (2009)

3.1 LAYER MAPPING

The complex-valued modulation symbols for each of the code words to be transmitted are mapped onto one or several layers (3GPP TS 36.211 2009). Complex-valued modulation symbols $d^{(q)}(0),...,d^{(q)}(M_{\text{symb}}^{(q)}-1)$ for code word q shall be mapped onto the layers $x(i)=\left[x^{(0)}(i) \quad ... \quad x^{(\upsilon-1)}(i)\right]^T$, $i=0,1,...,M_{\text{symb}}^{\text{layer}}-1$ where υ is the number of layers and $M_{\text{symb}}^{\text{layer}}$ is the number of modulation symbols per layer.

3.1.1 Layer Mapping For Transmission On A Single Antenna Port

For transmission on a single antenna port, a single layer is used, $\upsilon=1$, and the mapping is defined by

$$x^{(0)}(i)=d^{(0)}(i) \tag{3.1}$$

with $M_{\text{symb}}^{\text{layer}}=M_{\text{symb}}^{(0)}$.

3.1.2 Layer Mapping For Spatial Multiplexing

For spatial multiplexing, the layer mapping shall be done according to Table 3.1 (3GPP TS 36.211, 2009). The number of layers υ is less than or equal to the number of antenna ports P used for transmission of the physical channel. The case of a single codeword mapped to two layers is only applicable when the number of antenna ports is 4.

Table 3.1: Codeword-to-layer mapping for spatial multiplexing

Number of layers	Number of code words	Codeword-to-layer mapping $i = 0,1,\ldots,M_{\text{symb}}^{\text{layer}} - 1$
1	1	$x^{(0)}(i) = d^{(0)}(i)$ $\quad M_{\text{symb}}^{\text{layer}} = M_{\text{symb}}^{(0)}$
2	2	$x^{(0)}(i) = d^{(0)}(i)$ $x^{(1)}(i) = d^{(1)}(i)$ $\quad M_{\text{symb}}^{\text{layer}} = M_{\text{symb}}^{(0)} = M_{\text{symb}}^{(1)}$
2	1	$x^{(0)}(i) = d^{(0)}(2i)$ $x^{(1)}(i) = d^{(0)}(2i+1)$ $\quad M_{\text{symb}}^{\text{layer}} = M_{\text{symb}}^{(0)} / 2$
3	2	$x^{(0)}(i) = d^{(0)}(i)$ $x^{(1)}(i) = d^{(1)}(2i)$ $x^{(2)}(i) = d^{(1)}(2i+1)$ $\quad M_{\text{symb}}^{\text{layer}} = M_{\text{symb}}^{(0)} = M_{\text{symb}}^{(1)} / 2$
4	2	$x^{(0)}(i) = d^{(0)}(2i)$ $x^{(1)}(i) = d^{(0)}(2i+1)$ $x^{(2)}(i) = d^{(1)}(2i)$ $x^{(3)}(i) = d^{(1)}(2i+1)$ $\quad M_{\text{symb}}^{\text{layer}} = M_{\text{symb}}^{(0)} / 2 = M_{\text{symb}}^{(1)} / 2$

3.1.3 Layer Mapping For Transmit Diversity

For transmit diversity, the layer mapping shall be done according to Table 3.2 (3GPP TS 36.211, 2009). There is only one codeword and the number of layers υ is equal to the number of antenna ports P used for transmission of the physical channel.

Table 3.2: Codeword-to-layer mapping for transmit diversity

Number of layers	Number of code words	Codeword-to-layer mapping $i = 0,1,\ldots,M_{\text{symb}}^{\text{layer}} - 1$
2	1	$x^{(0)}(i) = d^{(0)}(2i)$ $x^{(1)}(i) = d^{(0)}(2i+1)$ $M_{\text{symb}}^{\text{layer}} = M_{\text{symb}}^{(0)} / 2$
4	1	$x^{(0)}(i) = d^{(0)}(4i)$ $x^{(1)}(i) = d^{(0)}(4i+1)$ $x^{(2)}(i) = d^{(0)}(4i+2)$ $x^{(3)}(i) = d^{(0)}(4i+3)$ $M_{\text{symb}}^{\text{layer}} = \begin{cases} M_{\text{symb}}^{(0)}/4 & \text{if } M_{\text{symb}}^{(0)} \bmod 4 = 0 \\ \left(M_{\text{symb}}^{(0)} + 2\right)/4 & \text{if } M_{\text{symb}}^{(0)} \bmod 4 \neq 0 \end{cases}$ If $M_{\text{symb}}^{(0)} \bmod 4 \neq 0$ two null symbols shall be appended to $d^{(0)}(M_{\text{symb}}^{(0)} - 1)$

3.2 PRECODING

The precoder takes as input a block of vectors $x(i) = \left[x^{(0)}(i) \quad \ldots \quad x^{(\upsilon-1)}(i)\right]^T$, $i = 0,1,\ldots,M_{\text{symb}}^{\text{layer}} - 1$ from the layer mapping and generates a block of vectors $y(i) = \left[\ldots \quad y^{(p)}(i) \quad \ldots\right]^T$, $i = 0,1,\ldots,M_{\text{symb}}^{\text{ap}} - 1$ to be mapped onto resources on each of the antenna ports, where $y^{(p)}(i)$ represents the signal for antenna port p (3GPP TS 36.211, 2009).

3.2.1 Precoding For Transmission On A Single Antenna Port

For transmission on a single antenna port, precoding is defined by

$$y^{(p)}(i) = x^{(0)}(i) \tag{3.2}$$

where $p \in \{0,4,5\}$ is the number of the single antenna port used for transmission of the physical channel and $i = 0,1,\ldots,M_{\text{symb}}^{\text{ap}} - 1$, $M_{\text{symb}}^{\text{ap}} = M_{\text{symb}}^{\text{layer}}$.

3.2.2 Precoding For Spatial Multiplexing

Precoding for spatial multiplexing is only used in combination with layer mapping for spatial multiplexing. Spatial multiplexing supports two or four antenna ports and the set of antenna ports used is $p \in \{0,1\}$ or $p \in \{0,1,2,3\}$, respectively (3GPP TS 36.211, 2009).

3.2.2.1 Precoding without CDD

Without cyclic delay diversity (CDD), precoding for spatial multiplexing is defined by

$$\begin{bmatrix} y^{(0)}(i) \\ \vdots \\ y^{(P-1)}(i) \end{bmatrix} = W(i) \begin{bmatrix} x^{(0)}(i) \\ \vdots \\ x^{(\upsilon-1)}(i) \end{bmatrix} \quad \textbf{(3.3)}$$

where the precoding matrix $W(i)$ is of size $P \times \upsilon$ and $i = 0,1,\ldots,M_{\text{symb}}^{\text{ap}} - 1$, $M_{\text{symb}}^{\text{ap}} = M_{\text{symb}}^{\text{layer}}$.

For spatial multiplexing, the values of $W(i)$ shall be selected among the precoder elements in the codebook configured in the eNodeB and the UE. The eNodeB can further confine the precoder selection in the UE to a subset of the elements in the codebook using codebook subset restrictions. The configured codebook shall be selected from Table 3.4 or 3.5 (3GPP TS 36.211, 2009).

3.2.2.2 Precoding for large delay CDD

For large-delay CDD, precoding for spatial multiplexing is defined by

$$\begin{bmatrix} y^{(0)}(i) \\ \vdots \\ y^{(P-1)}(i) \end{bmatrix} = W(i)D(i)U \begin{bmatrix} x^{(0)}(i) \\ \vdots \\ x^{(\upsilon-1)}(i) \end{bmatrix} \quad \textbf{(3.4)}$$

where the precoding matrix $W(i)$ is of size $P \times \upsilon$ and $i = 0,1,\ldots,M_{\text{symb}}^{\text{ap}} - 1$, $M_{\text{symb}}^{\text{ap}} = M_{\text{symb}}^{\text{layer}}$. The diagonal size-$\upsilon \times \upsilon$ matrix $D(i)$ supporting cyclic delay diversity and the size-$\upsilon \times \upsilon$ matrix U are both given by Table 3.3 for different numbers of layers υ.

The values of the precoding matrix $W(i)$ shall be selected among the precoder elements in the codebook configured in the eNodeB and the UE. The eNodeB can further confine the precoder selection in the UE to a subset of the elements in the codebook using

codebook subset restriction. The configured codebook shall be selected from Table 3.4 or 3.5.

i. For 2 antenna ports, the precoder is selected according to $W(i) = C_1$ where C_1 denotes the precoding matrix corresponding to precoder index 0 in Table 3.4.

ii. For 4 antenna ports, the UE may assume that the eNodeB cyclically assigns different precoders to different vectors $\left[x^{(0)}(i) \quad ... \quad x^{(\upsilon-1)}(i)\right]^T$ on the physical downlink shared channel as follows. A different precoder is used every υ vectors, where υ denotes the number of transmission layers in the case of spatial multiplexing. In particular, the precoder is selected according to $W(i) = C_k$, where k is the precoder index given by $k = \left(\left\lfloor \frac{i}{\upsilon} \right\rfloor \bmod 4\right) + 1$, where *k=1,2,3,4,* and C_1, C_2, C_3, C_4 denote precoder matrices corresponding to precoder indices 12,13,14 and 15, respectively, in Table 3.5 (3GPP TS 36.211, 2009).

3.2.2.3 Codebook for precoding

For transmission on two antenna ports, $p \in \{0,1\}$, the precoding matrix $W(i)$ shall be selected from Table 3.4 or a subset thereof. For the closed-loop spatial multiplexing transmission mode defined in (3GPP TS 36.211, 2009), the codebook index 0 is not used when the number layers is $\upsilon = 2$.

For transmission on four antenna ports, $p \in \{0,1,2,3\}$, the precoding matrix W shall be selected from Table 3.5 or a subset thereof.

The quantity $W_n^{\{s\}}$ denotes the matrix defined by the columns given by the set $\{s\}$ from the expression $W_n = I - 2u_n u_n^H / u_n^H u_n$ where I is the 4×4 identity matrix and the vector u_n is given by Table 3.5 (3GPP TS 36.211, 2009).

Table 3.3: Large-delay cyclic delay diversity

Number of layers υ	U	$D(i)$
2	$\frac{1}{\sqrt{2}}\begin{bmatrix}1 & 1\\ 1 & e^{-j2\pi/2}\end{bmatrix}$	$\begin{bmatrix}1 & 0\\ 0 & e^{-j2\pi i/2}\end{bmatrix}$
3	$\frac{1}{\sqrt{3}}\begin{bmatrix}1 & 1 & 1\\ 1 & e^{-j2\pi/3} & e^{-j4\pi/3}\\ 1 & e^{-j4\pi/3} & e^{-j8\pi/3}\end{bmatrix}$	$\begin{bmatrix}1 & 0 & 0\\ 0 & e^{-j2\pi i/3} & 0\\ 0 & 0 & e^{-j4\pi i/3}\end{bmatrix}$
4	$\frac{1}{2}\begin{bmatrix}1 & 1 & 1 & 1\\ 1 & e^{-j2\pi/4} & e^{-j4\pi/4} & e^{-j6\pi/4}\\ 1 & e^{-j4\pi/4} & e^{-j8\pi/4} & e^{-j12\pi/4}\\ 1 & e^{-j6\pi/4} & e^{-j12\pi/4} & e^{-j18\pi/4}\end{bmatrix}$	$\begin{bmatrix}1 & 0 & 0 & 0\\ 0 & e^{-j2\pi i/4} & 0 & 0\\ 0 & 0 & e^{-j4\pi i/4} & 0\\ 0 & 0 & 0 & e^{-j6\pi i/4}\end{bmatrix}$

Table 3.4: Codebook for transmission on antenna ports $\{0,1\}$.

Codebook index	**Number of layers υ**	
	1	**2**
0	$\frac{1}{\sqrt{2}}\begin{bmatrix}1\\ 1\end{bmatrix}$	$\frac{1}{\sqrt{2}}\begin{bmatrix}1 & 0\\ 0 & 1\end{bmatrix}$
1	$\frac{1}{\sqrt{2}}\begin{bmatrix}1\\ -1\end{bmatrix}$	$\frac{1}{2}\begin{bmatrix}1 & 1\\ 1 & -1\end{bmatrix}$
2	$\frac{1}{\sqrt{2}}\begin{bmatrix}1\\ j\end{bmatrix}$	$\frac{1}{2}\begin{bmatrix}1 & 1\\ j & -j\end{bmatrix}$
3	$\frac{1}{\sqrt{2}}\begin{bmatrix}1\\ -j\end{bmatrix}$	-

Table 3.5: Codebook for transmission on antenna ports $\{0,1,2,3\}$.

Codebook index	u_n	Number of layers υ			
		1	**2**	**3**	**4**
0	$u_0 = \begin{bmatrix} 1 & -1 & -1 & -1 \end{bmatrix}^T$	$W_0^{\{1\}}$	$W_0^{\{14\}}/\sqrt{2}$	$W_0^{\{124\}}/\sqrt{3}$	$W_0^{\{1234\}}/2$
1	$u_1 = \begin{bmatrix} 1 & -j & 1 & j \end{bmatrix}^T$	$W_1^{\{1\}}$	$W_1^{\{12\}}/\sqrt{2}$	$W_1^{\{123\}}/\sqrt{3}$	$W_1^{\{1234\}}/2$
2	$u_2 = \begin{bmatrix} 1 & 1 & -1 & 1 \end{bmatrix}^T$	$W_2^{\{1\}}$	$W_2^{\{12\}}/\sqrt{2}$	$W_2^{\{123\}}/\sqrt{3}$	$W_2^{\{3214\}}/2$
3	$u_3 = \begin{bmatrix} 1 & j & 1 & -j \end{bmatrix}^T$	$W_3^{\{1\}}$	$W_3^{\{12\}}/\sqrt{2}$	$W_3^{\{123\}}/\sqrt{3}$	$W_3^{\{3214\}}/2$
4	$u_4 = \begin{bmatrix} 1 & (-1-j)/\sqrt{2} & -j & (1-j)/\sqrt{2} \end{bmatrix}^T$	$W_4^{\{1\}}$	$W_4^{\{14\}}/\sqrt{2}$	$W_4^{\{124\}}/\sqrt{3}$	$W_4^{\{1234\}}/2$
5	$u_5 = \begin{bmatrix} 1 & (1-j)/\sqrt{2} & j & (-1-j)/\sqrt{2} \end{bmatrix}^T$	$W_5^{\{1\}}$	$W_5^{\{14\}}/\sqrt{2}$	$W_5^{\{124\}}/\sqrt{3}$	$W_5^{\{1234\}}/2$
6	$u_6 = \begin{bmatrix} 1 & (1+j)/\sqrt{2} & -j & (-1+j)/\sqrt{2} \end{bmatrix}^T$	$W_6^{\{1\}}$	$W_6^{\{13\}}/\sqrt{2}$	$W_6^{\{134\}}/\sqrt{3}$	$W_6^{\{1324\}}/2$
7	$u_7 = \begin{bmatrix} 1 & (-1+j)/\sqrt{2} & j & (1+j)/\sqrt{2} \end{bmatrix}^T$	$W_7^{\{1\}}$	$W_7^{\{13\}}/\sqrt{2}$	$W_7^{\{134\}}/\sqrt{3}$	$W_7^{\{1324\}}/2$
8	$u_8 = \begin{bmatrix} 1 & -1 & 1 & 1 \end{bmatrix}^T$	$W_8^{\{1\}}$	$W_8^{\{12\}}/\sqrt{2}$	$W_8^{\{124\}}/\sqrt{3}$	$W_8^{\{1234\}}/2$
9	$u_9 = \begin{bmatrix} 1 & -j & -1 & -j \end{bmatrix}^T$	$W_9^{\{1\}}$	$W_9^{\{14\}}/\sqrt{2}$	$W_9^{\{134\}}/\sqrt{3}$	$W_9^{\{1234\}}/2$
10	$u_{10} = \begin{bmatrix} 1 & 1 & 1 & -1 \end{bmatrix}^T$	$W_{10}^{\{1\}}$	$W_{10}^{\{13\}}/\sqrt{2}$	$W_{10}^{\{123\}}/\sqrt{3}$	$W_{10}^{\{1324\}}/2$
11	$u_{11} = \begin{bmatrix} 1 & j & -1 & j \end{bmatrix}^T$	$W_{11}^{\{1\}}$	$W_{11}^{\{13\}}/\sqrt{2}$	$W_{11}^{\{134\}}/\sqrt{3}$	$W_{11}^{\{1324\}}/2$
12	$u_{12} = \begin{bmatrix} 1 & -1 & -1 & 1 \end{bmatrix}^T$	$W_{12}^{\{1\}}$	$W_{12}^{\{12\}}/\sqrt{2}$	$W_{12}^{\{123\}}/\sqrt{3}$	$W_{12}^{\{1234\}}/2$
13	$u_{13} = \begin{bmatrix} 1 & -1 & 1 & -1 \end{bmatrix}^T$	$W_{13}^{\{1\}}$	$W_{13}^{\{13\}}/\sqrt{2}$	$W_{13}^{\{123\}}/\sqrt{3}$	$W_{13}^{\{1324\}}/2$
14	$u_{14} = \begin{bmatrix} 1 & 1 & -1 & -1 \end{bmatrix}^T$	$W_{14}^{\{1\}}$	$W_{14}^{\{13\}}/\sqrt{2}$	$W_{14}^{\{123\}}/\sqrt{3}$	$W_{14}^{\{3214\}}/2$
15	$u_{15} = \begin{bmatrix} 1 & 1 & 1 & 1 \end{bmatrix}^T$	$W_{15}^{\{1\}}$	$W_{15}^{\{12\}}/\sqrt{2}$	$W_{15}^{\{123\}}/\sqrt{3}$	$W_{15}^{\{1234\}}/2$

3.2.3 Precoding For Transmit Diversity

Precoding for transmit diversity is only used in combination with layer mapping for transmit diversity. The precoding operation for transmit diversity is defined for two and four antenna ports (3GPP TS 36.211, 2009).

For transmission on two antenna ports, $p \in \{0,1\}$, the output $y(i) = \begin{bmatrix} y^{(0)}(i) & y^{(1)}(i) \end{bmatrix}^T$, $i = 0,1,\ldots,M_{\text{symb}}^{\text{ap}} - 1$ of the precoding operation is defined by

$$\begin{bmatrix} y^{(0)}(2i) \\ y^{(1)}(2i) \\ y^{(0)}(2i+1) \\ y^{(1)}(2i+1) \end{bmatrix} = \frac{1}{\sqrt{2}} \begin{bmatrix} 1 & 0 & j & 0 \\ 0 & -1 & 0 & j \\ 0 & 1 & 0 & j \\ 1 & 0 & -j & 0 \end{bmatrix} \begin{bmatrix} \text{Re}\left(x^{(0)}(i)\right) \\ \text{Re}\left(x^{(1)}(i)\right) \\ \text{Im}\left(x^{(0)}(i)\right) \\ \text{Im}\left(x^{(1)}(i)\right) \end{bmatrix} \quad \textbf{(3.5)}$$

for $i = 0,1,\ldots,M_{\text{symb}}^{\text{layer}} - 1$ with $M_{\text{symb}}^{\text{ap}} = 2M_{\text{symb}}^{\text{layer}}$.

For transmission on four antenna ports, $p \in \{0,1,2,3\}$, the output $y(i) = \left[y^{(0)}(i) \quad y^{(1)}(i) \quad y^{(2)}(i) \quad y^{(3)}(i)\right]^T$, $i = 0,1,\ldots,M_{\text{symb}}^{\text{ap}} - 1$ of the precoding operation is defined by

$$\begin{bmatrix} y^{(0)}(4i) \\ y^{(1)}(4i) \\ y^{(2)}(4i) \\ y^{(3)}(4i) \\ y^{(0)}(4i+1) \\ y^{(1)}(4i+1) \\ y^{(2)}(4i+1) \\ y^{(3)}(4i+1) \\ y^{(0)}(4i+2) \\ y^{(1)}(4i+2) \\ y^{(2)}(4i+2) \\ y^{(3)}(4i+2) \\ y^{(0)}(4i+3) \\ y^{(1)}(4i+3) \\ y^{(2)}(4i+3) \\ y^{(3)}(4i+3) \end{bmatrix} = \frac{1}{\sqrt{2}} \begin{bmatrix} 1 & 0 & 0 & 0 & j & 0 & 0 & 0 \\ 0 & 0 & 0 & 0 & 0 & 0 & 0 & 0 \\ 0 & -1 & 0 & 0 & 0 & j & 0 & 0 \\ 0 & 0 & 0 & 0 & 0 & 0 & 0 & 0 \\ 0 & 1 & 0 & 0 & 0 & j & 0 & 0 \\ 0 & 0 & 0 & 0 & 0 & 0 & 0 & 0 \\ 1 & 0 & 0 & 0 & -j & 0 & 0 & 0 \\ 0 & 0 & 0 & 0 & 0 & 0 & 0 & 0 \\ 0 & 0 & 0 & 0 & 0 & 0 & 0 & 0 \\ 0 & 0 & 1 & 0 & 0 & 0 & j & 0 \\ 0 & 0 & 0 & 0 & 0 & 0 & 0 & 0 \\ 0 & 0 & 0 & -1 & 0 & 0 & 0 & j \\ 0 & 0 & 0 & 0 & 0 & 0 & 0 & 0 \\ 0 & 0 & 0 & 1 & 0 & 0 & 0 & j \\ 0 & 0 & 0 & 0 & 0 & 0 & 0 & 0 \\ 0 & 0 & 1 & 0 & 0 & 0 & -j & 0 \end{bmatrix} \begin{bmatrix} \text{Re}\left(x^{(0)}(i)\right) \\ \text{Re}\left(x^{(1)}(i)\right) \\ \text{Re}\left(x^{(2)}(i)\right) \\ \text{Re}\left(x^{(3)}(i)\right) \\ \text{Im}\left(x^{(0)}(i)\right) \\ \text{Im}\left(x^{(1)}(i)\right) \\ \text{Im}\left(x^{(2)}(i)\right) \\ \text{Im}\left(x^{(3)}(i)\right) \end{bmatrix} \quad \textbf{(3.6)}$$

for $i = 0,1,\ldots,M_{\text{symb}}^{\text{layer}} - 1$ with $M_{\text{symb}}^{\text{ap}} = \begin{cases} 4M_{\text{symb}}^{\text{layer}} & \text{if } M_{\text{symb}}^{(0)} \bmod 4 = 0 \\ \left(4M_{\text{symb}}^{\text{layer}}\right) - 2 & \text{if } M_{\text{symb}}^{(0)} \bmod 4 \neq 0 \end{cases}$

4. SCHEDULING IN LTE

Multi-user scheduling finds its basis at the interface between information theory and queuing theory. Before establishing an algorithm, a capacity-related metric is first formulated and then optimized across all possible resource allocation solutions satisfying a set of predetermined constraints. Such constraints may be physical (e.g. bandwidth and total power) or QoS-related. The eNodeB allocates physical layer resources for the physical uplink and downlink shared channels (PUSCH and PDSCH). Resources are composed of Physical Resource Blocks (PRB) and Modulation Coding Scheme (MCS). The MCS determines the bit rate, and thus the capacity, of PRBs. Allocations may be valid for one or more TTIs; each TTI interval is one subframe (1 ms) (Holma – Toskala 2009).

4.1 ROUND ROBIN SCHEDULING

In this scheduling strategy the terminals are assigned the shared resources in turn (one after another). Thus every user is equally scheduled without taking the CQI into account as illustrated in Figure 4.1.

The principal advantage of Round Robin scheduling is the guarantee of fairness for all users (Dikamba 2011). Furthermore Round Robin is easy to implement which is the reason why it is usually used by many systems. Since Round Robin does not take the channel quality information into account, it will result in low user throughput. However, round robin scheduler can schedule the cell edge users although their average throughput is very low.

Figure 4.1: Round Robin scheduling

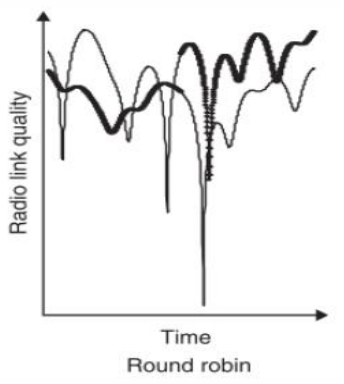

Source: Dikamba, (2011).

4.2 PROPORTIONAL FAIR SCHEDULER

Proportional fair scheduler schedules a user when its instantaneous link quality is high relative to its own average channel condition over time (Holma – Toskala 2009). It allocates user *k* in resource block *m* in any given subframe *f* if $k = \hat{k}_m$, where

$$\hat{k}_m = \arg\max_{k'=1,\ldots,K} \frac{R_{k'}(m, f)}{T_{k'}(f)} \qquad \textbf{(4.1)}$$

Where $T_k(f)$ denotes the long term average throughput of user *k* computed in subframe *f* and $R_k(m, f)$=log [1+SNR$_k$ (*m*,*f*)] is the achievable rate by user *k* in resource block *m* and subframe *f*. The long term average user throughputs are recursively computed by

$$T_k(f) = \left(1 - \frac{1}{t_c}\right) T_k(f-1) + \frac{1}{t_c} \sum_{m=1}^{M} R_k(m, f) \mathrm{I}\left\{\hat{k}_m = k\right\} \qquad \textbf{(4.2)}$$

where t_c is the time window over which fairness is imposed and I$\{\cdot\}$ is the indicator function equal to one if $\hat{k}_m$ = k and zero otherwise. A large time window t_c tends to maximize the total average throughput; in fact, in the limit of a very long time window,

PF scheduling and maximum-rate constant-power scheduling result in the same allocation of resources. For small t_c, the Proportional Fair Scheduler tends towards a round-robin scheduling of users in the system.

4.3 BEST CQI SCHEDULER

As the name implies, this scheduling strategy assigns resource blocks to the user with the best radio link conditions as illustrated in Figure 4.2 (Dikamba 2011). In order to perform scheduling, UEs send Channel Quality Indicator (CQI) to the eNodeB. Basically in the downlink, the eNodeBs transmit reference signal (downlink pilot) to UEs. These reference signals are used by UEs for the measurements of the CQI. A higher CQI value means better channel condition.

Figure 4.2: Best CQI scheduling

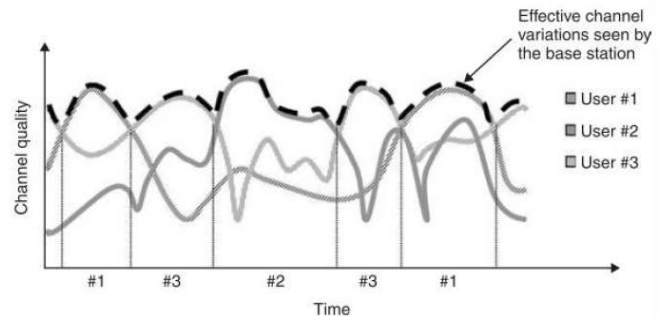

Source: Dikamba, (2011).

Best CQI scheduling can increase the cell capacity at the expense of the fairness. In this scheduling strategy, terminals located far from the base station (i.e. cell-edge users) are unlikely to be scheduled.

5. SIMULATION ANALYSIS

5.1 LTE SYSTEM LEVEL SIMULATOR OVERVIEW

In this study, a non-commercial LTE system level simulator is used to analyze the performance of LTE systems (Colom - Taranet 2011). The simulations are performed on both, the physical layer (link-level) and in the network (system-level) context, since the LTE system level simulator supplements LTE link level simulator. This combination allows detailed simulation of both the physical layer and system level simulations. While link level simulations allow for the investigation of issues such as Multiple-Input Multiple-Output (MIMO) gains, Adaptive Modulation and Coding (AMC) feedback, modeling of channel encoding and decoding or physical modeling for system level (Ikuno and et al 2010), system level simulations focus more on network related issues such as scheduling. Also, simulating the effects of issues such as cell planning, scheduling and interference and the totality of the radio links between the User Equipments (UEs) and eNodeBs is simplified by abstracting the physical layer parameters with high accuracy and simultaneously low complexity. This simulation covers the links between one eNodeB and multiple UEs. This setup additionally allows for the investigation of receiver structures that take into account the influence of scheduling, multi-user MIMO resource allocation, and multi-user gains. LTE system level simulator consists of two core parts: a link measurement model and a link performance model. A schematic block diagram of the LTE system level simulator is depicted in Figure 5.1.

The link measurement model reflects the link quality, given by the UE measurement reports, and is required to carry out link adaptation and resource allocation. The chosen link quality measure is evaluated per subcarrier. Based on the Signal to Interference and Noise Ratio (SINR), the UE computes the feedback (PMI, RI, and CQI), which is employed for link adaptation at the eNodeB as described in Section 3. The scheduling algorithm assigns resources to users in order to optimize the performance of the system (e.g., in terms of throughput) based on this feedback. Following the link measurement

model, the link performance model predicts the BLER of the link, based on the receiver SINR and the transmission parameters (e.g., modulation and coding).

The simulation is performed by defining a Region of Interest (ROI) in which the eNodeBs and UEs are distributed and a simulation length in Transmission Time Intervals (TTIs). It is designed that the UEs move only in this area. UEs average throughput results statistics interface and the eNodeBs and UEs positions in the ROI figures are depicted in Figure 5.2 and 5.3 respectively. In Figure 5.3, blue dots correspond to UEs and red dots show the eNodeB positions.

Figure 5.1: Schematic block diagram of the LTE system level simulator

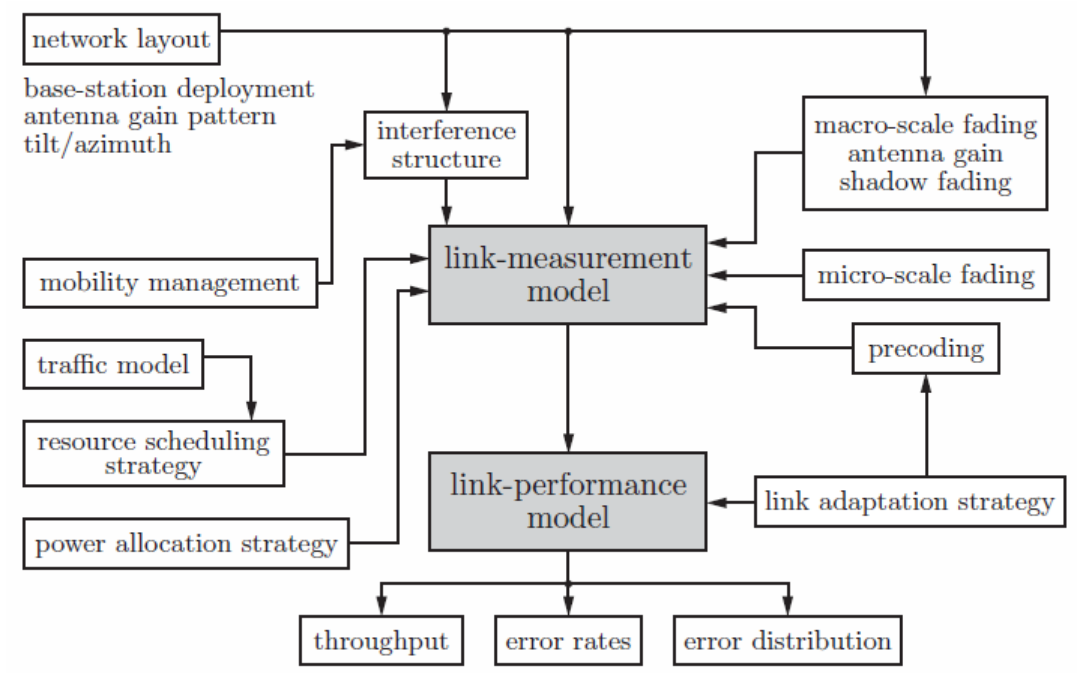

Source: Ikuno and et al, 2010,

Figure 5.2: The LTE system level simulator UEs throughput results statistics interface

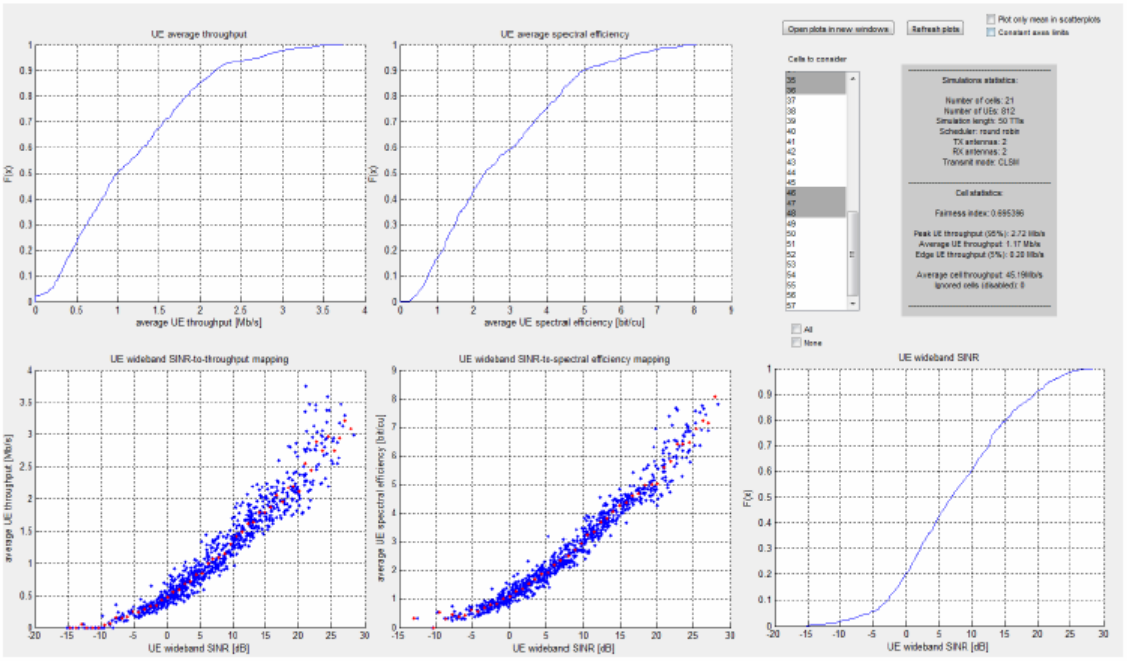

Figure 5.3: The eNodeBs and UEs positions are shown in ROI

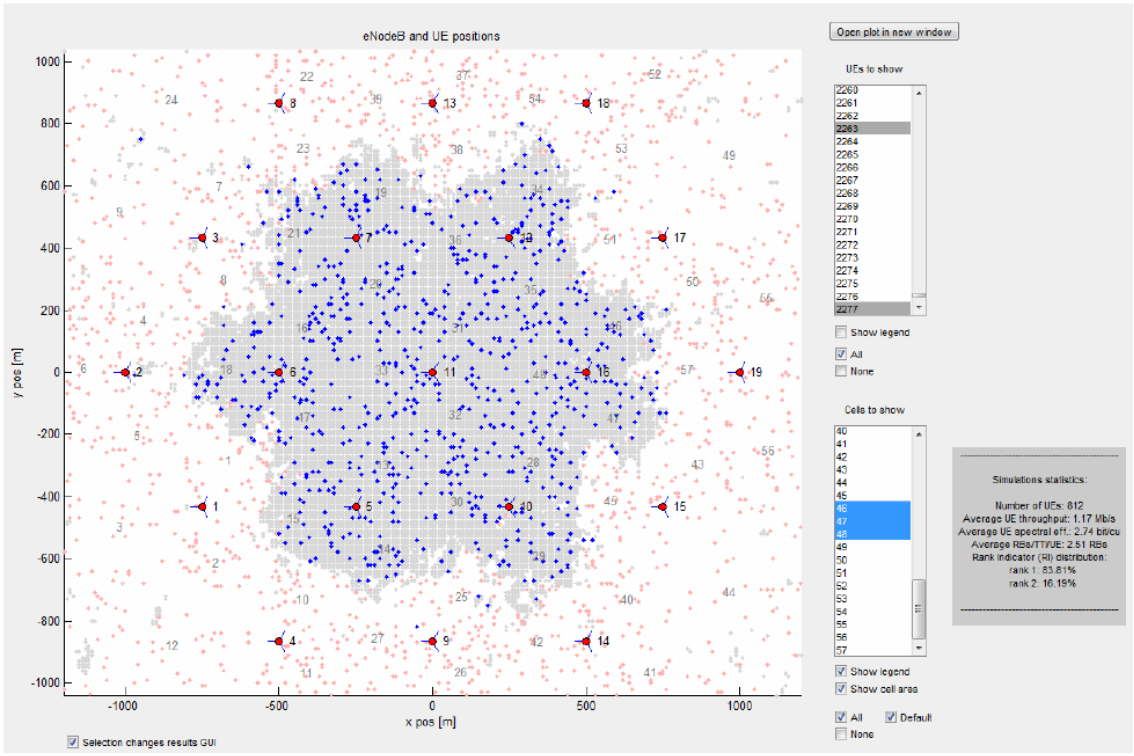

Source: Colom – Taranet, 2012

In LTE system level simulator, coverage analyze can be done by measuring the SINR in the ROI. Both macroscopic pathloss and shadow fading are taken into account to measure the SINR (Ikuno 2010). The macroscopic pathloss depends on both the propagation pathloss due to distance and the antenna gain and is measured between an eNodeB and UE. The eNodeB antenna radiation pattern to be used for each sector in 3-sector cell sites is plotted in Figure 5.4.

$$A(\theta) = -\min\left[12\left(\frac{\theta}{\theta_{3dB}}\right)^2,\ A_m\right] \quad \text{where} \quad -180 \le \theta \le 180 \tag{5.1}$$

where θ_{3dB} is the 3dB beam width which corresponds to 65 degrees, and $A_m = 15dB$ is the maximum attenuation.

Figure 5.4: The eNodeB antenna radiation pattern

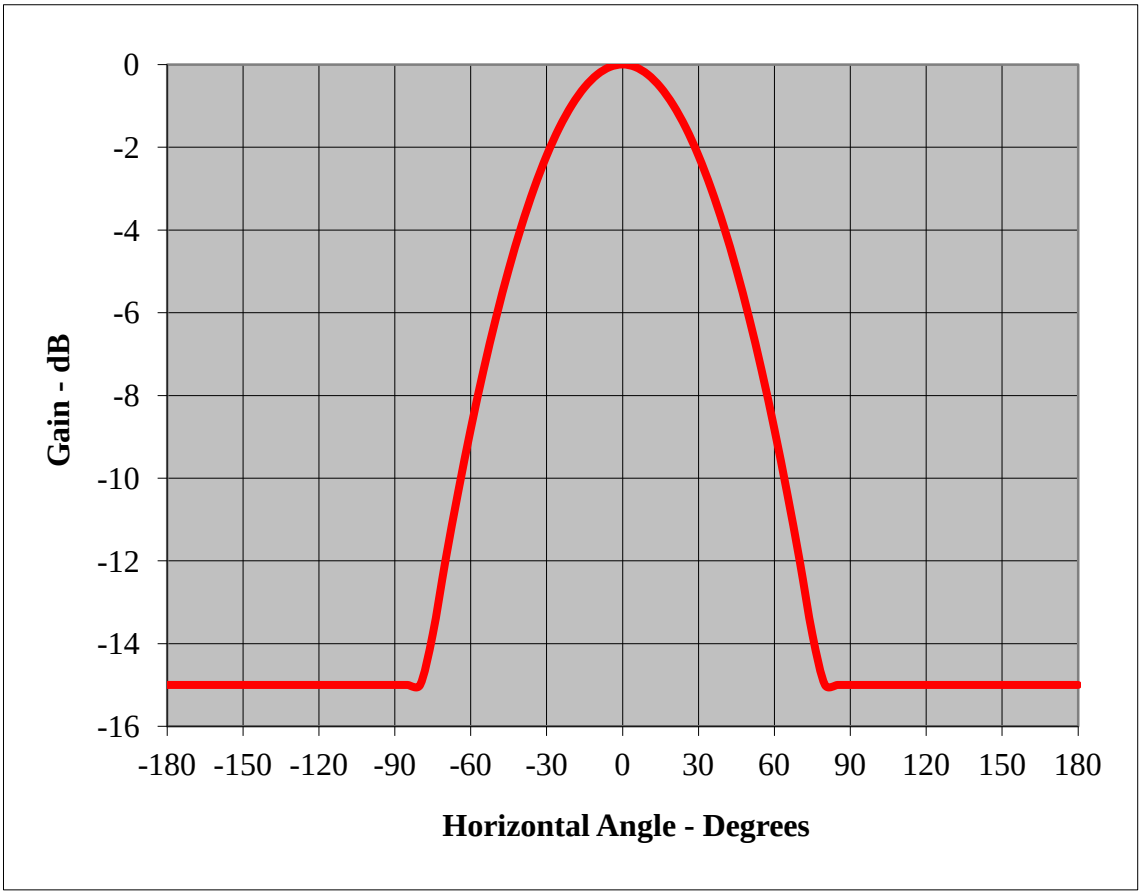

Shadow fading is caused by obstacles in the propagation path between the UE and the eNodeB and can be interpreted as the irregularities of the geographical characteristics of the terrain with respect to the average pathloss obtained from the macroscopic pathloss model. It is typically approximated by a log-normal distribution of mean 0 dB and standard deviation 10 dB (3GPP TS 36.942 2009).

In Figure 5.5, the effect of the macroscopic pathloss map and shadow fading is depicted. The SINR values in the ROI are decided according to the colors which indicate the SINR.

Figure 5.5: SINR measurement in ROI with the effects of macroscopic pathloss and shadow fading

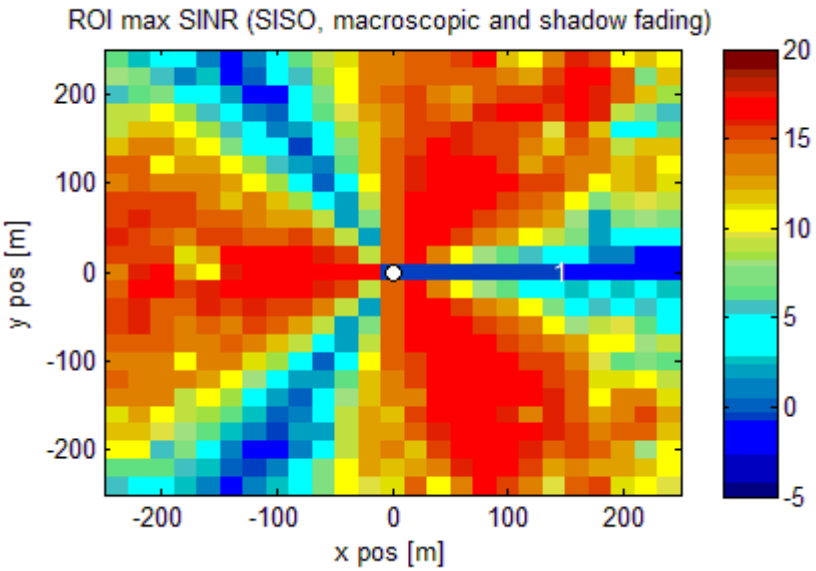

Source: Ikuno and et al, 2010,

Implementation-wise, the simulator follows the structure shown in Figure 5.7. Each network element is represented by a suitable class object, whose interactions are described below.

In order to generate the network topology, transmission sites are generated, to which three eNodeBs are appended, i.e., sectors, each containing a scheduler (see Figure 5.3). In the simulator, traffic modeling assumes full buffers in the downlink.

A scheduler assigns PHY resources, precoding matrices, and a suitable MCS to each UE attached to an eNodeB. The actual assignment depends on the scheduling algorithm and the received UE feedback. At the UE side, the received subcarrier post-equalization symbol SINR is calculated in the link measurement model. The SINR is determined by the signal, interference, and noise power levels, which are dependent on the cell layout (defined by the eNodeB positions, large-scale (macroscopic, macro-scale) pathloss, shadow fading) and the time-variant small-scale (microscopic, micro-scale) fading. The CQI feedback report is calculated based on the subcarrier SINRs and the target transport BLER. The CQI reports are generated by an SINR-to-CQI mapping as shown in Figure 5.6 and made available to the eNodeB implementation via a feedback channel with adjustable delay. At the transmitter, the appropriate MCS is selected by the CQI to achieve the target BLER during the transmission. Especially in high mobility scenarios, the feedback delay caused by computation and signaling timing can lead to performance degradation if the channel state changes significantly during the delay. In this study this delay value is assumed 3ms. In the link performance model, an AWGN equivalent SINR (AWGN) is obtained via Mutual Information Effective Signal to Interference and Noise Ratio Mapping (MIESM) (Schwarz 2010). In a second step, AWGN is mapped to BLER via AWGN link performance curves as described in section 2. The BLER value acts as a probability for computing ACK/NACKs, which are combined with the Transport Block (TB) size to compute the link throughput. The simulation output consists of traces, containing link throughput and error ratios for each user, as well as a cell aggregates, from which statistical distributions of throughputs and errors can be extracted as depicted in Figure 5.8.

Figure 5.6: SINR to CQI mapping

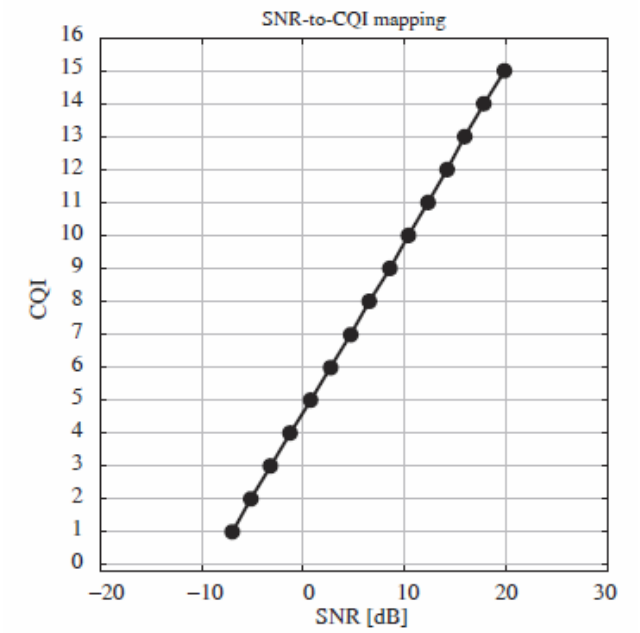

Source: Colom – Taranet 2012

Figure 5.7: Schematic class diagram showing the relation between the several components comprising the LTE System Level Simulator.

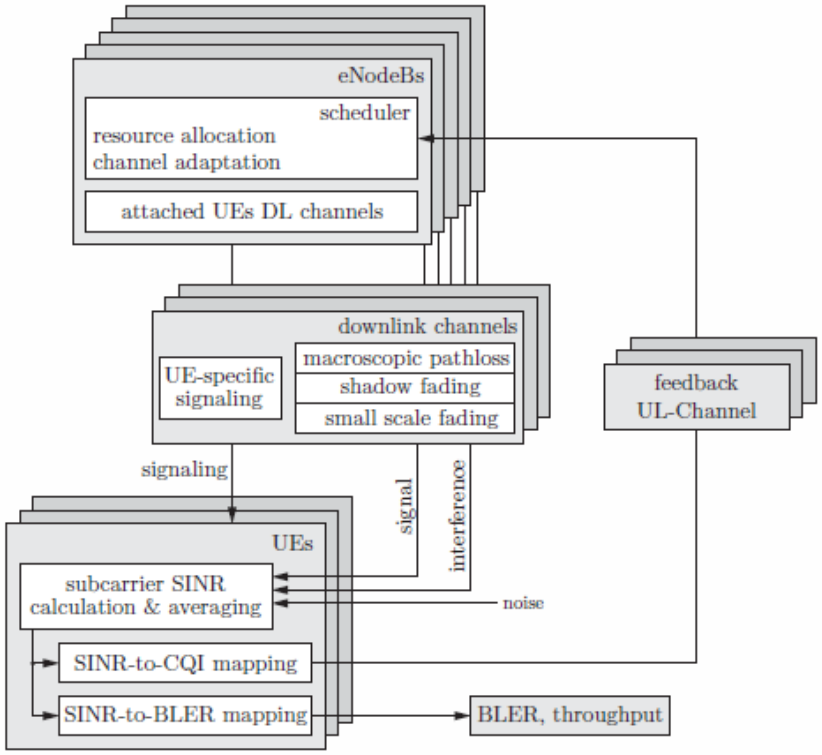

Source: Mehlführer and et al, 2011

Figure 5.8: The simulation outputs for UEs including average throughput, BLER and CQI values

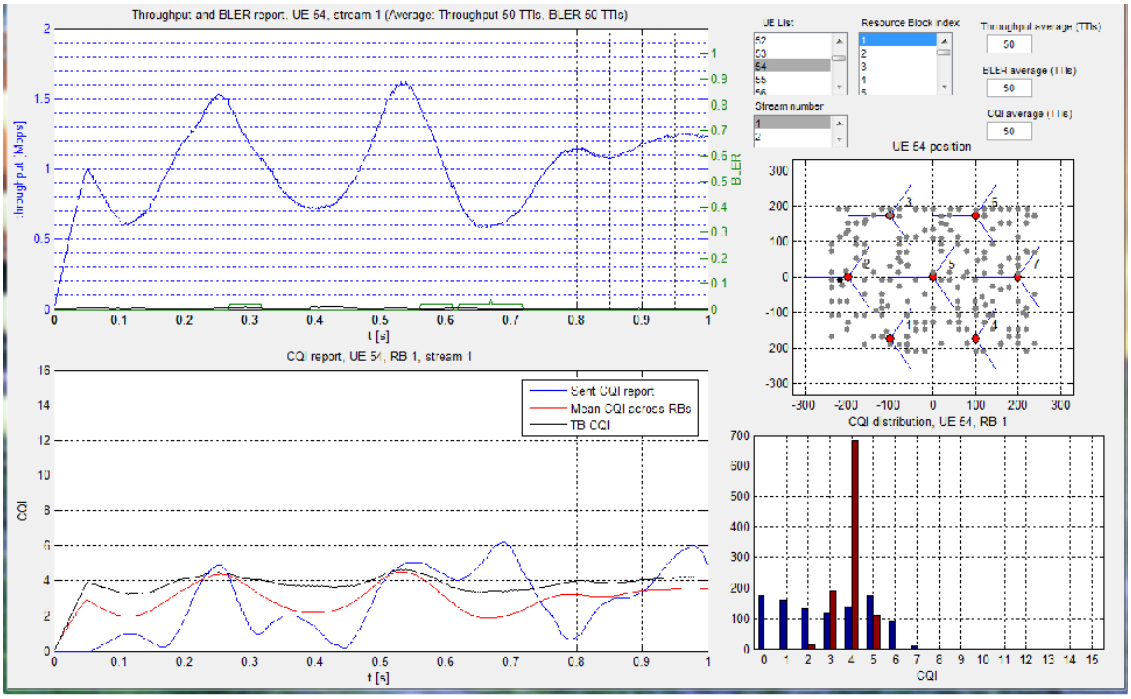

The performance of various multiuser LTE scheduling techniques including Round Robin, Proportional Fair and Best CQI is also compared by system level simulations. The considered schedulers pursue different goals for resource allocation. The best CQI scheduler tries to maximize total throughput and completely ignores fairness by just assigning resources to the users with the best channel conditions. Round robin scheduling does not consider the user equipment feedback and cyclically assigns the same amount of resources to each user. Thus, ignoring the user equipment feedback results in the worst throughput performance of all schedulers considered here. The proportional fair scheduler emphasizes multiuser diversity by scheduling the user who has the best current channel realization relative to its own average. The schedulers are compared in terms of total sector throughput and fairness (Jain's fairness index (Almatarneh and et al 2009)) as shown in Figure 5.9. Jain's fairness index is the standard traditional measure of network fairness and defined as follows,

$$f(x) = \frac{\left[\sum_{i=1}^{N} x_i\right]^2}{\sum_{i=1}^{N} x_i^{\,2}} \qquad \textbf{(5.2)}$$

where *xi* is the average traffic achieved by user *i*.

Figure 5.9: UE throughput and fairness comparison for Round Robin, Proportional Fair and Best CQI schedulers

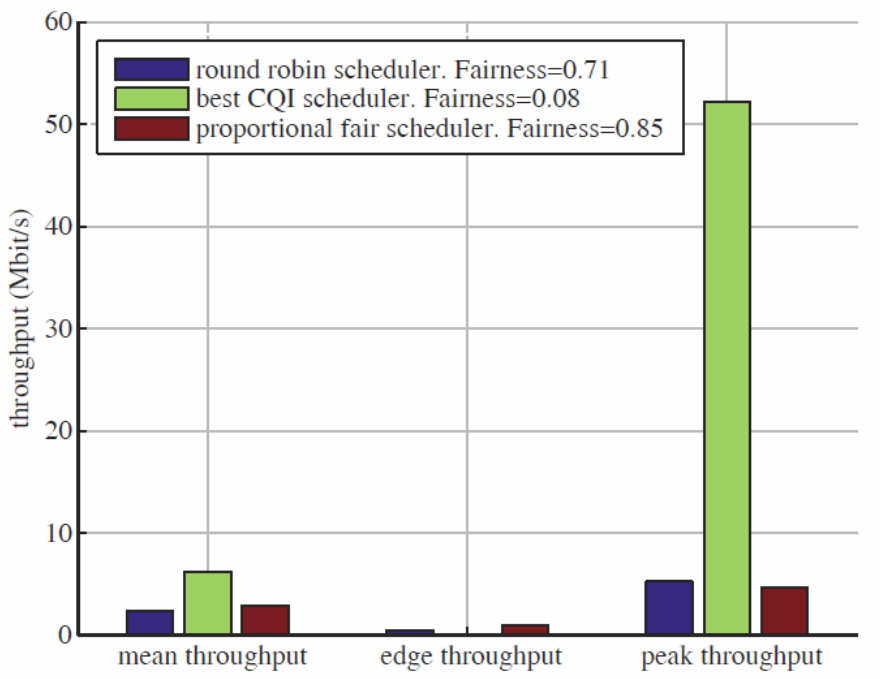

Source: Colom – Taranet 2012

5.2 COVERAGE AND CAPACITY COMPARISON FOR 2600 MHZ AND 800 MHZ BANDS

5.2.1 Coverage Analysis

Coverage in a cell is dependent upon the area covered by the signal. The distance travelled by the signal is dependent upon radio propagation characteristics in the given area. Radio propagation varies from region to region and should be studied carefully before predictions for both coverage and capacity are made. The requirement for the radio planners is generally a network design that covers 100% of the area. Fulfilling this

requirement is usually impossible, so efforts are made to design a network that covers all the regions that may generate traffic and to have 'holes' only in no-traffic zones.

There are two ways in which radio planners can use propagation models. They can either create their own propagation models for different areas in a cellular network, or they can use the existing standard models, which are generic in nature and are used for the entire area. The advantage of using their own model is that it will be more accurate, but it will also be immensely time-consuming to construct. Usage of the standard models is economical from the time and money perspectives, but these models have limited accuracy. Of course, there is a middle way out: the use of multiple generic models for urban, suburban and rural environments in terms of macro-cell or micro-cell structure. The cell and network coverage depend mainly on natural factors such as geographical aspect/propagation conditions, and on human factors such as the landscape (urban, suburban, rural), subscriber behavior etc. The ultimate quality of the coverage in the mobile network is measured in terms of location probability. For that, the radio propagation conditions have to be predicted as accurately as possible for the region.
The whole land area is divided into three major classes: urban, suburban and rural based on human-made structures and natural terrains. The cells (sites) that are constructed in these areas can be classified as outdoor and indoor cells (femto-cells). Outdoor cells can be further classified as macro-cellular, micro-cellular or pico-cellular. In this study, macro and micro cells are evaluated (Syed and et al 2009, Zhang and et al 2010, Tura and et al 2011, Dersch 1992, Nawrocki and et al 2006).

5.2.1.1 Macro-cells

When the base station antennas are placed above the average roof-top level, the cell is known as a macro-cell. As the antenna height is above the average roof-top level, the area that can be covered is wide. A macro-cell range may vary from a couple of kilometers to 35 km, the distance depending upon the type of terrain and the propagation conditions. Hence, this concept is generally used for suburban or rural environments.

5.2.1.2 Micro-cells

When the base station antennas are below the average roof-top level, then the cell is known as a micro-cell. The area that can be covered is small, so this concept is applied in urban and suburban areas. The range of micro-cells is from a few hundred meters to a couple of kilometers.

Coverage planning is an important step in deploying a cellular network. This process includes the selection of the proper propagation model based on the area's terrain, clutter, and population. Propagation models (empirical models) are too simplistic to predict the signal propagation behavior in an accurate fashion; they provide us with some relatively good accuracy of how things would behave.

Engineers rely on prediction tools to study and analyze the performance of the network for a geographic area via its coverage. Modeling and simulation using some current RF planning tools for LTE cells will give a good idea about the coverage performance of a certain grid within a specific area. Most cells are designed to be hexagonal in theory; in reality, this is not the case, as several factors affect the location selection decision (political, humanitarian, and economical).

5.2.1.3 Empirical path loss models

The path loss represents the mean (median) signal attenuation at a certain distance from the transmitter, and can be predicted by the distance and other macroscopic parameters such as carrier frequency, transmitter and receiver antenna heights, terrain contour and building concentration. The simplest form of path loss is the free space loss, which applies to the extreme case when nothing obstructs the propagation path and so and the corresponding received signal is called the LOS (Line of sight) signal.

$$\frac{P_r}{P_t} = \left[\frac{\sqrt{G_l}\lambda}{4\pi d} \right]^2 \qquad \textbf{(5.3)}$$

Thus, the received signal power falls off inversely proportional to the square of the distance *d* between the transmit and receive antennas. The received signal power is also proportional to the square of the signal wavelength, so as the carrier frequency increases, the received power decreases. If there is a NLOS (No Line of sight) connection, then the received signal attenuates more than the LOS case and also becomes independent of frequency. In this case the power relation between the receiver and the transmitter is

$$\frac{P_r}{P_t} = \left[\frac{\sqrt{G_l} h_t h_r}{d^2} \right]^2 \qquad \textbf{(5.4)}$$

where h_t and h_r denote the transmitter and the receiver heights respectively.

Path loss estimation is performed by empirical models if land cover is known only roughly, and the parameters required for semi-deterministic models cannot be determined. The empirical path loss model for urban-micro environment is Cost 231 Walfish-Ikegami (COST 231 Final Report 2012) model which allows for improved path-loss estimation by consideration of more data to describe the character of the urban environment, namely

i. heights of buildings hRoof,
ii. widths of roads w,
iii. building separation b and
iv. road orientation with respect to the direct radio path φ.

and in this study, their values are 10 meters, 25 meters, 50 meters and 30^o respectively. The parameters are defined in Figures 5.10 and 5.11.

Figure 5.10: Typical propagation situation in urban areas and definition of the parameters used in the COST-WI model

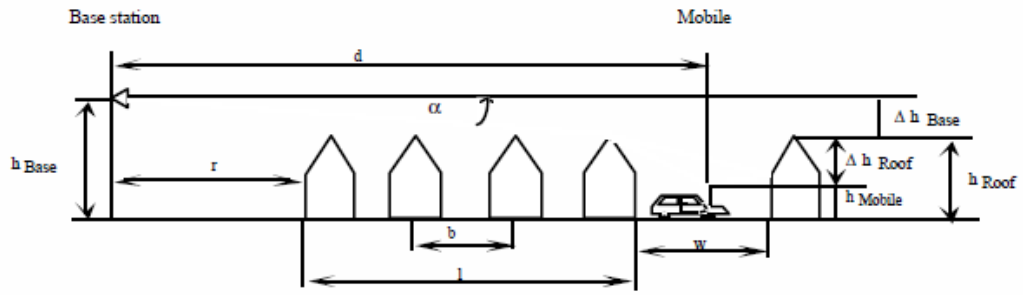

Source: DIGITAL MOBILE RADIO TOWARDS FUTURE GENERATION SYSTEMS COST 231 Final Report, 2012

These elements block the signal path and give rise to random variations of the received power at a given distance and generally attenuate the signal value. For example a building coverage will add about 16-20 dB and in car about 7 dB of extra signal loss which are known as shadowing effect.

The model distinguishes between line-of-sight (LOS) and non-line-of-sight (NLOS) situations. In the LOS case -between base and mobile antennas within a street canyon - a simple propagation loss formula different from free space loss is applied.

$$L_b(\text{dB}) = 42.6 + 26\log(d/\text{km}) + 20\log(f/\text{MHz}) \quad \text{for } d \geq 20 \text{ m} \qquad \textbf{(5.5)}$$

where the first constant is determined in such a way that L_b is equal to freespace loss for d = 20 m. In the NLOS-case the basic transmission loss is composed of the terms free space loss L_0, multiple screen diffraction loss L_{msd}, and roof-top-to-street diffraction and scatter loss L_{rts}.

$$L_b = \begin{cases} L_0 + L_{rts} + L_{msd} & \text{for } L_{rts} + L_{msd} > 0 \\ L_0 & \text{for } L_{rts} + L_{msd} \leq 0 \end{cases} \qquad \textbf{(5.6)}$$

The free-space loss is given by:

$$L_0(\text{dB}) = 32.4 + 20\log(d/\text{km}) + 20\log(f/\text{MHz}) \qquad \textbf{(5.7)}$$

The term L_{rts} describes the coupling of the wave propagating along the multiple-screen path into the street where the mobile station is located. The determination of L_{rts} is mainly based on Ikegami's model. It takes into account the width of the street and its orientation. COST 231, however, has applied another street-orientation function than Ikegami:

$$L_{rts} = -16.9 - 10\log\frac{w}{m} + 10\log\frac{f}{MHz} + 20\log\frac{\Delta h_{Mobile}}{m} + L_{Ori}$$

$$L_{Ori} = \begin{cases} -10 + 0.354\dfrac{\varphi}{\text{deg}} & \text{for } 0^\circ \le \varphi < 35^\circ \\ 2.5 + 0.075\left(\dfrac{\varphi}{\text{deg}} - 35\right) & \text{for } 35^\circ \le \varphi < 55^\circ \\ 4.0 + 0.114\left(\dfrac{\varphi}{\text{deg}} - 55\right) & \text{for } 55^\circ \le \varphi < 90^\circ \end{cases} \qquad \textbf{(5.8)}$$

$$\Delta h_{Mobile} = h_{Roof} - h_{Mobile}$$

$$\Delta h_{Base} = h_{Base} - h_{Roof}$$

Figure 5.11: Definition of the street orientation angle φ.

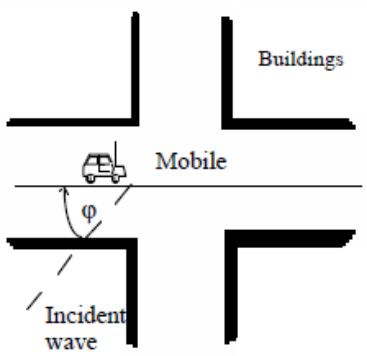

Source: DIGITAL MOBILE RADIO TOWARDS FUTURE GENERATION SYSTEMS COST 231 Final Report, 2012

In urban-macro and suburban-macro environment, COST 231 extended Hata model is used as an empirical path loss model. Four parameters are used for estimation of the propagation loss by Hata's well-known model: frequency f, distance d, base station antenna height hBase and the height of the mobile antenna hMobile. In Hata´s model, which is based on Okumura´s various correction functions (COST 231 Final Report 2012), the basic transmission loss, L_b, in urban areas is:

$$L_b = 69.55 + 26.16.\log\frac{f}{MHz} - 13.82.\log\frac{hBase}{m} - a(h_{Mobile}) + (44.9 - 6.55.\log\frac{h_{Base}}{m}).\log\frac{d}{km} \quad \textbf{(5.9)}$$

where:

$$a(h_{Mobile}) = (1.1.\log\frac{f}{MHz} - 0.7)\frac{h_{Mobile}}{m} - (1.56.\log\frac{f}{MHz} - 0.8) \quad \textbf{(5.10)}$$

The model is restricted to:

i. *f* : 150 ... 1000 MHz
ii. *hBase* : 30 ...200 m
iii. *hMobile*: 1 ...10 m
iv. *d* : 1 ...20 km

COST 231 has extended Hata´s model to the frequency band 1500 < f(MHz) < 2000 by analysing Okumura´s propagation curves in the upper frequency band. This combination is called "COST-Hata-Model" (Cost 231 Final Report 2012):

$$L_b = 46.3 + 33.9.\log\frac{f}{MHz} - 13.82.\log\frac{hBase}{m} - a(h_{Mobile}) + (44.9 - 6.55.\log\frac{h_{Base}}{m}).\log\frac{d}{km} + C_m \quad \textbf{(5.11)}$$

where *a(hMobile)* is defined in equation (5.10) and

$$C_m = \begin{cases} 0 \text{ dB for medium sized city and suburban} \\ \text{centres with medium tree density} \\ 3 \text{ dB for metropolitan centres} \end{cases} \quad \textbf{(5.12)}$$

Note that in suburban-macro environment C_m value is 3 dB while in urban-macro environment this value is 0 dB.

In rural-macro environment the Hata model was used in the work item UMTS900 (3GPP TR 25.816 2009), this model can be reused:

$$L(R) = 69.55 + 26.16\log_{10}(f) - 13.82\log_{10}(Hb) + [44.9 - 6.55\log_{10}(Hb)]\log(R) - 4.78(\text{Log}_{10}(f))^2 + 18.33\log_{10}(f) - 40.94 \quad \textbf{(5.13)}$$

where:

i. R is the base station-UE separation in kilometres

ii. f is the carrier frequency in MHz

iii. Hb is the base station antenna height above ground in metres

After L is calculated, log-normally distributed shadowing (LogF) with standard deviation of 10 dB should be added (3GPP TR 25.816 2009), (3GPP TR 25.942 2009). A Shadowing correlation factor of 0.5 for the shadowing between sites (regardless aggressing or victim system) and of 1 between sectors of the same site shall be used.

In Figure 5.12, path loss comparison related to 800 MHz and 2600 MHz bands in different environments is shown. Urban-micro environment in 2600 MHz band gives the worst result and rural-macro environment in 800 MHz band gives the best result in terms of signal level as expected. Since urban-micro environment consists of dense buildings, cars, trees etc. and the antenna height is below the rooftop, the signal

attenuates rapidly compared to the other environments. Also, there is a difference in signal level between the two different frequency bands (800 MHz and 2600 MHz) in the same environment which is about 10 dBm for urban-macro, suburban-macro and rural-macro environment and more than 20 dBm for urban-micro environment.

Figure 5.12: Pathloss comparison for all environments in 800 MHz & 2600 MHz frequency

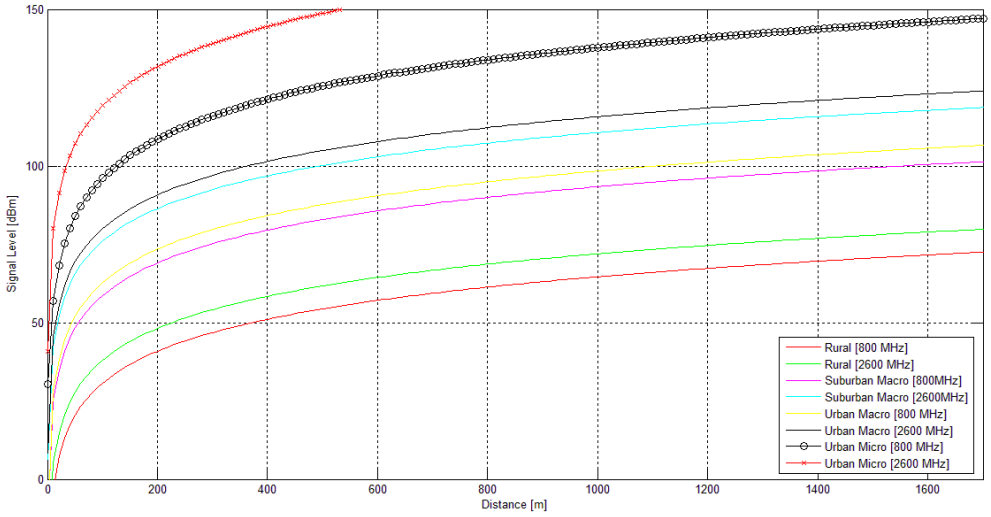

5.2.2 Simulation Results

In this part, the coverage behavior of different environments are analyzed for 800 MHz and 2600 MHz bands. The results are obtained with LTE system level simulator. Propagation models are used to simulate the coverage results for different environments. The coverage is analyzed with respect to path loss and shadowing effects and the results are obtained in SINR (Signal to interference plus noise ratio) value. The results are compared for different frequency bands according to the furthest distance can be reached and the widest area can be covered. Also it is assumed that only one eNodeB deployed to the area with one user exist in each sector as shown in figure 5.13 and so it is unlikely to see the effect of intercell interference.

The simulations are run in the urban-micro, urban-macro, suburban-macro and rural-macro environments. The results are taken according to the SINR values related to the

distances from the eNodeB. The parameters used for the system level simulator are summarized in Table 5.1.

Figure 5.13: One cell and a UE per sector deployment for coverage analysis

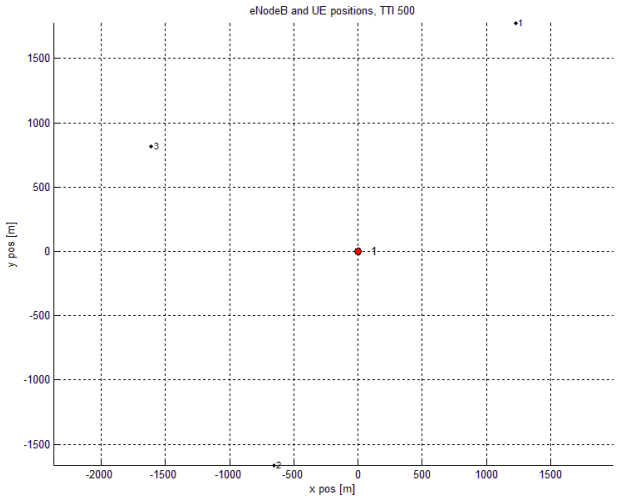

Table 5.1: LTE System Level simulator parameters

System Level simulator parameters				
Deployment scenario for the evaluation process	Urban micro-cell (UMi)	Urban macro-cell (UMa)	Suburban macro-cell	Rural macro-cell (RMa)
Layout	Hexagonal grid	Hexagonal grid	Hexagonal grid	Hexagonal grid
Inter-site distance	200 m	500 m	1300 m	1 732 m
Channel model	Urban micro model (UMi)	Urban macro model (UMa)	Suburban macro model (SMa)	Rural macro model (RMa)
User distribution	Randomly and uniformly distributed over area. 100% users outdoor (pedestrian users) (10 users per sector)	Randomly and uniformly distributed over area. 100% of users outdoors in vehicles (10 users per sector)	Randomly and uniformly distributed over area. 100% users vehicles (10 users per sector)	Randomly and uniformly distributed over area. 100% of users outdoors in high speed vehicles (10 users per sector)
User mobility model	Fixed and identical speed |v| of all UTs, randomly and uniformly distributed direction	Fixed and identical speed |v| of all UTs, randomly and uniformly distributed direction	Fixed and identical speed |v| of all UTs, randomly and uniformly distributed direction	Fixed and identical speed |v| of all UTs, randomly and uniformly distributed direction
UE speeds of interest	3 km/h	30 km/h	90 km/h	120 km/h
System Bandwidth	20 MHz	20 MHz	20 MHz	20 MHz
Carrier frequency	800 MHz & 2.6 GHz	800 MHz & 2.6 GHz	800 MHz & 2.6 GHz	800 MHz & 2.6 GHz
Transmission Mode	SISO, TxD OLSM & CLSM	SISO, TxD OLSM & CLSM	SISO, TxD OLSM & CLSM	SISO, TxD OLSM & CLSM
UT noise figure	9 dB	9 dB	9 dB	9 dB
BS antenna gain (boresight)	17 dBi	17 dBi	17 dBi	17 dBi
UT antenna gain	0 dBi	0 dBi	0 dBi	0 dBi
Thermal noise level	–174 dBm/Hz	–174 dBm/Hz	–174 dBm/Hz	–174 dBm/Hz
Base station (BS) antenna height	10 m, below rooftop	25 m, above rooftop	35 m, above rooftop	45 m, above rooftop
Number of BS and UE antenna elements	1 RX & 1 TX for SISO 2 RX & 2 TX	1 RX & 1 TX for SISO 2 RX & 2 TX	1 RX & 1 TX for SISO 2 RX & 2 TX	1 RX & 1 TX for SISO 2 RX & 2 TX
Total BS transmit power	44 dBm for 20 MHz	49 dBm for 20 MHz	49 dBm for 20 MHz	49 dBm for 20 MHz
Shadow fading	Log-normal, 10 dB std	Log-normal, 10 dB std	Log-normal, 10 dB std	Log-normal, 10 dB std
Multipath fading	Winner+	Winner+	Winner+	Winner+
Scheduling	Round Robin, Proportional Fair & Best CQI	Round Robin, Proportional Fair & Best CQI	Round Robin, Proportional Fair & Best CQI	Round Robin, Proportional Fair & Best CQI
CQI report delay	3 ms	3 ms	3 ms	3 ms
Simulation time	1000 TTI	1000 TTI	1000 TTI	1000 TTI

In urban-micro environment, inter site distance is 200 meters and the antenna height is 10 meters which is below the rooftop and the antenna gain is 17 dBi. The transmit power for urban-micro environment is accepted as 44 dBm (25 Watts) for 20 MHz bandwidth. The shadowing is assumed Log-normal distributed with zero mean and 10 dB variance (Gudmundson 1991). According to these parameters, coverage comparison of 800 Mhz and 2600 MHz was evaluated.

As illustrated in Figure 5.14, 800 MHz band has better coverage than 2600 MHz band. Since urban-micro environment consists of many high buildings, streets and other moving or static objects and the antenna is below the rooftop, the effect of shadowing can be seen clearly. Especially at the edge of the sectors the SINR degrades around 5 dB in which the SINR value is approximately 15 dB in 800 MHz and 10 dB in 2600 MHz. But up to 100 meters the signal levels are almost the same, particularly around the antenna radiation direction.

Figure 5.14: Urban-micro environment coverage comparison (800 MHz left and 2600 MHZ right).

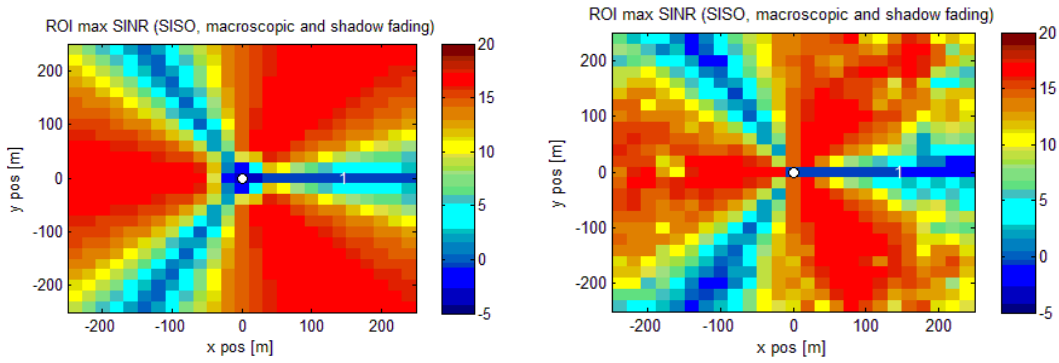

In urban-macro environment, inter site distance is 500 meters and the antenna height is 25 meters which is above the rooftop and the antenna gain is 17 dBi. The transmit power for urban-macro environment is accepted as 49 dBm (80 Watts) for 20 MHz bandwidth. The shadowing is assumed Log-normal distributed with zero mean and 10 dB variance.

In urban-macro environment the propagation is influenced by terrain effects: shadowing and scattering due to earth surface irregularities, buildings, vegetation, etc. Since the antenna is above the roof top it can be assumed the scattering topology is open.

In Figure 5.15, 800 MHz (on the left) and 2600 MHz (on the right) bands are compared as a coverage in urban-macro environment. It is clear that 800 MHz band surpasses at the cell edge. The signal levels vary between 0-15 dB at the cell edge for 2600 MHz band simulation since the shadowing effect occured. As a result, it is observed that there is about 5-10 dB SINR difference between two frequency bands at the cell edge. But in the near zone, moreover, up to 300 meters, the signal levels are almost the same.

In suburban-macro environment, inter site distance is 1300 meters and the antenna height is 35 meters which is above the rooftop and the antenna gain is 17 dBi. The transmit power for suburban-macro environment is accepted as 49 dBm (80 Watts) for 20 MHz bandwidth. The shadowing is assumed Log-normal distributed with zero mean and 10 dB variance. In suburban-macro environment, antenna is higher according to urban-macro case and the density of the buildings is less. So the effect of the shadowing is less in this environment.

Figure 5.15: Urban-macro environment coverage comparison (800 MHz left and 2600 MHZ right).

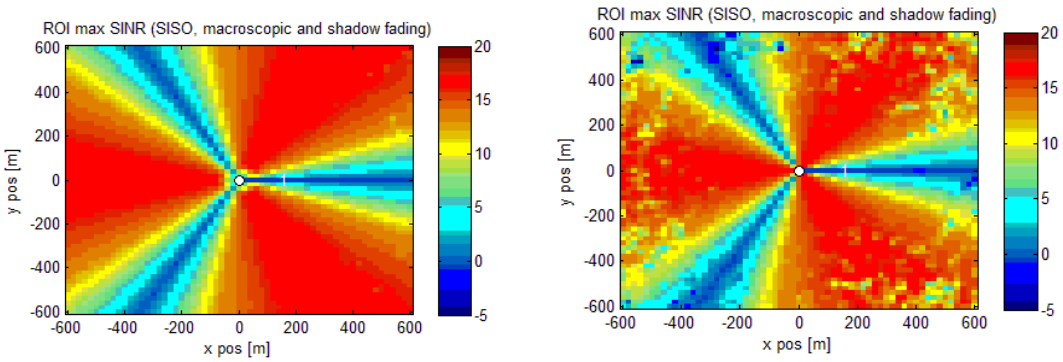

In Figure 5.16, it can be observed easily that 800 MHz band coverages better than 2600 MHz band. Particularly, at the cell edge the signal degrades explicitly and at the sector intersection areas the SINR value falls below 0 dB, however at the zone of antenna radiation direction, it is possible to get high SINR values. In general, the SINR difference at the cell edge between the two frequency bands is about 10 dB. In addition, up to 500 meters distance the signal level is the same for both frequency bands.

Figure 5.16: Suburban-macro environment coverage comparison (800 MHz left and 2600 MHZ right)

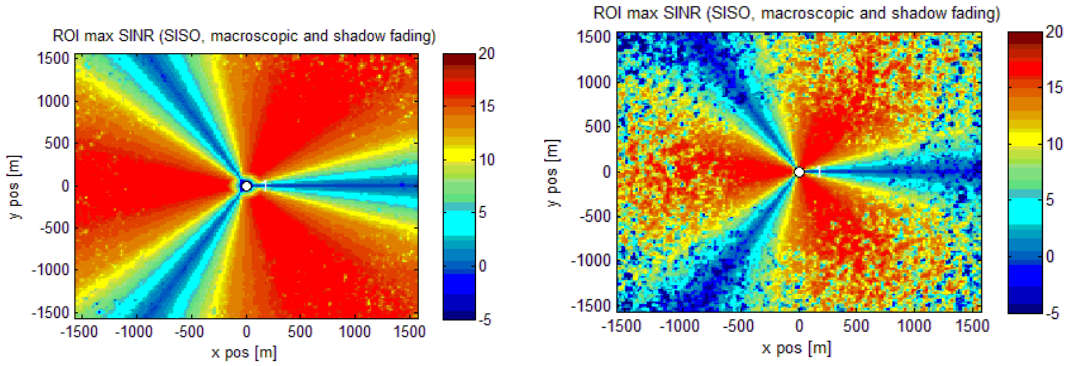

In rural-macro environment, inter site distance is 1732 meters and the antenna height is 45 meters which is above the rooftop and the antenna gain is 17 dBi. The transmit power for rural-macro environment is accepted as 49 dBm (80 Watts) for 20 MHz bandwidth. The shadowing is assumed Log-normal distributed with zero mean and 10 dB variance. The scattering topology is open for rural environments and it is possible to cover several kilometers.

In rural-macro environment, the coverage is more important than capacity. In Figure 5.17, the results show that 800 MHz band ensures better coverage, however 2600 MHz band performs better in near zone. As the inter site distance is 1732 meters, even in 800 MHz band the cell edge users may not be connected but still it reaches more users than 2600 MHz band coverage. In addition, 2600 MHz band provides better SINR values up to 1000 meters distance. One of the main reason for this difference between two bands is the geographical environment which is covered by hilly mountains etc. So the shadowing effect can also be seen here. Therefore, in rural-macro environments, it is more suitable to use lower frequencies to be able to cover the whole site since the inter site distance is more than enough for the signals to attenuate to unacceptable level.

Figure 5.17: Rural-macro environment coverage comparison (800 MHz left and 2600 MHZ right).

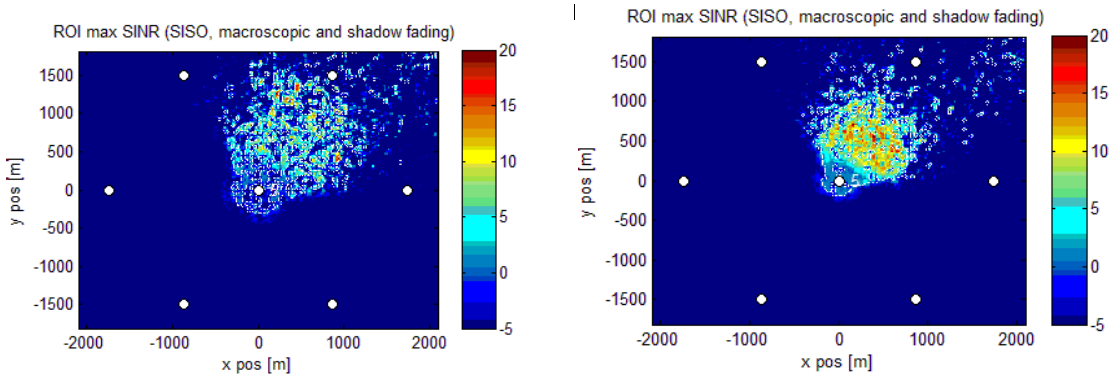

5.2.3 Capacity Analysis Results

In this part, LTE Release 8 capacity results are compared in micro and macro environments with respect to 800 MHz and 2600 MHz frequency bands, different MIMO modes and scheduling algorithms. These parameters are compared in terms of the average cell and cell edge throughputs. The results are presented in four different environments. The main idea of this analyse is to give idea about future deployment scenarios for LTE. Simulation parameters are summarized in Table 5.1.

Firstly, performance comparison of Round Robin (RR), Proportional Fair (PF) and Best CQI (BCQI) schedulers in terms of fairness (Jain's fairness index) is shown in Figure 5.18. These results are valid for all the capacity results in the following part. The results show that the proportional fair scheduler outperforms the other schedulers in terms of fairness thereby resulting in a good trade-off between throughput and fairness as can be understood from the capacity results in the following part.

Figure 5.18: Fairness index comparison for RR, PF and BCQI schedulers

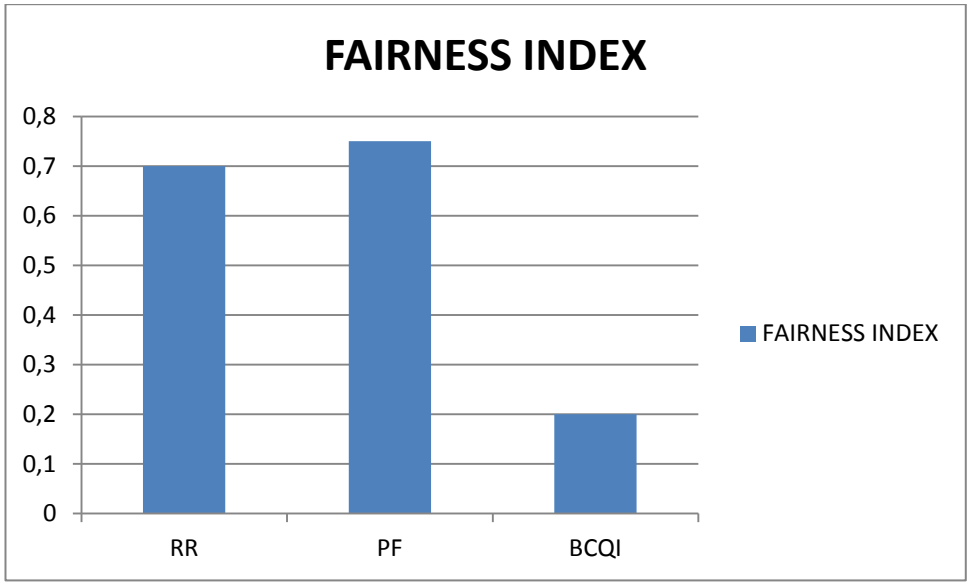

In the following part, average throughput and cell-edge throughput results are compared in different environments with respect to frequency bands, SISO and MIMO modes and scheduling algorithms.

In urban-micro environment, average throughput results are listed in Table 5.2 and shown in Figure 5.19. The results show that, in all cases it is possible to get higher throughputs in 2600 MHz than in 800 MHz. It is clear that the lowest throughput is achieved for SISO case. The MIMO mode 4 which is referred to CLSM (Closed Loop Spatial Multiplexing) outperforms in all cases. TxD (Transmit Diversity – MIMO mode 2) and OLSM (Open Loop Spatial Multiplexing – MIMO mode 3) performs almost equal. Otherwise, Best CQI scheduling algorithm maximizes the throughput since it selects the user which has the best channel quality in the current resource block. Round Robin scheduling algorithm has the worst performance between the scheduling algorithms since it allocates the resource blocks without dealing the channel quality of each user. Proportional Fair scheduling algorithm is fairer than Best CQI but gives lower throughputs but it performs better than Round Robin scheduling algorithm.

Table 5.2: Urban-micro environment average cell throughput results

	AVERAGE CELL THROUGHPUT [Mb/s]					
	800 MHz			**2600 MHz**		
	RR	PF	BEST CQI	RR	PF	BEST CQI
SISO	17,69	29,7	42,79	22,6	33,52	58,57
TxD	29,7	39,53	62,13	33,91	44,83	71,03
OLSM	26,45	33,6	62,69	32,41	40,97	79,02
CLSM	37,19	46,73	70,34	45,57	50,83	81,79

Figure 5.19: Urban-micro environment average cell throughput results

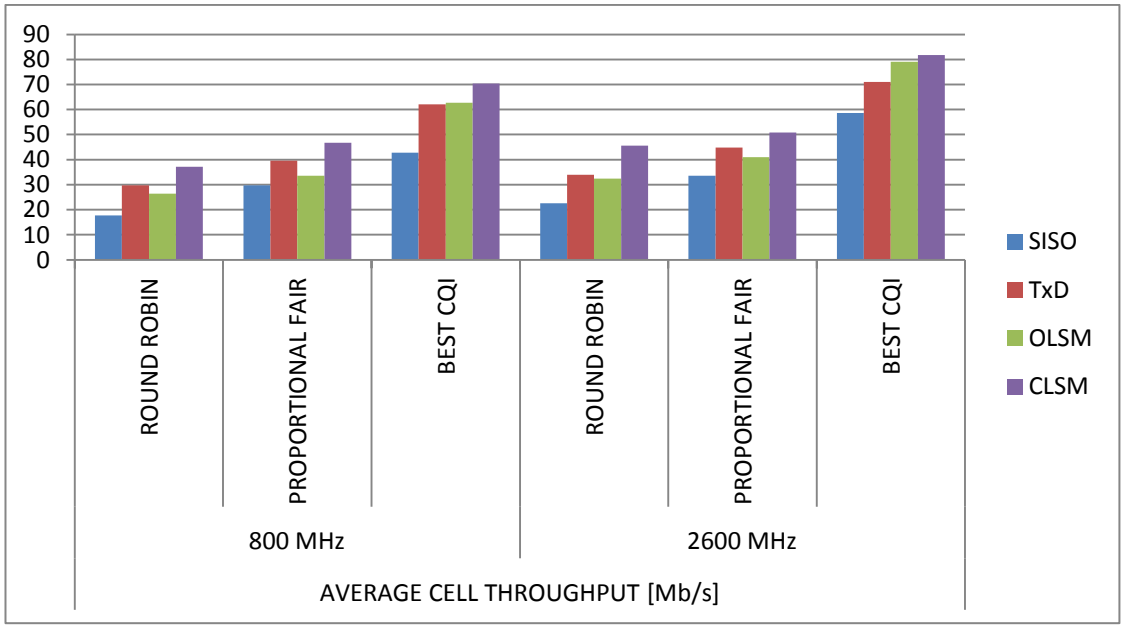

When the cell edge throughput performance is evaluated, the situation changes. As shown in Figure 5.20 and Table 5.3, Best CQI algorithm cannot produce any throughput in any case since it schedules the users close to the eNodeB. But, Round robin and Proportional Fair scheduling algorithms can still provide some throughput. CLSM and Proportional Fair scheduler performs as the best at the cell edge. At the cell edge, the maximum throughput that can be obtained is around 1,5 Mb/s while in SISO mode it degrades to 0,3 Mb/s. In most cases, 2600 MHz throughputs are better than 800 MHz especially with Round Robin scheduler.

Table 5.3: Urban-micro environment cell edge throughput results

	CELL EDGE UE THROUGHPUT [Mb/s]					
	800 MHz			2600 MHz		
	RR	PF	BEST CQI	RR	PF	BEST CQI
SISO	0,28	0,76	0	0,32	0,73	0
TxD	0,78	1,23	0	0,89	1,36	0
OLSM	0,47	0,52	0	0,49	1,18	0
CLSM	0,88	1,48	0	1,16	1,44	0

Figure 5.20: Urban-micro environment cell edge throughput results

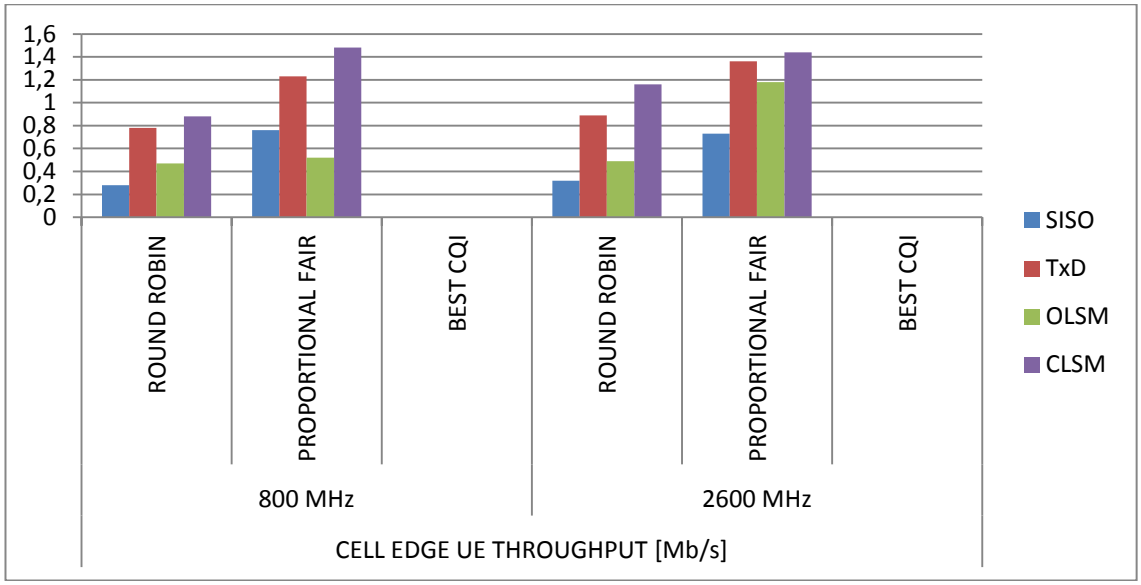

In Urban-macro environment, average throuhput values degrade more in general according to urban micro environment case since the intercell distance increases to 500 meters and the average cell SINR decreses. In this case, throughput values between the two different frequency bands is almost the same, even in some cases 800 MHz exceeds 2600 MHz. Also, TxD performs better than the other MIMO modes and the maximum throuhgput value is achieved in TxD mode with Best CQI scheduling algorithm as 40,3 Mb/s and the lowest value is clearly obtained in SISO mode with Proportional fair scheduling algorithm. Beacuse, the CQI reporting delay time is assumed 3 ms and each user speed is 30 Km/h, the channel response changes more rapidly which means the channel coherence time shrinks and channel tracking and adapting performance decreases. Best CQI scheduling algorithm outperforms again between all the scheduling algorithms in urban-macro environment. The throughput drops considerably for Proportional Fair scheduler with respect to Round Robin scheduler when the mobile

speed increases to 30 km/h because the feedback is not able to follow the fast fading, and the frequency domain scheduling gain is lost.

Table 5.4: Urban-macro environment average cell throughput results

	AVERAGE CELL THROUGHPUT [Mb/s]					
	800 MHz			**2600 MHz**		
	RR	PF	BEST CQI	RR	PF	BEST CQI
SISO	17,69	3,93	12,01	12,79	3,98	15,39
TxD	28,41	11,76	40,3	28,22	11,95	38,24
OLSM	24,95	14,64	33,91	24,87	13,72	33,38
CLSM	29,18	18,11	33,71	32,12	19,34	29,65

Figure 5.21: Urban-macro environment average cell throughput results

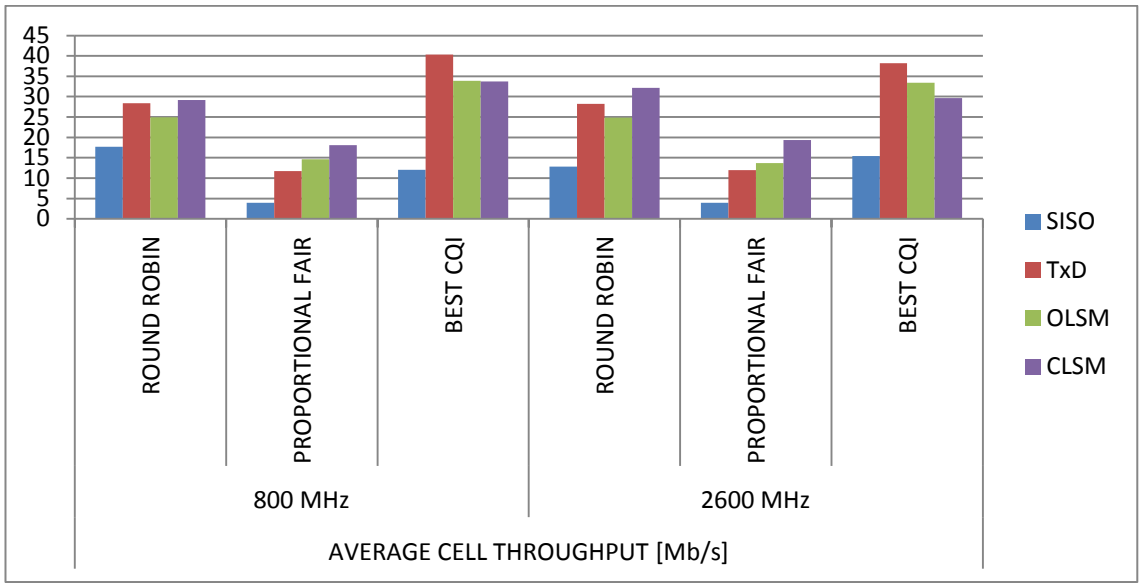

Cell edge performance in urban-macro environment is similar to urban-micro case. Unlike to average cell throughput results, CLSM produces more throughput than the other cases. Best CQI scheduler cannot produce any throughput as in urban-micro case. Round Robin scheduler performs better than Proportional Fair scheduler in this case. The maximum throughput that can be achieved is around 0,8 Mb/s with Round Robin scheduler while with using Proportional Fair scheduler, the maximum throughput is 0,6 Mb/s. On the other hand, 800 MHz band results are better than 2600 MHz band at the cell edge in some cases and almost the same for the remaining results.

Table 5.5: Urban-macro environment cell edge throughput results

	CELL EDGE UE THROUGHPUT [Mb/s]					
	800 MHz			2600 MHz		
	RR	PF	BEST CQI	RR	PF	BEST CQI
SISO	0,28	0,05	0	0,11	0,04	0
TxD	0,59	0,3	0	0,54	0,32	0
OLSM	0,5	0,38	0	0,4	0,27	0
CLSM	0,76	0,56	0	0,83	0,6	0

Figure 5.22: Urban-macro environment cell edge throughput results

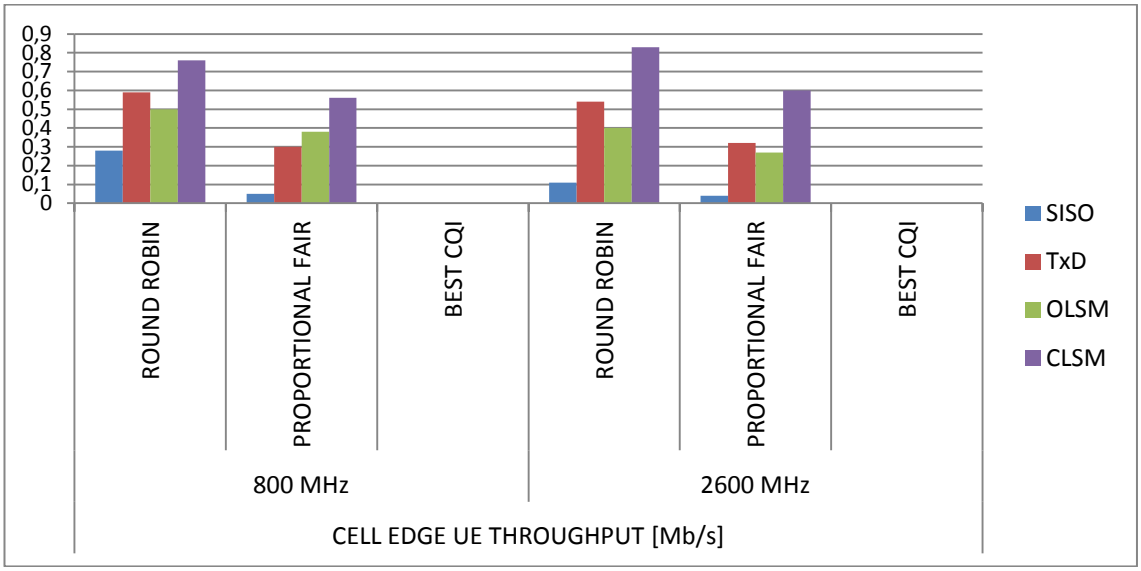

In suburban-macro environment, average throughput results are better than urban-macro environment results, especially in TxD mode. As listed in table 5.1, user speed is 90 Km/h in this environment. So, increasing speed also increases the doppler speed and the channel varies more frequently than the previous cases. Also, inter eNodeB distance is 1300 meters and the users are spread to a larger area and the received signal level is poorer according to the path loss formula described in section 5.2.1.3. But the antenna is located to a higher position in this case and so according to equation 5.4, it provides more received power. If all these parameters evaluated, as seen in table 5.5, TxD mode has the best performance almost in all cases. Also, the throughput difference between 800 Mhz and 2600 MHz bands decreases, even in some cases 800 Mhz band results are better than 2600 MHz band. CLSM mode performs better than OLSM in suburban-macro environment in all cases. If the schedulers are compared, the result is similar as in urban-macro environment. Best CQI has the best throughput results in all cases and

Round Robin scheduler is greater than Proportional Fair scheduler which is almost double in all results.

Table 5.6: Suburban-macro environment average cell throughput results

AVERAGE CELL THROUGHPUT [Mb/s]						
	800 MHz			2600 MHz		
	RR	PF	BEST CQI	RR	PF	BEST CQI
SISO	12,46	8,31	19,43	12,51	8,54	19,09
TxD	33,09	16,84	52,26	28,22	16,77	50,52
OLSM	23,52	11,61	34,46	25,81	12,6	36,62
CLSM	31,67	17,09	34,99	29,3	16,16	43,06

Figure 5.23: Suburban-macro environment average cell throughput results

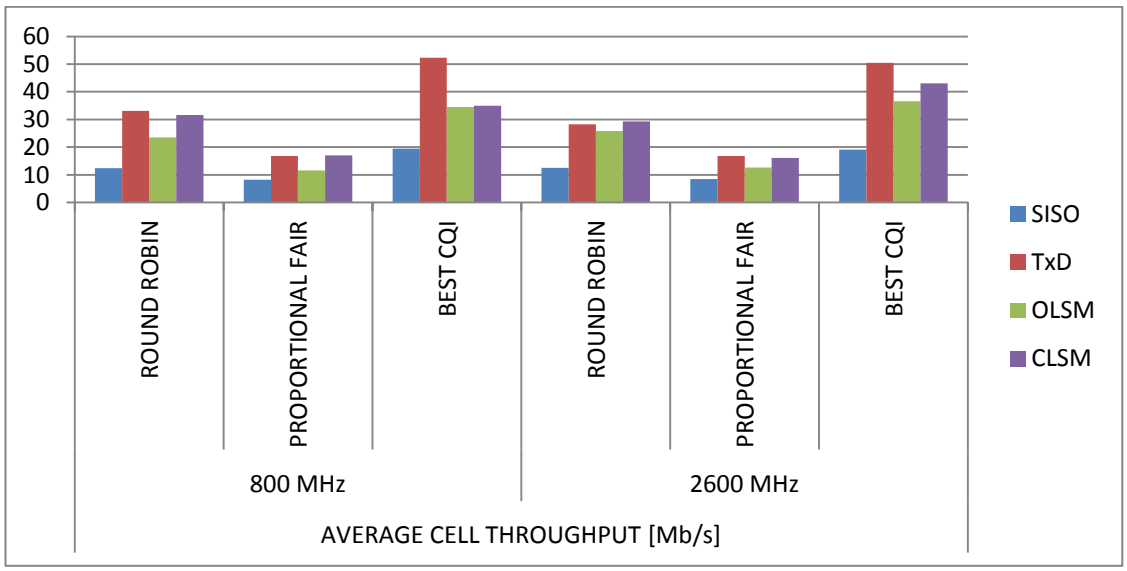

Cell edge performance according to the schedulers is similar to urban-micro environment. While Best CQI scheduler is disabled at the cell edge and Round Robin scheduler maximizes the throughput levels and Proportional Fair scheduler follows it very closely. The highest throughput is obtained with CLSM and Round Robin scheduler which is around 0,9 Mb/s and almost the same as in urban-macro environment result. In addition, maximum throughput value for Proportional Fair scheduler is around 0,5 Mb/s which is also obtained in CLSM mode. Also 800 MHz band performs better particularly with Round Robin scheduler and almost the same with Proportional Fair scheduler.

Table 5.7: Suburban-macro environment cell edge throughput results

	CELL EDGE UE THROUGHPUT [Mb/s]					
	800 MHz			2600 MHz		
	RR	PF	BEST CQI	RR	PF	BEST CQI
SISO	0,1	0,13	0	0,08	0,12	0
TxD	0,62	0,43	0	0,63	0,49	0
OLSM	0,57	0,32	0	0,42	0,25	0
CLSM	0,89	0,47	0	0,66	0,51	0

Figure 5.24: Suburban-macro environment cell edge throughput results

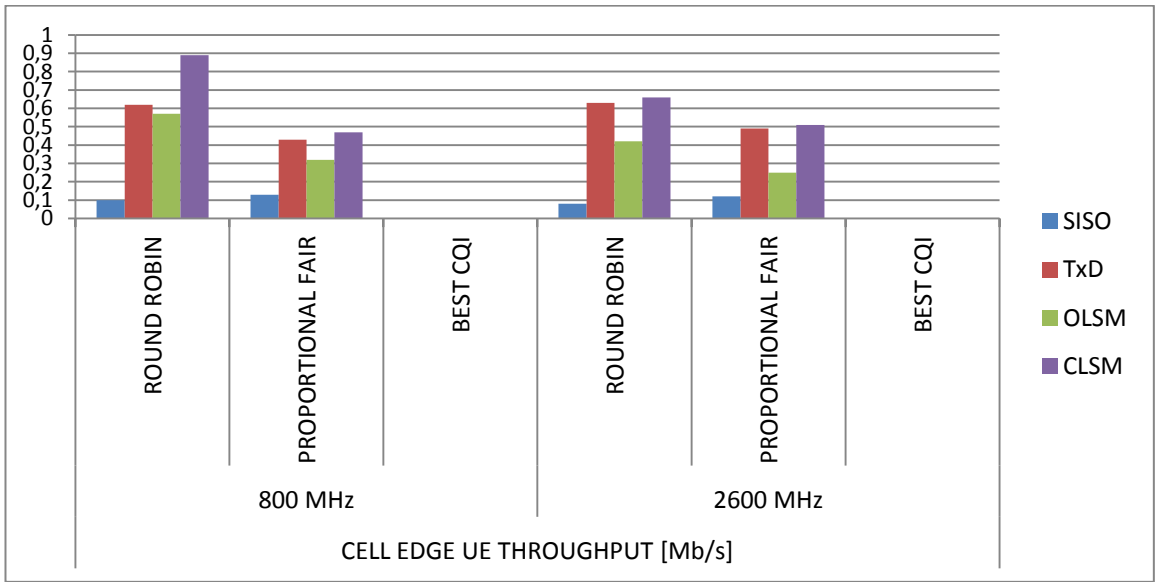

So far, various urban environment simulation results are shown and discussed. Also rural-macro environment is simulated and will be compared in this part. In this case, it is assumed that users are on the highway and each has a speed of 120 Km/h. The inter eNodeB distance is 1732 which is comparable to urban environment values and the antenna height (45 meters above the rooftop) is more than the others. The users are spread to a wide area and as shown in Figure 5.3, rural-macro environment has the best path loss performance than the others since there are fewer obstacles in the cell coverage area. But according to equation (5.3), the received signal will be poorer at the far points to the eNodeB. Also, unlike other situations, minimum coupling loss which describes the minimum loss in signal (dB) between the eNodeB and user equipment is 80 dB in rural-macro environment while in all urban environments this value is 70 dB. The results show that in Figure 5.25, average cell throughput is better in 2600 MHz band and again TxD leads almost in all cases as well as Best CQI is the best choice for

maximizing the average cell throughput in any case. Round Robin scheduler comes after Best CQI scheduler as in the other macro environment results. In rural-macro environment, average cell throughput values, especially CLSM mode results highly drop comparing to urban environment simulation results.

Table 5.8: Rural-macro environment average cell throughput results

AVERAGE CELL THROUGHPUT [Mb/s]						
	800 MHz			2600 MHz		
	RR	PF	BEST CQI	RR	PF	BEST CQI
SISO	3,15	2,14	6,31	5,72	3,58	8,03
TxD	12,07	7,27	25,46	16,8	10,85	25,34
OLSM	5,5	3,78	8,38	9,44	6,83	15,37
CLSM	11,7	4,52	11,12	18,81	5,84	17,02

Figure 5.25: Rural-macro environment average cell throughput results

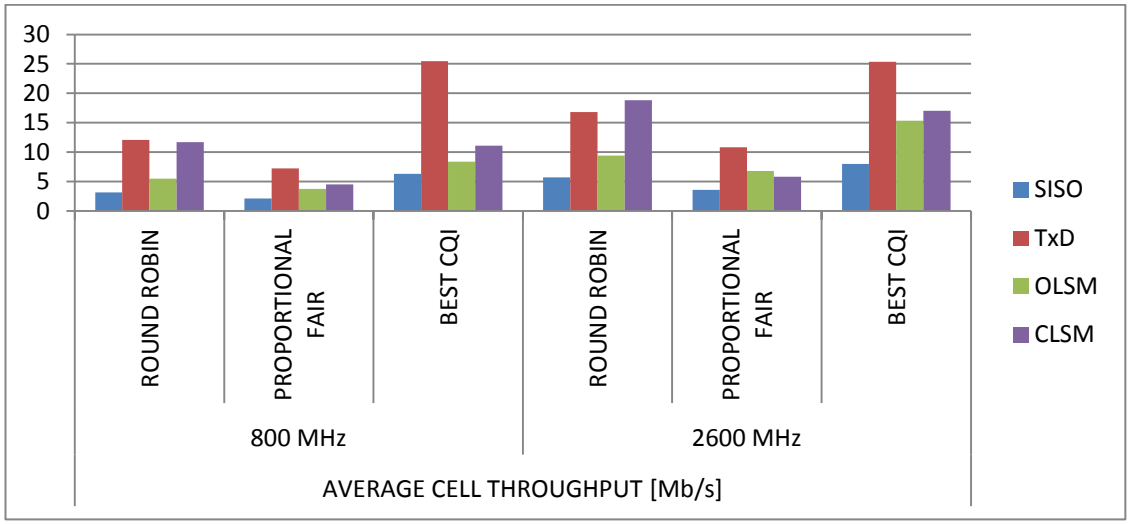

Cell edge throughputs compared to urban environment simulations are worse, even in most cases the difference is more than five to one ratio. Best CQI scheduler gives nothing as expected and Proportional Fair scheduler has better throughputs in 800 MHz band while in 2600 MHz band, Round Robin scheduler has the best performance. But in all cases, 2600 MHz band produces better throughput. The maximum value for the cell edge is 0,45 Mb/s with CLSM and Round Robin scheduler while Proportional Fair scheduler performs best with a 0,29 Mb/s throughput value in TxD mode.

Table 5.9: Rural-macro environment cell edge throughput results

	CELL EDGE UE THROUGHPUT [Mb/s]					
	800 MHz			2600 MHz		
	RR	PF	BEST CQI	RR	PF	BEST CQI
SISO	0,01	0,04	0	0,05	0,06	0
TxD	0,22	0,26	0	0,37	0,29	0
OLSM	0,02	0,03	0	0,15	0,17	0
CLSM	0,06	0,13	0	0,45	0,12	0

Figure 5.26: Rural-macro environment cell edge throughput results

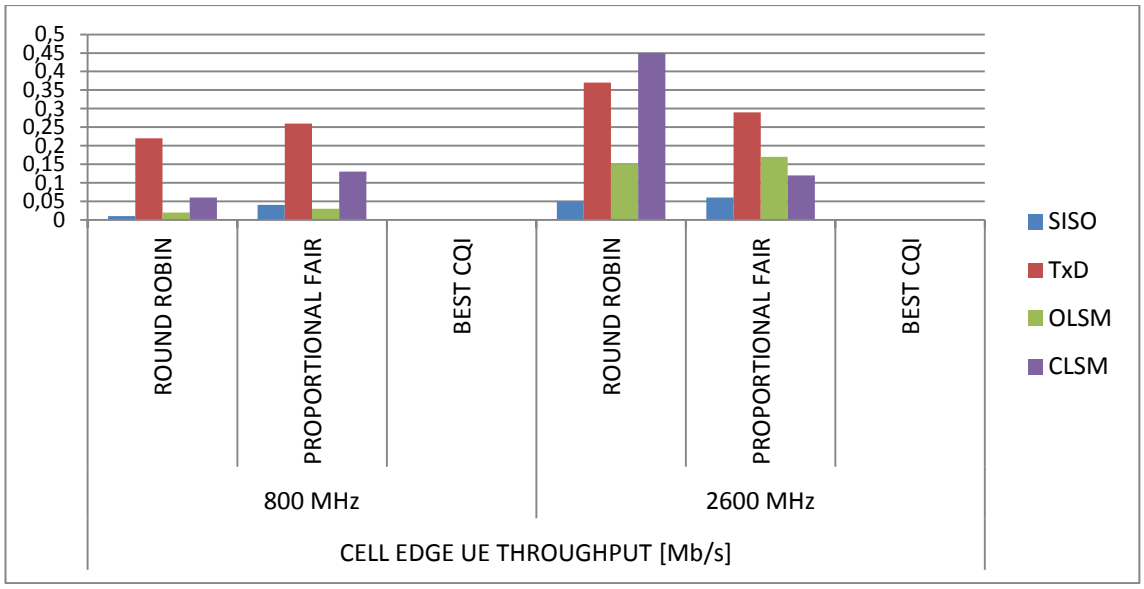

6. CONCLUSION

In this Master's thesis, a simulation based performance analysis of the Long Term Evolution (LTE) is presented. LTE intends to support high peak data rates to improve the system capacity and coverage. OFDM has been adopted as the downlink transmission scheme and SC-FDMA has been adopted as the uplink transmission scheme. LTE supports Multiple-Input Multiple-Output (MIMO) antenna technology which offers up to 300 Mbit/s in the downlink and 75 Mbit/s in the uplink. LTE is the future of the Mobile broadband and the most important rival for the wireline technologies.

I have done research on the LTE coverage and capacity comparison in various environments which are urban-micro, urban-macro, suburban-macro and rural-macro environments. I have used a Matlab based system level simulator which provides different types of simulations for the downlink very similar to real scenarios.

I have compared 800 MHz and 2600 MHz bands to investigate the coverage difference between them. It is assumed that only one eNodeB deployed to the area so the effect of intercell interference is omitted. However, this study gives idea about deployment scenarios for two different frequencies. The results showed that the best coverage was achieved in rural-macro environment with using 800 MHz band and the minimum coverage occurred in urban-micro environment in 2600 MHz band. Also, in all cases 800 MHz band coverage outperforms 2600 MHz band.

I have compared capacity results of four environments with respect to SISO or MIMO mode, frequency band, scheduling algorithms. I have used three types of MIMO modes which are Transmit Diversity (TxD), Open Loop Spatial Multiplexing (OLSM) and Closed Loop Spatial Multiplexing (CLSM). Also I have used Round Robin, Proportional Fair and Best CQI scheduling algorithms. In each simulation it assumed that 210 users were deployed randomly to an area within seven cells exist. The results are compared according to average cell throughput and cell-edge throughput of the users. The highest throughput could be achieved was 81,79 Mbit/s and the lowest was 2,14 Mbit/s in average cell throughput results and for cell-edge throughputs the results

varies between 0 to 1,5 Mbit/s. I have investigated that the highest throughputs was achieved in urban-micro environment with CLSM mode and Best CQI scheduler in 2600 MHz band and the lowest result was obtained in rural-macro environment in 800 MHz band with SISO mode and Proportional Fair scheduler. Since the users are pedestrian and so their speed are very low (3 km/h), the best channel condition was experienced in urban-micro environment and on the contrary, in rural-macro environment, the channel quality was so low due to the high speed of the users and their further distances to eNodeBs. Almost in all simulations, throughput results in 2600 MHz band were higher than the results in 800 MHz band. Best CQI scheduler has the highest throughputs when evaluating the average cell throughputs but for cell-edge performance Best CQI scheduler could not produce any throughput since it schedules only the users with good channel quality. Furthermore, Round Robin and Proportional Fair schedulers could have produced throughput in cell-edge throughput simulations since they do not take into account the channel conditions. Also the results showed that, Round Robin scheduler has better results than Proportional Fair scheduler almost in all simulations. On the other hand, CLSM mode performs slightly better than OLSM and TxD modes in urban-micro and urban-macro environments. Because the channel variations are slow, i.e. the channel is almost flat during the transmission period, so that feedback reporting in CLSM and OLSM worked fine in these cases. Beside, in suburban-macro and rural-macro environments TxD produces the highest throughputs since it is more robust in bad channel conditions. SISO mode was the worst performer in all cases.

REFERENCES

Books

Goldsmith, A., 2005. *Wireless Communications.* U.S.A: Cambridge University Press.

Sesia, S., Toufik, I., Baker, M., 2009. *LTE – The UMTS Long Term Evolution : From Theory to Practice.* U.K: Wiley.

Holma, H., Toskala, A., 2009. *LTE for UMTS – OFDMA and SC-FDMA Based Radio Access*. U.K: Wiley.

Rumney, M., 2009. *LTE and the Evolution to 4G Wireless : Design and Measurement Challanges*. U.K: Agilent Technologies.

Abu-Rgheff, MA., 2007. *Introduction to CDMAWireless Communications.* U.S.A: Academic Press.

Proakis, JG., 2001. *Digital Communications*. Republic of China: Mc Graw Hill.

Madhow, U., 2008. *Fundamentals of Digital Communication*. U.K: Cambridge University Press.

Yang, SC., 2010. *OFDMA System Analysis and Design*. U.K: Artech House.

Furht, B., Ahson, SA., 2009. *Long Term Evolutıon 3GPP LTE Radio and Cellular Technology*. U.K: CRC Press.

Song, L., Shen, J., 2011. *Evolved Cellular Network Planning and Optimization for UMTS and LTE*. U.S.A: CRC Press.

Nawrocki, MJ., Dohler, M., Aghvami, AH., 2006. *Understanding UMTS Radio Network Modelling, Planning and Automated Optimisation Theory and Practice*. U.S.A: Wiley

Tse, D., Viswanath, P., 2004. *Fundamentals of Wireless Communications.* U.K: Cambridge University Press.

Periodicals

3GPP, 2012, Overview of 3GPP Release 8 V0.2.7.

3GPP TS 36.211, 2009, 3rd Generation Partnership Project; Technical Specification Group Radio Access Network; Evolved Universal Terrestrial Radio Access (E-UTRA); Physical Channels and Modulation (Release 8).

3GPP TS 36.212, 2009, 3rd Generation Partnership Project; Technical Specification Group Radio Access Network; Evolved Universal Terrestrial Radio Access (E-UTRA); Multiplexing and channel coding (Release 8).

3GPP TR 36.942, 2009, 3rd Generation Partnership Project; Technical Specification Group Radio Access Network; Evolved Universal Terrestrial Radio Access (E-UTRA); Radio Frequency (RF) system scenarios; (Release 8).

3GPP TS 36.213, 2009, 3rd Generation Partnership Project; Technical Specification Group Radio Access Network; Evolved Universal Terrestrial Radio Access (E-UTRA); Physical layer procedures (Release 8).

3GPP TR 25.816, 2009, 3rd Generation Partnership Project; Technical Specification Group Radio Access Network; UMTS 900 MHz Work Item Technical Report (Release 8).

3GPP TR 25.942, 2009, 3rd Generation Partnership Project; Technical Specification Group Radio Access Networks; Radio Frequency (RF) system scenarios (Release 8).

Alamouti, S. M., 1998. A Simple Transmit Diversity Technique for Wireless Communications. *IEEE Journal on Select Areas in Communications*. **16**(8), pp.1451-1458.

Dersch, U., 1992. Physical modelling of macro, micro and inhouse cell mobile radio channels. *Third IEEE International Symposium on Personal, Indoor and Mobile Radio Communications.,* pp.64-68.

Spiegel, C., Zijian Bai, Bruck, G.H., Jung, P., Horvat, M., Berkmann, J., Drewes, C., and Gunzelmann, B., 2011. Closed-Loop Schemes in UTRA LTE and LTE-Advanced. *International Conference on Communications, Computing and Control Applications (CCCA).*, pp. 1-5.

Tura, O., Soysal, A., Yuksel, G., 2011. Comparison of LTE 800 MHz and LTE 2600 MHz Frequency Bands in terms of Cell Coverage. *IEEE 19th Conference on Signal Processing and Communications Applications (SIU).*, pp. 837-840.

Giancristofaro, D., 1996. Correlation model for shadow fading in mobile radio channels. *Electronics Letters.* **32**(11), pp. 958-959.

Gudmundson, M., 1991. Correlation model for shadow fading in mobile radio systems. *Electronics Letters.* **27**(23), pp. 2145-2146.

Ozdemir, M. and Arslan, H., 2007. Channel Estimation for Wireless OFDM System. *IEEE Communications Surveys*. **9**(2), pp. 19-48.

Adhikari, S., 2011. Downlink Transmission Mode Selection And Switching Algorithm For LTE. *Third International Conference on Communication Systems and Networks (COMSNETS).*, pp. 1-10.

Claussen, H., 2005. Efficient modelling of channel maps with correlated shadow fading in mobile radio systems. *IEEE 16th International Symposium on Personal, Indoor and Mobile Radio Communications* .**1**., pp. 512-516.

Simonsson, A., Qian, Y., and Östergaard, J., 2010. LTE Downlink 2x2 MIMO With Realistic CSI: Overview and Performance Evaluation. *IEEE Wireless Communications and Networking Conference (WCNC.)*, pp. 1-6.

Astely, D., Dahlman, E., Furuskar, A., Jading, Y., Lindstrom, M., Parkvall, S., 2009. LTE: The Evolution of Mobile Broadband. *IEEE Communications Magazine.* **47**(4)., pp. 44-51.

Schwarz, S., Wrulich, M., and Rupp, M., 2010. Mutual Information based Calculation of the Precoding Matrix Indicator for 3GPP UMTS/LTE. *International ITG Workshop on Smart Antennas (WSA).*, pp. 52-58.

Schwarz, S., Mehlführer, C., and Rupp, M., 2010. Calculation of the spatial preprocessing and link adaption feedback for 3GPP UMTS/LTE. 6th Conference on Wireless Advanced (WiAD)., pp. 1-6.

Ball, C.F., Mullner, R., Lienhart, J., and Winkler, H., 2009. Performance Analysis of Closed and Open Loop MIMO in LTE. *EW 2009. European Wireless Conference.*, pp. 260-265.

Lee, J., Han, J.K., and Zhang, J., 2009. MIMO Technologies in 3GPP LTE and LTE-Advanced. *EURASIP Journal on Wireless Communications and Networking.* **2009**(302092).

Rumney, M., 2008. 3GPP LTE: Introducing Single-Carrier FDMA. *Agilent Measurement Journal.* **1**.

Zyren, J., 2007. Overview of the 3GPP Long Term Evolution Physical Layer, *Freescale Semiconductor*. **1.**

Coleri, S., Ergen, M., Puri, A., Bahai, A., 2002. Channel estimation techniques based on pilot arrangement in OFDM systems. *IEEE Transactions.* 48(4)., pp. 223-229.

Bagadi, K.P., Das, S., 2010. MIMO-OFDM Channel Estimation using Pilot Carries. *International Journal of Computer Applications.* 2(3)., pp. 81-88.

Shen, Y., Martinez, E., 2006. Channel Estimation in OFDM Systems. Freescale Semiconductor Application Note.

Ikuno, J.C., Wrulich, M., Rupp, M., 2010. System level simulation of LTE networks. *IEEE 71st Vehicular Technology Conference*: *VTC2010-Spring*

Almatarneh, R., Ahmed, M., Dobre, O., 2009. Frequency-time scheduling algorithm for OFDMA systems. *Canadian Conference on Electrical and Computer Engineering, CCECE '09*., pp. 766 - 771

Other Publications

MATLAB. 2011, Available: http://www.mathworks.com/products/matlab/ (cited 5 September, 2011).

Colom, J., Taranet, M., 2011, Vienna LTE Simulators System Level Simulator, Available: http://www.nt.tuwien.ac.at/ltesimulator/ (cited 4, October, 2011).

3GPP. 2012, Availale: http://www.3gpp.org/ftp/Specs/html-info/21101.htm (cited 15, May, 2012)

Pagès, A.S., (2009). A Long Term Evolution Link Level Simulator. *Master of Science Thesis*: Polytechnic University of Catalunya

Dikamba, T. (2011). Downlink Scheduling in 3GPP Long Term Evolution (LTE). *Master of Science Thesis*: Delft University of Technology. NAS.

Zhang, L., 2010. Network Capacity, Coverage Estimation and Frequency Planning of 3GPP Long Term Evolution. *Master of Science Thesis*: Linköping University. Institute of Technology.

Syed, A.B. (2009). Dimensioning of LTE Network Description of Models and Tool, Coverage and Capacity Estimation of 3GPP Long Term Evolution radio interface. *Master of Science Thesis*: Helsinki University of Technology. Department of ECE

Akram, M.S. (2007). Pilot-based Channel Estimation in OFDM Systems. *Master of Science Thesis*: Technical University of Denmark.

Simko, M., (2009). Channel Estimation for UMTS Long Term Evolution. *Master of Science Thesis*: Vienna University of Technology. Faculty of Electrical Engineering and Information Technology.

De Jong, Y. L. C., Camir´e, D., and Rogers, D. V., 2011. COMPARISON OF RADIO PROPAGATION CHARACTERISTICS AT 700 AND 2,500 MHz PERTAINING TO MACROCELLULAR COVERAGE. [online] http://www.ic.gc.ca/eic/site/smt-gst.nsf/vwapj/smse-005-11-bell-apndix3.pdf/$FILE/smse-005-11-bell-apndix3.pdf [accessed 30 March 2012]

DIGITAL MOBILE RADIO TOWARDS FUTURE GENERATION SYSTEMS COST 231 Final Report. [online] http://www.lx.it.pt/cost231/final_report.htm [accessed 31 March 2012]

MIMO Transmission Schemes for LTE and HSPA Networks. 2009. [online] http://www.4gamericas.org/documents/Mimo_Transmission_Schemes_for_LTE_and_HSPA_Networks_June-2009.pdf [accessed 28 March 2012]

TD-LTE: Exciting Alternative, Global Momentum. 2010. [online] http://www.3gamericas.org/documents/Moto_TD-LTE_WP.pdf [accessed 28 March 2012]

The Seven Modes of MIMO in LTE. 2009. [online] http://www.tsiwireless.com/docs/whitepapers/The%20Seven%20Modes%20of%20MIMO%20in%20LTE.PDF [accessed 16 April 2012]